

Decays of the Lightest Squark in the MSSM with Flavor Violation

Masterarbeit
von

Alexander Wlotzka

An der Fakultät für Physik
Institut für Theoretische Physik

Referentin: Prof. Dr. M. Mühlleitner

Korreferent: Prof. Dr. D. Zeppenfeld

Bearbeitungszeit: 1. Mai 2013 – 25. April 2014

Ich versichere, dass ich diese Arbeit selbstständig verfasst und ausschließlich die angegebenen Hilfsmittel verwendet habe, die wörtlich oder inhaltlich übernommenen Stellen als solche kenntlich gemacht und die Satzung des KIT zur Sicherung guter wissenschaftlicher Praxis beachtet habe.

Alexander Wlotzka
Karlsruhe, den 25. April 2014

Als Masterarbeit anerkannt.

Prof. Dr. M. Mühlleitner
Karlsruhe, den 25. April 2014

1. Introduction	1
2. Basics of the Standard Model and Supersymmetry	3
2.1. The Standard Model	3
2.1.1. Particles and Interactions in the Standard Model	3
2.1.2. The Higgs Mechanism in the Standard Model	5
2.2. Supersymmetry	6
2.2.1. Motivation and Principles	7
2.2.2. The Minimal Supersymmetric Extension of the Standard Model	9
2.2.3. Flavor Structure of the MSSM	12
2.2.4. Light Up-Type Squarks	13
3. Calculation of the Decay Width	17
3.1. The Decay Width at Next-to-Leading Order	18
3.1.1. Dimensional Regularization	18
3.1.2. Phase Spaces	19
3.1.2.1. Two-Particle Phase Space	19
3.1.2.2. Three-Particle Phase Space	20
3.1.3. Factorization of the $d\Phi_{2+1}$ Phase Space	21
3.2. Renormalization	23
3.2.1. Lagrangian and Vertex Corrections	23
3.2.2. The On-Shell Renormalization Scheme	27
3.2.2.1. Matrix Renormalization	28
3.2.2.2. Renormalization Constants in the On-Shell Scheme	28
3.2.2.3. Limits and Special Cases	32
3.2.3. Self-Energies	33
3.2.4. Kinematics of the Decay	36
3.3. Real Corrections: Gluon Radiation	37
3.3.1. Feynman Diagrams and Amplitudes	37
3.3.2. Re-Parametrization of the Phase Space and the Amplitudes	39
3.3.2.1. Integration Bounds	41
3.3.2.2. Transformation of the Integrand	42
3.3.3. Divergences and Finite Terms	44

3.4. Four-Body Decay	45
4. Implementation and Constraints	47
4.1. Implementation of the Calculation	47
4.2. Spectrum Generator	48
4.3. Experimental Constraints	50
4.3.1. Higgs	50
4.3.2. Dark Matter	52
4.3.3. Low Energy Flavor Observables	54
4.3.4. Mass Exclusion Bounds	54
5. Results	57
5.1. Random Scan	57
5.2. Random Scan with a $\mathbf{U(3)} \times \mathbf{U(2)} \times \mathbf{U(3)}$ Symmetry	63
6. Conclusion and Future Prospects	69
7. Appendix	71
A. CMS Limits on Stop Pair-Production	71
B. Dirac Gamma-Matrices	72
Bibliography	75

The launch of the Large Hadron Collider (LHC) at the 'Conseil Européen pour la Recherche Nucléaire' (CERN) in September 2008 marked the beginning of a new era in particle physics. In the first investigation periods until the beginning of 2013 the LHC accelerated protons to a center-of-mass energy of 7 TeV and 8 TeV and current upgrades of both the accelerator and the detectors make proton collisions with a center-of-mass energy of up to 14 TeV possible, thereby enabling physicists to probe the fundamental laws of nature at yet unreachable energies. Moreover, the number of recorded collisions will considerably increase during the upcoming operation periods of the LHC. In this way the LHC and the detectors meet two requirements for detecting rare processes: the high center-of-mass energy can raise the probability for these processes to occur and a high number of recorded events helps to make statistically significant observations. Furthermore, the high energy released in the proton collisions allows for the production of new, heavy particles as long as they are in the kinematic reach. All this enabled the two particle detectors ATLAS and CMS to discover a new particle with a mass of about 125 GeV at the LHC in July 2012 [1, 2], which constitutes a landmark of particle physics. The generally accepted theoretical concept of describing interactions of elementary particles in physics is called Standard Model. Within this theory the masses of the particles are generated through the Higgs mechanism. This procedure predicts a new, scalar particle, the Higgs boson, which had not been observed before the launch of the LHC. After its discovery then, refined measurements of the properties of the particle showed that it is compatible with the Higgs boson predicted by the Higgs mechanism in the Standard Model [3–5]. In consequence François Englert and Peter Higgs were awarded the Nobel Prize in Physics 2013 for their theoretical work on the Higgs mechanism [6].

Now all free parameters of the model are determined by experiments making the Standard Model a conclusive framework for the description of fundamental interactions of elementary particles. But nevertheless, there are open questions in particle physics which cannot be addressed within the Standard Model. To name but a few: a fundamental force experienced in everyday life, gravity, is not described in the Standard Model and the astronomical observation of Dark Matter cannot be explained by it.

For this reason physicists investigate theories beyond the Standard Model. At present, various approaches undergo intense studies, each of them being able to answer one or few open questions. A promising idea in this context is Supersymmetry. It takes up the concept of describing elementary particles and their interactions of the Standard Model, but adds a

symmetry relating particles with half integer spin (fermions) to particles with integer spin (bosons). As a result the particle spectrum is enriched by new, supersymmetric partners of Standard Model particles which, in the case of soft Supersymmetry breaking, can be heavier than their Standard Model equivalents. In order to interpret experimental results precise predictions for both the production and decay processes of these particles are required.

This thesis focuses on the calculation of the decay width at next-to-leading order of an up-type squark into the lightest neutralino and a charm- or an up-quark within the framework of the Minimal Supersymmetric Extension of the Standard Model with flavor violation. The up-type squark and the lightest neutralino are two of the superpartners predicted by Supersymmetry and in our case the lightest neutralino is a candidate for Dark Matter. In Chapter 2, first, essentials of the Standard Model including the particle spectrum, interactions and the Higgs mechanism will be explained, followed by a short introduction to Supersymmetry, the model and the decay process studied in this work. The calculation of the decay width comprising the leading order process, virtual one-loop corrections and real corrections is part of Chapter 3. In particular, details on dimensional regularization, the renormalization of the Lagrangian and the cancellation of divergences occurring in loop-corrected amplitudes are given. Chapter 4 contains information on the implementation of the calculation in a computer program and a description of the procedure of deriving valid predictions of the chosen model. Experimental constraints taken into account are presented there as well. Finally, results of the calculation and their implications on the experimental search for the up-type squark considered in this thesis are discussed in Chapter 5, followed by a conclusion and an outlook in Chapter 6.

CHAPTER 2

BASICS OF THE STANDARD MODEL AND SUPERSYMMETRY

2.1. The Standard Model

The Standard Model (SM) has been highly developed over the past few decades and it successfully describes a variety of phenomena observed in particle physics. Although it is well understood in many respects and has been tested at highest precision it is a popular field of research as, for example, driving the theoretical predictions of the SM to higher precision can reveal deviations to results obtained by experiments. Moreover, the processes within the SM act as background to New Physics and a detailed study of the Higgs mechanism remains to be done. The Minimal Supersymmetric Extension of the SM (MSSM) described in Section 2.2.2 is explicitly based on the SM. For that reason, some major aspects shall be stated in the next sections, following [7–10].

2.1.1. Particles and Interactions in the Standard Model

The SM is a Quantum Field Theory (QFT) with all elementary matter particles being represented by fermion fields with spin one-half. The free field theory can be formulated in terms of a Lagrangian, which yields the correct equations of motion for the fields by using the Euler-Lagrange-Equations. Interactions are introduced to the free theory by requiring local gauge invariance of the Lagrangian with respect to corresponding symmetry groups. In that way the SM covers three fundamental interactions: the strong interaction by invariance under the symmetry group $SU(3)_C$, the weak interaction by invariance under $SU(2)_L$ and the electromagnetic interaction by the $U(1)_Y$ gauge invariance. The complete symmetry group of the SM is then given by

$$SU(3)_C \times SU(2)_L \times U(1)_Y , \quad (2.1)$$

where the index C stands for color, L denotes left, since only left-handed particles participate in the weak interaction, and Y represents hypercharge. From the Lagrangian Feynman rules can be derived for computing transition amplitudes. However, not all matter fields take part in all interactions and they differ in the quantum numbers, i.e. Noether charges corresponding to the symmetry groups. The quantum number for the $SU(3)_C$ is called color, for the $SU(2)_L$ it is the weak isospin, and for the $U(1)_Y$ it is called hypercharge. This allows for a classification of the fermion fields: there are two basic classes, one comprising the leptons, the other comprising the quarks. Leptons only undergo the electromagnetic and the weak interaction

whereas quarks undergo all three interactions. Schematically, the particles of the SM can be arranged as

$$\begin{pmatrix} \nu_e \\ e_L^- \end{pmatrix}, \begin{pmatrix} \nu_\mu \\ \mu_L^- \end{pmatrix}, \begin{pmatrix} \nu_\tau \\ \tau_L^- \end{pmatrix}, e_R^-, \mu_R^-, \tau_R^-, \quad (2.2)$$

$$\begin{pmatrix} u_L \\ d_L \end{pmatrix}, \begin{pmatrix} c_L \\ s_L \end{pmatrix}, \begin{pmatrix} t_L \\ b_L \end{pmatrix}, u_R, d_R, c_R, s_R, t_R, b_R. \quad (2.3)$$

The leptons are shown in Eq. (2.2) with e denoting the electron, μ for the muon and τ for the tau. The left-handed particles, with index L , are part of $SU(2)_L$ doublets together with partners with opposite third component of the isospin, called neutrinos, whereas the right-handed particles, denoted by the index R , carry isospin zero and are $SU(2)_L$ singlets. According to the Goldhaber experiment, right handed neutrinos do not exist [11]. The only difference between the electron, the muon and the tau is their mass. These three representatives of one and the same gauge multiplet are called generations. Taking the absolute value of the electric charge of the electron as unit, the electron, muon and tau carry an electric charge of -1 , the neutrinos are uncharged and assumed to be massless.

A similar picture holds for the quarks as shown in Eq. (2.3). Here, u represents the up-quark, d the down-quark, s the strange-, c the charm-, b the bottom-, and t the top-quark. These six types of quarks are called flavors. Again, the left-handed particles form isospin doublets and the right-handed particles are $SU(2)$ singlets and the only difference between the doublets is the mass of the particles. The up-, charm- and top-quarks are called up-type quarks and carry an electric charge of $+2/3$ and the down-, strange- and bottom-quarks are called down-type quarks with the charge $-1/3$. All quarks are triplets in color space. For all particles shown in Eqs. (2.2) and (2.3) there are anti-particles with the same mass but opposite charge.

A major achievement in order to establish the SM was the successful unification of the electromagnetic and the weak interaction by Glashow, Salam and Weinberg [7–9]. In the $SU(2)_L \times U(1)_Y$ -invariant Lagrangian the gauge field W_3 corresponding to the third generator of the $SU(2)_L$ and the gauge field B for the $U(1)_Y$ can be mixed to give two physical fields, one is then identified with the photon, the other one is called Z boson. The rotation angle to accomplish that is called Weinberg angle θ_W . This is the reason, why the Noether charge for the $U(1)_Y$ is not directly the electric charge, but is called hypercharge Y . The connection between the third component of the isospin I_3 , the hypercharge Y and the electric charge Q is given by the Gell-Mann-Nishijima formula [12–14]

$$Q = I_3 + \frac{Y}{2}. \quad (2.4)$$

The two gauge fields corresponding to the first and second generator of the $SU(2)_L$ can be combined to form two fields W^\pm with charges $Q = \pm 1$. Thus, the interaction particles of the SM are

$$\gamma, Z, W^\pm, g, \quad (2.5)$$

with g denoting gluons which are the gauge bosons for the $SU(3)_C$.

In anticipation of Section 2.2.3, where the flavor structure of the MSSM will be presented, a few facts for the SM shall be stated here. All up-type quarks carry the same gauge quantum numbers. Thus, the interaction eigenstates do not necessarily have to coincide with the mass eigenstates constituting the physical particles. This is indeed the case for the weak interaction and the rotation in generation space from mass to interaction eigenstates is given by the unitary matrix $U^{uL,R}$. The same holds for the down-type quarks with a unitary matrix

$U^{d_{L,R}}$. In an interaction of an up-type quark and a down-type quark with a W boson there will be a product of two such rotation matrices which is defined as the Cabbibo-Kobayashi-Maskawa (CKM) matrix [15, 16]

$$V_{\text{CKM}} = U^{u_L \dagger} U^{d_L} . \quad (2.6)$$

This means that the coupling of up-type and down-type quarks of different generations is possible due to the distinct rotations of up- and down-type quarks. By contrast, it is not possible for the interactions with the photon and the Z boson: the interaction of quarks with the photon or Z boson is diagonal in generation space. This means, that at tree-level flavor changing neutral currents (FCNCs) are impossible in the SM. Also note, that in the SM mass eigenstates coincide with flavor eigenstates.

2.1.2. The Higgs Mechanism in the Standard Model

The discovery of massive W and Z bosons confronted the concept of local gauge invariance described in the previous section with a problem. The gauge fields introduced to make the Lagrangian invariant under a local gauge transformation have to be massless since a mass term for the gauge fields in the Lagrangian is not gauge invariant. A method to overcome this problem is the Higgs mechanism [17–21]. The clue is that in the Lagrangian the whole symmetry is maintained but it is broken by the ground state. This concept is called spontaneous symmetry breaking (SSB) [22].

In detail, a complex spin zero particle field Φ is introduced as an $SU(2)_L$ doublet with the Lagrangian

$$\mathcal{L}_{\text{Higgs}} = (\partial_\mu \Phi)(\partial^\mu \Phi)^\dagger - V(\Phi) \quad (2.7)$$

and the potential

$$V(\Phi) = \mu^2 \Phi \Phi^\dagger + \lambda (\Phi \Phi^\dagger)^2 . \quad (2.8)$$

In order to have a potential V bounded from below, λ must be greater than zero. Replacing the pure derivative ∂_μ by a covariant one the Lagrangian of Eq. (2.7) becomes gauge invariant. To determine the ground state of the scalar field Φ which is the state with the lowest energy, the potential V has to be minimized. The two results are

$$\Phi^\dagger \Phi = \begin{cases} 0 & ; \mu^2 > 0 \\ \frac{-\mu^2}{2\lambda} & ; \mu^2 < 0 . \end{cases} \quad (2.9)$$

The first solution for the ground state does not break any symmetry and is rejected. But in the case of $\mu^2 < 0$ the scalar field has a non-vanishing vacuum expectation value (vev) v

$$|\Phi| = \sqrt{\frac{-\mu^2}{2\lambda}} := \frac{v}{\sqrt{2}} . \quad (2.10)$$

The $SU(2)_L$ doublet has hypercharge $Y = +1$. The upper component of the doublet will contain a Higgs field with charge $Q = +1$ while the lower component is uncharged. Hence, to have an uncharged vacuum the vev is assigned to the lower component. After SSB the expansion of the Higgs field around the ground state yields

$$\Phi = \frac{1}{\sqrt{2}} \begin{pmatrix} 0 \\ v + H(x) \end{pmatrix} . \quad (2.11)$$

It is this ground state which breaks the $SU(2)_L$ symmetry and according to the Goldstone theorem [22] this leads to $N^2 - 1 = 3$ spare degrees of freedom. However, inserting the Higgs field of Eq. (2.11) into the Lagrangian of Eq. (2.7), with covariant instead of pure derivatives, illustrates that these degrees of freedom are absorbed by the gauge bosons to acquire a mass. The remaining field $H(x)$ is the Higgs field. Its mass and self-couplings result from the potential V in Eq. (2.8). Also the fermion masses for each generation are generated by interactions of the Higgs field with the fermions in the Lagrangian [19]

$$\mathcal{L}_f = -y_{q_d} \bar{Q}_L \Phi q_{d,R} - y_{q_u} \bar{Q}_L i\sigma_2 \Phi^* q_{u,R} - y_l \bar{L}_L \Phi l_R, \quad (2.12)$$

where Q_L and L_L are the left-handed fermion doublets for quarks and leptons, respectively, and $q_{u,R}, q_{d,R}, l_R$ the corresponding right-handed fermion singlets. The coupling strengths of the fermions to the Higgs field are given by the Yukawa couplings $y_{q_u, q_d, l}$. The resulting masses are

$$m_W^2 = \frac{g^2 v^2}{4}, \quad (2.13)$$

$$m_Z^2 = \frac{(g^2 + g'^2)v^2}{4}, \quad (2.14)$$

$$m_f = \frac{y_f v}{\sqrt{2}}, \quad (2.15)$$

with the $SU(2)_L$ and $U(1)_Y$ gauge couplings g and g' , respectively. Due to the Higgs mechanism couplings of the Higgs boson to the SM particles are proportional to the respective masses of the particles: combining Eqs. (2.11), (2.12) and (2.15) shows that the coupling of the Higgs field to the fermions g_f is given by

$$g_f = \frac{\sqrt{2}m_f}{v}. \quad (2.16)$$

A similar relation holds for the gauge boson masses, *cf.* Eqs. (2.13) and (2.14). Therefore methods to probe the Higgs mechanism in the SM are

1. Find a scalar particle. Test its spin and parity quantum numbers and compare them to the SM prediction for the Higgs boson $J^P = 0^+$.
2. Verify that couplings of fermions and gauge bosons to this particle are proportional to their mass.
3. Measure the self-couplings of the Higgs boson. This allows to reconstruct the Higgs potential, which with its typical minimax form is responsible for the non-vanishing vev.

While a new particle with couplings compatible with the SM predictions has been found by the ATLAS and CMS experiments at the LHC [1, 2, 23], its quantum numbers are not determined uniquely, yet, and the self couplings remain to be investigated.

2.2. Supersymmetry

Although many predictions of the SM are compatible with the results of experiments there are reasons to study theories beyond the SM, such as Supersymmetry (SUSY). In Section 2.2.1 a motivation and brief introduction to the idea of Supersymmetry will be given, followed by a general description of the MSSM. In Section 2.2.3 the general flavor structure of the MSSM and assumptions used in this thesis will be explained and at the end, in Section 2.2.4, superpartners of the top-quark predicted by SUSY will be introduced as well as the process considered in this thesis.

2.2.1. Motivation and Principles

There are both experimental and theoretical reasons to investigate theories beyond the SM and in particular SUSY. An obvious reason is, that the SM only covers three fundamental forces, but does not include gravity. At energies around the TeV scale which are in the reach of current particle accelerators, gravity is not as important as the other interactions due to the small value of the gravity constant G_N . But in order to describe physics at energies up to the Planck scale $M_{Pl} \propto 10^{19}$ GeV a consistent description of all four forces is needed. Supersymmetric theories take a step in this direction [24–26].

In the search of grand unified theories (GUTs) it is also desirable to have the gauge coupling constants unify at a high energy scale. The dependence of the gauge coupling constants on the energy is described by renormalization group equations (RGEs) [27]. In the SM they show that the three couplings do not meet at a single point. However, in SUSY the RGEs are modified and the unification becomes possible [28–30]. In Section 2.1.2 the Higgs mechanism in the SM was explained. However, in the SM the Higgs potential V of Eq. (2.8) is added ad hoc and not generated by underlying dynamics. The condition $\mu^2 < 0$ in Eq. (2.9) is crucial to enable SSB. In supersymmetric models this can be achieved through RGE running [31, 32]. Moreover, the Higgs propagator acquires loop corrections containing quadratic divergences. The larger the energy scale where New Physics enters, the more tuned the theory has to be to keep the Higgs mass at its measured value of $m_{h,\text{phys}} \approx 125$ GeV. By introducing a new symmetry the fine-tuning can be avoided, for example in Supersymmetry the superpartners of the SM particles cancel the quadratic divergences.

Measuring the cosmic microwave background with a lensing technique, the Planck space telescope measured invisible mass centers [33]. An idea is, that these mass centers could consist of weakly interacting massive particles (WIMPs). They must be weakly interacting since no experiment could report direct evidence for such a particle, yet. But as they are observed by gravitational effects, the particles must have a mass. Similar measurements have been performed by the WMAP experiment [34]. In the SM there are no possible particles for this phenomenon called Dark Matter (DM), while in SUSY there can be promising candidates.

Precision measurements of SM observables prove that local gauge invariance is a striking concept in explaining the interactions of elementary particles. Provided that SUSY is a space-time symmetry and not a gauge symmetry, it is an elegant way to extend the SM and still maintain all gauge interactions unchanged.

In detail, the Lorentz algebra is extended to the Poincaré Superalgebra by introducing new generators for the SUSY transformation Q_a ($a = 1\dots 4$). These generators Q_a transform as a Dirac spinor under Lorentz transformation, leading to non-trivial commutation relations with the Lorentz generators. The complete Poincaré Superalgebra is given by [35]

$$[P^\mu, P^\nu] = 0, \quad (2.17a)$$

$$[P^\mu, M^{\rho\sigma}] = i(g^{\mu\rho}P^\sigma - g^{\mu\sigma}P^\rho), \quad (2.17b)$$

$$[M^{\mu\nu}, M^{\rho\sigma}] = -i(g^{\mu\nu}M^{\rho\sigma} - g^{\mu\sigma}M^{\nu\rho} - g^{\nu\rho}M^{\mu\sigma} + g^{\nu\sigma}M^{\mu\rho}), \quad (2.17c)$$

$$[P^\mu, Q_a] = 0, \quad (2.17d)$$

$$[M^{\mu\nu}, Q_a] = -\Sigma_{ab}^{\mu\nu}Q_b, \quad (2.17e)$$

$$\{Q_a, \bar{Q}_b\} = 2\gamma_{ab}^\mu P^\mu, \quad (2.17f)$$

where P^μ and $M^{\mu\nu}$ are the generators of the Lorentz group and

$$\Sigma^{\mu\nu} = \begin{pmatrix} \sigma^{\mu\nu} & 0 \\ 0 & \bar{\sigma}^{\mu\nu} \end{pmatrix}, \quad (2.18)$$

$$\bar{\sigma}^{\mu\nu} = \frac{i}{4}(\sigma^\mu \bar{\sigma}^\nu - \sigma^\nu \bar{\sigma}^\mu), \quad (2.19)$$

$$\sigma^\mu = (\mathbf{1}, \sigma_k), \quad (2.20)$$

$$\bar{\sigma}^\mu = (\mathbf{1}, -\sigma_k), \quad (2.21)$$

with the Pauli matrices σ_k ($k = 1, 2, 3$). The Coleman-Mandula-Theorem [36] in combination with the Haag-Łopuszański-Sohnius Theorem [37] prove that this is the largest continuous space-time symmetry for S -matrix elements consistent with QFT. Dirac spinors are bispinors in the $(\frac{1}{2}, 0) \oplus (0, \frac{1}{2})$ representation of the Lorentz group and can be decomposed into two left- and right-handed Weyl spinors in the $(\frac{1}{2}, 0)$ and $(0, \frac{1}{2})$ representation, respectively. This is also possible for the SUSY generators Q_a . From the non-trivial commutation relation of the SUSY generator with the Lorentz generators in Eq. (2.17e) it can be shown that acting with the SUSY generators on a state changes the spin of this state by one half. At the same time, due to Eq. (2.17d), the mass of the corresponding particle remains unchanged. Next, from Eq. (2.17f) it can be derived that subsequent application of the same SUSY generator gives zero [38]. In that way, the SUSY generators generate multiplets of states having the same mass and the same gauge quantum numbers, but a different spin. These multiplets are called supermultiplets and in each of them the number of fermionic and bosonic degrees of freedom coincides. Among the members of the supermultiplets it is possible to identify the SM matter fields and others, which are the superpartners of the SM fields. The symbols for the superpartners are the same as for the SM particles, but with a tilde on top. The partners for the SM fermions and are denoted by the SM name with a preceding 's'. So the superpartner of a quark q is called a squark \tilde{q} , the partner of a tau τ is called stau $\tilde{\tau}$, etc. The superpartners of the gauge bosons are called gauginos and the ones for the Higgs fields are named higgsinos.

An on-shell Dirac fermion has four degrees of freedom, therefore two complex scalar fields are needed as superpartners. These two complex scalar fields are assigned as superpartners for the left- and right-handed components of the Dirac fermion. Thus, the superpartners of the fermion f are then called \tilde{f}_L, \tilde{f}_R . Note that the lower indices L, R do not mark a chiral property of the sfermions themselves as they are scalar fields, but only indicate which SM fermion component they correspond to.

Contrary to the SM, two Higgs doublets are needed to give mass to up- and down-type fermions as $i\sigma_2\Phi^*$ transforms as a right chiral field which is not allowed in a SUSY-invariant Lagrangian [39, 40]. Thus, two Higgs doublets are introduced, one with hypercharge $Y = -1$

$$H_1 = \begin{pmatrix} h_1^{0*} \\ h_1^- \end{pmatrix}, \quad (2.22)$$

which gives mass to down-type fermions by acquiring a vev v_1 for h_1^0 and another one with hypercharge $Y = +1$

$$H_2 = \begin{pmatrix} h_2^+ \\ h_2^0 \end{pmatrix} \quad (2.23)$$

to give mass to up-type fermions with a vev v_2 for h_2^0 . The ratio of the two vevs is defined as

$$\tan \beta = \frac{v_2}{v_1}. \quad (2.24)$$

By imposing SUSY-invariance superpartners for the Higgs fields are introduced. Through EWSB three degrees of freedom are taken over by the gauge bosons to acquire a mass leaving five degrees of freedom open which form five Higgs bosons: two CP -even neutral Higgs bosons h^0, H^0 which are mixtures of the real components of the two neutral Higgs fields with the mixing parametrized by the angle α , one CP -odd neutral Higgs boson A^0 with mass m_A resulting from the imaginary parts of the neutral Higgs fields and two charged Higgs bosons H^\pm coming from the charged components of the Higgs fields.

In the decoupling limit [41] which is reached for $m_A \gg m_Z$ the lightest CP -even neutral Higgs boson h^0 has couplings similar to Higgs boson of the SM. Therefore the Higgs boson already discovered could also be a SUSY Higgs boson.

2.2.2. The Minimal Supersymmetric Extension of the Standard Model

In the MSSM all new SUSY particles have a SM equivalent and the Higgs sector contains only the two required Higgs doublets. So the particles of the MSSM are

1. All SM particles.
2. Superpartners for left- and right-chiral components \tilde{f}_L, \tilde{f}_R of the SM fermions f .
3. Superpartners for the gauge fields $\tilde{B}, \tilde{W}_i (i = 1, 2, 3), \tilde{g}_j (j = 1 \dots 8)$.
4. Two Higgs doublets H_1 and H_2 with superpartners \tilde{H}_1, \tilde{H}_2 .

Just as in the SM states with the same charge, color and spin can mix. In particular, the superpartners of the gauge fields \tilde{B} and \tilde{W}_3 mix with the two neutral Higgsinos \tilde{h}_1^0 and \tilde{h}_2^0 forming four neutral, weakly interacting fermions called neutralinos $\tilde{\chi}_l^0, l = 1 \dots 4$, which are ordered in mass with $l = 1$ being the lightest one. Additionally, the superpartners of the W bosons \tilde{W}^\pm mix with the superpartners of the charged Higgs bosons to build two charginos $\tilde{\chi}_{1,2}^\pm$. The EWSB through the Higgs mechanism shall be maintained in SUSY as it allows to have both local gauge invariance and massive gauge bosons [42–44]. Then also the fermion masses are given by the Yukawa coupling terms as in the SM. In SUSY, this additionally holds for the superpartners of the SM fields and it is possible to express the three Yukawa terms by superfields \hat{E}, \hat{L} for (s)leptons and \hat{Q}, \hat{U} and \hat{D} for (s)quarks and \hat{H}_1 and \hat{H}_2 for the Higgs fields, combining both SM fields and their superpartners. The gauge group of the SM as stated in Eq. (2.1) is taken over by the MSSM and the behavior of the fields under gauge transformations and the hypercharges are

$$\begin{aligned} \hat{L} &: (1, 1, -1), & \tilde{\hat{E}} &: (1, 1, 2), \\ \hat{Q} &: \left(3, 2, \frac{1}{3}\right), & \tilde{\hat{U}} &: \left(\bar{3}, 1, -\frac{4}{3}\right), & \tilde{\hat{D}} &: \left(\bar{3}, 1, \frac{2}{3}\right), \\ \hat{H}_1 &: (1, 2, -1), & \hat{H}_2 &: (1, 2, 1), \end{aligned} \quad (2.25)$$

where the first two numbers stand for the transformation behavior under $SU(3)_C$ and the $SU(2)_L$ transformations: 1 denotes a singlet, 2 a doublet and 3 a triplet. The third number is the hypercharge Y . The Yukawa terms together with another term connecting the two Higgs doublets specify the superpotential of the MSSM

$$W_{\text{MSSM}} = y_{ij}^u \tilde{U}_i \hat{Q}_j \cdot \hat{H}_2 + y_{ij}^d \tilde{D}_i \hat{Q}_j \cdot \hat{H}_1 + y_{ij}^e \tilde{E}_i \hat{L}_j \cdot \hat{H}_1 - \mu \hat{H}_1 \cdot \hat{H}_2, \quad (2.26)$$

where the ‘ \cdot ’ stands for the $SU(2)_L$ -invariant coupling of the left-handed $SU(2)_L$ doublets with the Higgs doublets, y_{ij}^f are generic Yukawa coupling matrices and $i, j = 1, 2, 3$ are

generation indices. The Higgsino parameter μ is a new, free parameter of the theory. At this point it is worth mentioning, that within conserved SUSY the MSSM contains only one new parameter μ with respect to the SM, as all new particles have the same mass and gauge quantum numbers as their SM equivalents. There are other terms respecting SUSY invariance, gauge invariance and renormalizability which could be added to the Lagrangian. However, these terms would violate lepton or baryon number conservation. As there is no experimental evidence for such processes, yet, either the corresponding couplings must be very small or there is a mechanism excluding these terms. Such a mechanism is given by requiring the conservation of R -parity [43] defined by

$$R := (-1)^{3B+L+2s} , \quad (2.27)$$

where B, L are baryon and lepton numbers and s is the spin of the particle. We have

$$R = +1 \quad \text{for SM particles} , \quad (2.28)$$

$$R = -1 \quad \text{for SUSY particles} . \quad (2.29)$$

The conservation of R -parity has important phenomenological consequences:

1. The lightest supersymmetric particle (LSP) is stable.
2. Starting with SM particles, SUSY particles can only be produced in pairs.
3. The final states of decays of SUSY particles always contain an odd number of SUSY particles.

The first point is the reason why the LSP can be a good candidate for DM, provided that it is only weakly interacting and neutral. Thereby, SUSY models with conserved R -parity can provide candidates for DM.

Up to now, the Lagrangian was taken to be SUSY invariant which led to superpartners with the same mass as the corresponding SM particles. None of the SUSY particles have been observed so far and current experiments derive lower bounds for their masses. This is one reason, why SUSY must be broken. A theoretical argument that SUSY must be broken comes from the Higgs sector. In Section 2.1.2 it was explained that the scalar potential V of Eq. (2.8) with the second case of Eq. (2.9) is vital for SSB. It turns out, that within conserved SUSY it is not possible to form a potential with non-vanishing expectation values for the two neutral Higgs fields. Therefore SUSY breaking terms in the Lagrangian relevant for the Higgs potential must be generated by a SUSY breaking mechanism [32].

Possible breaking mechanisms are for example gravity mediated SUSY breaking (mSUGRA) or gauge mediated SUSY breaking (GMSB), more information on these can be found for example in Ref. [38]. In this work, a rather general approach will be pursued: all terms explicitly breaking SUSY, but maintaining renormalizability and gauge invariance will be added to the Lagrangian, as long as they do not introduce new quadratic divergences. These terms are called soft SUSY breaking terms and parametrize the lack of knowledge of the SUSY breaking mechanism in a general way [40]. They are given by bilinear terms for the superpartners of the gauge fields

$$\mathcal{L}_{\text{bilinear, gauginos}} = -\frac{1}{2} \left(M_1 \tilde{B}\tilde{B} + M_2 \sum_{i=1}^3 \tilde{W}_i \tilde{W}_i + M_3 \sum_{i=1}^8 \tilde{g}_i \tilde{g}_i \right) , \quad (2.30)$$

with M_i , $i = 1, 2, 3$ as soft SUSY breaking masses for the gauginos and bilinear terms for the sfermions

$$\mathcal{L}_{\text{bilinear, sfermions}} = -\mathbf{m}_{\tilde{Q},ij}^2 \tilde{Q}_{L,i}^* \tilde{Q}_{L,j} - \mathbf{m}_{\tilde{U},ij}^2 \tilde{U}_{R,i}^* \tilde{U}_{R,j} - \mathbf{m}_{\tilde{D},ij}^2 \tilde{D}_{R,i}^* \tilde{D}_{R,j} \quad (2.31)$$

$$- \mathbf{m}_{\tilde{L},ij}^2 \tilde{L}_{L,i}^* \tilde{L}_{L,j} - \mathbf{m}_{\tilde{E},ij}^2 \tilde{E}_{R,i}^* \tilde{E}_{R,j} , \quad (2.32)$$

where $\mathbf{m}_{\tilde{Q}}^2$, $\mathbf{m}_{\tilde{U}}^2$, $\mathbf{m}_{\tilde{D}}^2$, $\mathbf{m}_{\tilde{L}}^2$ and $\mathbf{m}_{\tilde{E}}^2$ are soft SUSY breaking mass matrices in generation space and the tilde indicates that only the scalar component of the fields is taken. Additionally, there are bilinear terms for the Higgs fields

$$\mathcal{L}_{\text{bilinear, Higgs}} = -m_{H_1}^2 |H_1|^2 - m_{H_2}^2 |H_2|^2 - m_A^2 \sin \beta \cos \beta (H_1 \cdot H_2 + \text{h.c.}) , \quad (2.33)$$

where the soft SUSY breaking masses for the Higgs fields are denoted by $m_{H_1}^2$ and $m_{H_2}^2$. Furthermore, trilinear terms coupling the sfermions to the Higgs fields are added

$$\mathcal{L}_{\text{trilinear}} = -(T_E)_{ij} H_1 \cdot \tilde{L}_i \tilde{E}_j^* - (T_D)_{ij} H_1 \cdot \tilde{Q}_i \tilde{D}_j^* - (T_U)_{ij} H_2 \cdot \tilde{Q}_i \tilde{U}_j^* + \text{h.c.} , \quad (2.34)$$

where $T_{ij} = y_{ij} A_{ij}$ for each $i, j = 1, 2, 3$ separately with the Yukawa matrices y_{ij} and the trilinear coupling matrices A_{ij} . All soft SUSY breaking parameters are new, free parameters entering the theory. It is then convenient to reduce the parameter space by only keeping parameters of phenomenological importance. The basic assumptions of the model called phenomenological MSSM (pMSSM) [45] which is used in this thesis are

- general MSSM with real parameters and R -parity conservation,
- Minimal Flavor Violation, soft SUSY breaking masses and trilinear couplings are diagonal in flavor space,
- soft SUSY-breaking masses for the first and the second generation of sfermions coincide,
- trilinear couplings for the first and the second generation can be neglected.

The concept of Minimal Flavor Violation will be explained in Section 2.2.3. As only flavor diagonal entries are present in the mass matrices and trilinear couplings, the generation can explicitly be indicated. These assumptions lead to a reduction of the parameter space to 19 free parameters given by

$$\begin{aligned} m_{\tilde{L}_1} &= m_{\tilde{L}_2}, m_{\tilde{L}_3} , \\ m_{\tilde{E}_1} &= m_{\tilde{E}_2}, m_{\tilde{E}_3} \end{aligned} \quad (2.35)$$

for the sleptons,

$$\begin{aligned} m_{\tilde{Q}_1} &= m_{\tilde{Q}_2}, m_{\tilde{Q}_3} , \\ m_{\tilde{U}_1} &= m_{\tilde{U}_2}, m_{\tilde{U}_3} , \\ m_{\tilde{D}_1} &= m_{\tilde{D}_2}, m_{\tilde{D}_3} \end{aligned} \quad (2.36)$$

for the squarks,

$$M_1, M_2, M_3 \quad (2.37)$$

for the gauginos,

$$A_t, A_b, A_\tau \quad (2.38)$$

as trilinear couplings for particles of the third generation and

$$\mu, m_A, \tan \beta \quad (2.39)$$

from the Higgs sector.

2.2.3. Flavor Structure of the MSSM

Above, the mixing of the superpartners of the gauge bosons and Higgs fields was explained, but also the sfermions can mix. Here, the focus is on the up-type squarks, similar results hold for down-type squarks and sleptons as well.

As explained, having superpartners for left- and right-handed components of the quarks is only a matter of choice. The squarks are spin zero particles and therefore the gauge properties of \tilde{q}_L and \tilde{q}_R are identical and the mass eigenstates do not necessarily coincide with this basis. Here, the notation of Ref. [38] is adopted. To describe a general mixing of up-type squarks \tilde{q} a six component vector containing left- and right-handed squarks of all generations can be defined as

$$\tilde{q} = \begin{pmatrix} \tilde{q}_{1L} \\ \tilde{q}_{2L} \\ \tilde{q}_{3L} \\ \tilde{q}_{1R} \\ \tilde{q}_{2R} \\ \tilde{q}_{3R} \end{pmatrix}. \quad (2.40)$$

The mass term in the Lagrangian then reads [38]

$$\mathcal{L} = -\tilde{q}^\dagger \mathcal{M}_{\tilde{q}}^2 \tilde{q}, \quad (2.41)$$

with the mass matrix $\mathcal{M}_{\tilde{q}}^2$ consisting of four 3×3 blocks

$$\mathcal{M}_{\tilde{q}}^2 = \begin{pmatrix} \mathcal{M}_{\tilde{q}LL}^2 & \mathcal{M}_{\tilde{q}LR}^2 \\ \mathcal{M}_{\tilde{q}RL}^2 & \mathcal{M}_{\tilde{q}RR}^2 \end{pmatrix}. \quad (2.42)$$

The 3×3 blocks are given by

$$\mathcal{M}_{\tilde{q}LL}^2 = \mathbf{m}_{\tilde{Q}}^2 + M_Z^2 (I_3^q - Q_q \sin^2 \theta_W) \cos 2\beta \mathbf{1}_{3 \times 3} + \mathbf{m}_q \mathbf{m}_q^\dagger, \quad (2.43)$$

$$\mathcal{M}_{\tilde{q}LR}^2 = -\mathbf{m}_q (\mathbf{A}_q + \mu \cot \beta), \quad (2.44)$$

$$\mathcal{M}_{\tilde{q}RL}^2 = -(\mathbf{A}_q + \mu \cot \beta) \mathbf{m}_q^\dagger, \quad (2.45)$$

$$\mathcal{M}_{\tilde{q}RR}^2 = \mathbf{m}_{\tilde{U}}^2 + Q_q M_Z^2 \cos 2\beta \sin^2 \theta_W \mathbf{1}_{3 \times 3} + \mathbf{m}_q^\dagger \mathbf{m}_q. \quad (2.46)$$

Here, $\mathbf{m}_{\tilde{Q}, \tilde{U}}^2$ are the soft SUSY breaking mass matrices, I_3^q and Q_q are third component of the isospin and charge of the quark q , \mathbf{m}_q is the quark mass matrix, \mathbf{A}_q the trilinear coupling matrix for the quark-type q and M_Z, θ_W, μ and β as defined before. The matrix $\mathcal{M}_{\tilde{q}}^2$ is diagonalized by a 6×6 unitary matrix \tilde{W} , which rotates the squark states \tilde{q} to their mass eigenstates \tilde{q}^m

$$\tilde{q}^m = \tilde{W} \tilde{q}. \quad (2.47)$$

This matrix accounts for both L, R -mixing which is induced by $\mathcal{M}_{\tilde{q}LR}^2$ and $\mathcal{M}_{\tilde{q}RL}^2$ and flavor mixing generated by flavor off-diagonal elements.

Now suppose an interaction of a squark, with a quark and a neutralino. In this interaction isospin is conserved so the quark must have the same isospin as the squark. Recall the end of Section 2.1.1 where it was explained, that FCNCs are not possible at tree-level in the SM. Rotations of quarks and squarks are in principle independent of each other. Thus, the product of the quark and squark rotation matrices is in general not diagonal in generation

space and as a consequence, FCNCs are possible at tree-level. However, the magnitude of FCNCs is strongly constrained by precision experiments in flavor physics.

To fulfill these constraints, two possibilities will be explained here. The first one is to just set the off-diagonal elements in generation space to zero. Additionally, the mixing of left- and right-handed components is only considered for the third generation of sfermions. This is motivated by the L, R -mixing elements $\mathcal{M}_{\tilde{q}_{LR}}^2$ and $\mathcal{M}_{\tilde{q}_{RL}}^2$ being proportional to the mass of the corresponding SM fermion. Hence, the mixing in the first and the second generation is negligible in comparison to the third generation. Another idea to constrain the flavor changing elements in the rotation matrix \widetilde{W} is to demand, that the rotation in generation space for the squarks shall be the same as for the quarks. The rotation matrix can be factorized by $\widetilde{W}_{L,R} = W_{L,R} U^{qL,R}$, where $U^{qL,R}$ is the quark rotation matrix and the remaining rotation W only contains the L, R -mixing. Then the case of the SM is recovered and FCNCs are forbidden at tree-level. However, due to differences in the RGEs of quarks and squarks this property cannot be maintained at all energy scales. Thus, a scale has to be chosen where this condition is fulfilled, at other scales the rotation matrix W will still contain generation off-diagonal elements generated by RGE running. Nevertheless, these elements are sufficiently small to be compatible with the experimental limits. Details and further assumptions of this concept called Minimal Flavor Violation (MFV) can be found in References [46–50]. The situation for quarks and squarks at the MFV scale can be summarized as

$$q_L^{\text{int}} \xrightarrow{U^{uL}} q_L^{\text{flav}} = q_L^{\text{mass}} , \quad (2.48)$$

$$\tilde{q}_L^{\text{int}} \xrightarrow{U^{uL}} \tilde{q}_L^{\text{flav}} \xrightarrow{W_L} \tilde{q}_L^{\text{mass}} , \quad (2.49)$$

where q_L^{int} and \tilde{q}_L^{int} denote interaction eigenstates. In the basis $\tilde{q}_L^{\text{flav}}$, also called Super-CKM-basis, the squarks are flavor-diagonal. A framework for the general flavor structure is given by the SUSY Les Houches Accord 2 [51] which will be used for the implementation in Chapter 4.

In this work the general flavor structure mixing all up- and down-type squarks and sleptons is used and the flavor off-diagonal elements in the rotation matrices induced by the CKM matrix are generated by RGE running.

2.2.4. Light Up-Type Squarks

Let us first assume that the squark mass matrix only contains flavor diagonal elements. As already stated, the off-diagonal elements in the squark mass matrix (Eqs. (2.44) and (2.45)) mixing left- and right-handed states are proportional to the mass of the corresponding SM particle. Since the top quark is the heaviest particle of the SM, the mass splitting of the two corresponding stop mass eigenstates can be large, leading to a light stop. Together with a slightly lighter neutralino, it is possible to reproduce the correct relic density, *cf.* Sec. 4.3.2. Light stops are consistent with the measurements of $b \rightarrow s\gamma$ (Sec. 4.3.3) and the measurements of the Higgs mass and lower limits for the masses of SUSY particles (Sec. 4.3.1 and Sec. 4.3.4). Moreover, the stops can be light enough to be produced at the LHC. Therefore it is necessary to calculate possible decays of the stops to analyze relevant search channels.

In this context, an important quantity is the mass difference between the stop and the lightest neutralino which are taken to be NLSP and LSP, respectively, since it determines which decay channels are kinematically forbidden or allowed. In this work the parameter region where the mass difference of the light superpartner of the top quark \tilde{t}_1 and the lightest neutralino $\tilde{\chi}_1^0$

$$\Delta m = m_{\tilde{t}_1} - m_{\tilde{\chi}_1^0} \quad (2.50)$$

is smaller than the W mass is considered. In this region the flavor diagonal decay into top quark and neutralino is forbidden as well as the three-body decay into a bottom quark, a W boson and a neutralino. Then, a possible decay mode is the FCNC two-body decay

$$\tilde{t}_1 \rightarrow c\tilde{\chi}_1^0, \quad (2.51)$$

where the charm-quark could also be replaced by an up-quark. Without FCNCs at tree-level, this decay is loop induced by electroweak interactions [52, 53]. In this work, however, according to the previous section a general flavor structure is used enabling this process at tree-level. Due to the strong coupling constant being the largest one, loop corrections with respect to α_s can be important.

In the general case the squark mass eigenstates are no flavor eigenstates any more. Hence, the NLSP is not a light stop, but simply the lightest up-type squark, denoted by \tilde{u}_1 . Nevertheless, as flavor off-diagonal elements in the mixing matrices are small, the \tilde{u}_1 will be stop-like. From now on, the formal notation \tilde{u}_s , $s = 1..6$ is chosen for the up-type squark mass eigenstates.

Of course also the experiments are searching for SUSY particles and in particular for light squarks. No squark has been observed so far which is why only upper limits on the cross sections or lower limits on the masses of the particles can be derived. Currently, the strongest limits on the mass of the light stop in our parameter region are reported by ATLAS. In Figure

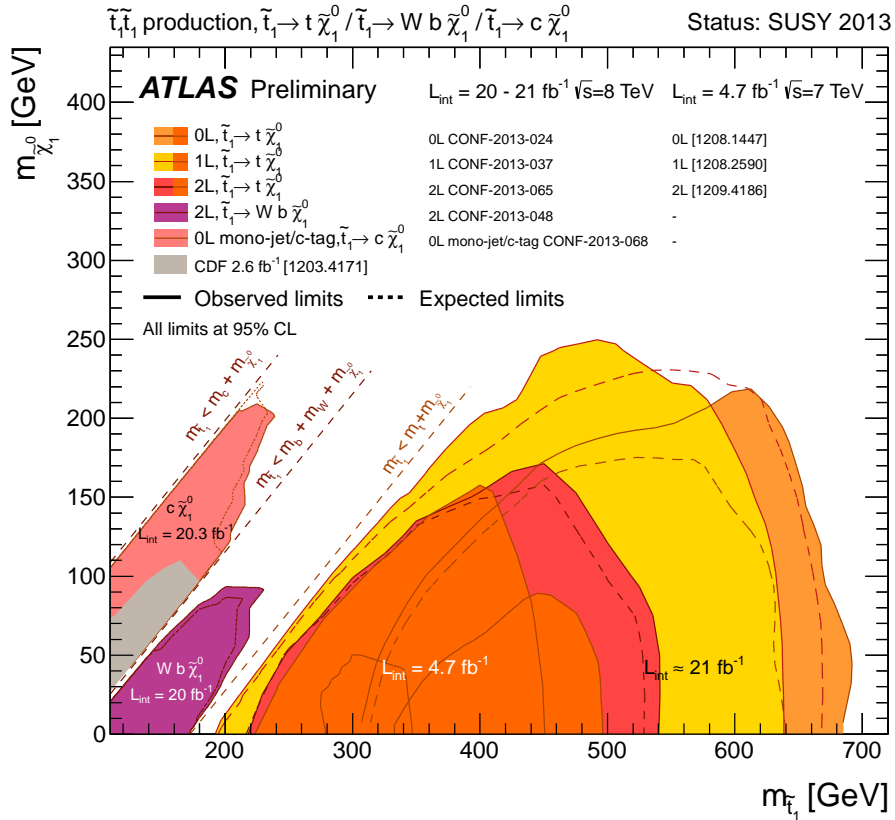


Figure 2.1: Limits in the $(m_{\tilde{t}_1}, m_{\tilde{\chi}_1^0})$ -plane measured by ATLAS.

2.1 a summary plot of the searches for stops by ATLAS and CDF, published in [54–58], is shown, combining the search in different mass regions and decay channels. As explained above, the mass difference Δm of Eq. (2.50) is important for the phenomenology of the decay.

The dashed lines in the summary plot correspond to three values of the mass difference: the right one indicates $\Delta m = m_t$, the dashed line in the middle corresponds to $\Delta m = m_W + m_b$ and the left one corresponds to $\Delta m = m_c$. Obviously, the mass limits for the stop drastically drop once the mass difference is lower than the top quark mass m_t . As in this work the region of $\Delta m < m_W$ is studied the relevant region in the plot is located between the left and the mid-line. Thus, stop masses down to $m_{\tilde{t}_1} \approx 200$ GeV, depending on the neutralino mass, are not excluded, yet. The limits reported on the stops are taken over as limits for the \tilde{u}_1 and explicit cuts employed in this thesis are given in Section 4.3. In the experimental analysis for the parameter region of $\Delta m \in [m_c, m_W + m_b]$ the branching ratio of the stop decaying into a charm quark and a neutralino is assumed to be one. However, another possible process competing with the two-body decay is the four-body decay of the \tilde{u}_1 into a neutralino and three SM fermions. The fermions can be both up-type and down-type quarks and leptons excluding the top-quark. This process has already been calculated without flavor changing elements in the squark mixing matrix [59], but to account for the flavor structure used here, the four-body decay has been recalculated by other members of our research group [60]. Furthermore, in this calculation the masses of the b -quark and the τ have been taken into account in the final states. Combining the calculations of both the two- and the four-body decay the branching ratios shall be calculated and compared to the assumed value of 1 in the experimental analysis.

The CMS collaboration also published exclusion limits for the \tilde{t}_1 pair-production [61, 62], but so far no limits are available for $\Delta m < m_W$. The current limits of CMS can be found in Appendix A.

With this motivation in mind, in this thesis the decay width of the lightest up-type squark \tilde{u}_1 decaying into a charm- or an up-quark and a neutralino will be calculated at next-to-leading order with respect to the strong interaction. The parameter space of the pMSSM will be scanned and confronted with existing experimental bounds and results for the parameter points passing the constraints will be presented.

CHAPTER 3

CALCULATION OF THE DECAY WIDTH

For unstable particles the probability to decay is the same at all times. Thus, assuming a probe of $N(t)$ identical, unstable particles, the decay is governed by the differential equation

$$\frac{dN(t)}{dt} = -\Gamma N(t) , \quad (3.1)$$

where t represents time and Γ is the probability per time of each particle to decay. The solution of this differential equation is directly obtained for example by separation of variables and reads

$$N(t) = N_0 e^{-\Gamma t} , \quad (3.2)$$

with N_0 as the number of particles at the time $t = 0$. In case of n possible decays with probabilities Γ_i into final states f_i Eq. (3.1) turns into

$$\frac{dN(t)}{dt} = \sum_{i=1}^n (-\Gamma_i N(t)) = - \left(\sum_{i=1}^n \Gamma_i \right) N(t) , \quad (3.3)$$

and the solution changes to

$$N(t) = N_0 e^{-(\sum_{i=1}^n \Gamma_i)t} . \quad (3.4)$$

Hence, it is possible to define a total probability per time to decay into any of the final states f_i as

$$\Gamma_{\text{tot}} = \sum_{i=1}^n \Gamma_i . \quad (3.5)$$

The resonance curve of unstable states with respect to the energy is given by a Breit-Wigner distribution. The quantity Γ_{tot} is the full width at half maximum of the Breit-Wigner distribution corresponding to the decay of the unstable particle. Therefore in particle physics Γ_{tot} is called total decay width and the Γ_i for each final state f_i are called partial decay widths. If the probe of particles is large enough to be statistically valid, the fraction with which each final state f_i contributes to the total result is given by

$$\text{BR}_i = \frac{\Gamma_i}{\Gamma_{\text{tot}}} . \quad (3.6)$$

These fractions BR_i are called branching ratios (BR) and are of great importance in particle physics as the signal rates in different search channels are proportional to them. Thereby the branching ratios are essential to give precise predictions for signal rates and to confront these with experimental data.

In the context of time-dependent perturbation theory the partial decay width of an initial particle i into a generic final state f is found to be

$$\Gamma(i \rightarrow f) = \frac{1}{2m_i} \int \overline{|\mathcal{M}_{if}|^2} d\text{LIPS} , \quad (3.7)$$

where m_i is the mass of the initial particle i , $\overline{|\mathcal{M}_{if}|^2}$ is the squared, spin-averaged transition amplitude for the particle i decaying into the final state f and the integral is over the Lorentz invariant phase space, denoted by $d\text{LIPS}$.

3.1. The Decay Width at Next-to-Leading Order

In order to improve theoretical predictions for the branching ratios, the decay widths they are composed of are calculated in higher orders of perturbation theory. This work concentrates on the next-to-leading order (NLO) with respect to the strong interaction. This means that only one-loop corrections proportional to the strong coupling constant α_s are taken into account. In the relevant diagrams ultraviolet (UV) and infrared (IR) divergences can occur. However, the physical parameters measured by experiments are finite. The running coupling constant α_s is decreasing with increasing energy and the mass of the squark which is considered in this work is sufficiently high to allow for a perturbative treatment of the strong interaction. Therefore perturbation theory is applicable and the divergences must disappear.

How the divergences are canceled is a matter of choice. In this work the UV divergences will be canceled by introduction of counterterms (see Section 3.2), which is possible since the MSSM is a renormalizable theory. The IR divergences cancel among the virtual and real NLO contributions (Section 3.3), as guaranteed by the Kinoshita-Lee-Nauenberg theorem [63, 64]. The first step in order to render the physical parameters finite is to regularize the integrand of the phase space integral, namely the transition amplitude, and the integral itself.

3.1.1. Dimensional Regularization

The task of the regularization is to make the evaluation of the integral (3.7) possible and thereby to isolate the divergences. In this work, we will apply dimensional regularization [65, 66]. Basically the dimension d of the space time is changed from $d = 4$ to

$$d = 4 - 2\epsilon , \quad (3.8)$$

with $\epsilon > 0$, so that in the limit $\epsilon \rightarrow 0$ we recover the four-dimensional space time and the divergences in the transition amplitudes will appear as poles in ϵ . Consequently, four-dimensional integrals over momenta appearing in the phase space or in loops turn into d -dimensional integrals as may be

$$\int \frac{d^4 p}{(2\pi)^4} \rightarrow \mu^{4-d} \int \frac{d^d p}{(2\pi)^d} . \quad (3.9)$$

The new parameter μ is an arbitrary parameter with the dimension of mass to keep the mass dimension of the integral at the same value as in the case of $d = 4$. The metric tensor $g^{\mu\nu}$ becomes d -dimensional, leading to

$$g^\mu{}_\mu = d . \quad (3.10)$$

The Dirac gamma-matrices still satisfy

$$\{\gamma^\mu, \gamma^\nu\} = 2g^{\mu\nu} , \quad (3.11)$$

but all consequences resulting from the modified metric (3.10) have to be taken into account, e.g.

$$\gamma^\mu \gamma_\mu = d\mathbf{1}_d , \quad (3.12)$$

where $\mathbf{1}_d$ is the $d \times d$ unit matrix. The generalization of $\gamma_5 := i\gamma^0\gamma^1\gamma^2\gamma^3$ ($d = 4$) to $d \neq 4$ dimensions is non-trivial. Useful relations in d dimensions also involving γ_5 can be found in Appendix B or, for example, in [67].

3.1.2. Phase Spaces

In this work a decay into two particles is considered at NLO. Hence, for the tree-level part and the virtual corrections a two-particle phase space is needed, whereas for the real corrections with an additional gluon in the final state a three-particle phase space is required. They are now derived in d dimensions to make dimensional regularization applicable.

3.1.2.1. Two-Particle Phase Space

The general two-particle phase space in d dimensions denoted by $d\Phi_2$ is

$$d\Phi_2 = \frac{d^{d-1}p_1}{(2\pi)^{d-1}2p_1^0} \frac{d^{d-1}p_2}{(2\pi)^{d-1}2p_2^0} (2\pi)^d \delta^{(d)}(p - p_1 - p_2) , \quad (3.13)$$

where p is the four-momentum of the decaying particle and p_1 and p_2 are the four-momenta of the final state particles, respectively. Keeping in mind that the integral is over the whole momentum space for both p_1 and p_2 , the first step to simplify the expression is to use the δ -function to eliminate one integration. As a matter of choice the evaluation of the p_2 integration leads to

$$d\Phi_2 = \frac{d^{d-1}p_1}{(2\pi)^{d-2}} \frac{1}{4p_1^0 p_2^0} \delta(p^0 - p_1^0 - p_2^0) \Big|_{\vec{p}_2 = \vec{p} - \vec{p}_1} . \quad (3.14)$$

Introducing spherical coordinates in d dimensions results in

$$d\Phi_2 = \frac{d\Omega_{d-1} |\vec{p}_1|^{d-2} d|\vec{p}_1|}{(2\pi)^{d-2} 4p_1^0 p_2^0} \delta(p^0 - p_1^0 - p_2^0) \Big|_{\vec{p}_2 = \vec{p} - \vec{p}_1} , \quad (3.15)$$

where $d\Omega_{d-1}$ is the solid angle element in $d - 1$ dimensions. In order to evaluate the $|\vec{p}_1|$ integration with the remaining δ -function it is convenient to choose the rest frame of the decaying particle with four-momentum p . Hence,

$$p^0 = m_{\bar{q}} , \quad \vec{p} = 0 , \quad \vec{p}_1 = -\vec{p}_2 , \quad |\vec{p}_1| = |\vec{p}_2| =: x , \quad (3.16)$$

with $m_{\bar{q}}$ being the mass of the decaying particle. As the argument of the δ -function is a function of the integration variable the relation

$$\delta(f(x)) = \frac{1}{|f'(x_0)|} \delta(x - x_0) \quad (3.17)$$

has to be used with x_0 denoting the root of $f(x)$. According to Eq. (3.15) the argument of the δ -function in terms of x is

$$f(x) = m_{\bar{q}} - \sqrt{x^2 + m_1^2} - \sqrt{x^2 + m_2^2} . \quad (3.18)$$

Therefore

$$f'(x) = -\frac{xm_{\bar{q}}}{p_1^0 p_2^0} \quad \text{and} \quad x_0 = \frac{1}{2m_{\bar{q}}} \sqrt{(m_{\bar{q}}^2 - m_1^2 + m_2^2)^2 - 4m_{\bar{q}}^2 m_2^2}, \quad (3.19)$$

where m_1 and m_2 are the masses of the final state particles. The second solution for the root of $f(x)$ is given by $-x_0$ which is not compatible with the definition of x in Eq. (3.16) and is therefore discarded. Combining everything the phase space then reads

$$d\Phi_2 = \frac{d\Omega_{d-1}}{(2\pi)^{d-2}} \frac{x^{d-3} dx}{4m_{\bar{q}}} \delta(x - x_0) \quad (3.20a)$$

$$= \frac{d\Omega_{d-1}}{(2\pi)^{d-2}} \frac{1}{4m_{\bar{q}}} \left(\frac{1}{2m_{\bar{q}}} \sqrt{(m_{\bar{q}}^2 - m_1^2 + m_2^2)^2 - 4m_{\bar{q}}^2 m_2^2} \right)^{d-3}. \quad (3.20b)$$

For the special case of $m_1 = 0$ the expression reduces to

$$d\Phi_2 = \frac{d\Omega_{d-1}}{(2\pi)^{d-2}} \frac{1}{4m_{\bar{q}}} \left(\frac{m_{\bar{q}}}{2} (1 - r^2) \right)^{d-3}, \quad (3.21)$$

with $r^2 = m_2^2/m_{\bar{q}}^2$. The solid angle integrations can be performed by

$$\int d\Omega_d = \frac{2\pi^{\frac{d}{2}}}{\Gamma(\frac{d}{2})}, \quad \text{with} \quad \Gamma(z) = \int_0^\infty e^{-t} t^{z-1} dt. \quad (3.22)$$

In $d = 4$ dimensions and with $\int d\Omega_3 = 4\pi$ it is

$$d\Phi_2 = \frac{1}{8\pi} (1 - r^2). \quad (3.23)$$

3.1.2.2. Three-Particle Phase Space

The strategy for calculating the three-particle phase space is essentially the same as for the two-particle phase space. However, as there are three particles in the final state instead of two, more integrations have to be considered. The three-particle phase space $d\Phi_3$ is

$$d\Phi_3 = \frac{d^{d-1}p_1}{(2\pi)^{d-1} 2p_1^0} \frac{d^{d-1}p_2}{(2\pi)^{d-1} 2p_2^0} \frac{d^{d-1}p_3}{(2\pi)^{d-1} 2p_3^0} (2\pi)^d \delta^{(d)}(p - p_1 - p_2 - p_3), \quad (3.24)$$

where p is the four-momentum of the decaying particle and p_i , $i = 1 \dots 3$ are the four-momenta of the decay products, respectively. To clarify that the third particle with momentum p_3 will be a gluon it is convenient to set $p_3 = k$. Using the δ -function for the p_2 integration yields

$$d\Phi_3 = \frac{1}{8} \frac{d^{d-1}p_1}{(2\pi)^{d-1}} \frac{d^{d-1}k}{(2\pi)^{d-2}} \frac{1}{p_1^0 p_2^0 k^0} \delta(p^0 - p_1^0 - p_2^0 - k^0) \Big|_{\vec{p}_2 = \vec{p} - \vec{p}_1 - \vec{k}}. \quad (3.25)$$

Note, that p_2 is fixed completely thereby since $p_2^0 = \sqrt{(\vec{p} - \vec{p}_1 - \vec{k})^2 + m_2^2}$. In the rest frame of the decaying particle two directions are left, namely \vec{p}_1 and \vec{k} . Choosing \vec{p}_1 as reference axis, the solid angle integration for p_1 can be kept as a whole whereas the integration for k will be split up in an angle θ between \vec{p}_1 and \vec{k} and the remaining solid angle, leading to

$$d^{d-1}p_1 = d\Omega_{d-1} |\vec{p}_1|^{d-2} d|\vec{p}_1|, \quad (3.26)$$

$$d^{d-1}k = d\Omega_{d-2} |\vec{k}|^{d-2} d|\vec{k}| \sin^{d-3} \theta d\theta. \quad (3.27)$$

By changing the integration variable in Eq. (3.27) from θ to $\cos \theta$, $d\cos \theta = \sin \theta d\theta$ the three-particle phase space turns into

$$\begin{aligned} d\Phi_3 = & \frac{1}{8} \frac{d\Omega_{d-1}}{(2\pi)^{d-1}} |\vec{p}_1|^{d-2} d|\vec{p}_1| \frac{d\Omega_{d-2}}{(2\pi)^{d-2}} |\vec{k}|^{d-2} d|\vec{k}| \sin^{d-4} \theta d\cos \theta \\ & \cdot \frac{1}{p_1^0 p_2^0 k^0} \delta(p^0 - p_1^0 - p_2^0 - k^0) \Big|_{\vec{p}_2 = \vec{p} - \vec{p}_1 - \vec{k}} . \end{aligned} \quad (3.28)$$

Now the last δ -function can be used to determine the integration over $\cos \theta$. In the rest frame of the decaying particle and by setting the gluon on-shell the δ -function in Eq. (3.28) is

$$\delta \left(\sqrt{|\vec{p}_1|^2 + m_1^2} + \sqrt{|\vec{p}_1|^2 + |\vec{k}|^2 + m_2^2} + 2|\vec{p}_1||\vec{k}| \cos \theta + k^0 - m_{\bar{q}} \right) , \quad (3.29)$$

where m_1 and m_2 are the masses of the two massive decay products and $m_{\bar{q}}$ is the mass of the decaying particle. Applying relation (3.17) with f being the argument of the delta function (3.29) and x being $\cos \theta$, one has

$$\delta(f(x)) = \frac{p_2^0}{|\vec{p}_1||\vec{k}|} \delta(\cos \theta - \cos \theta_0) ; \quad f(\cos \theta_0) = 0 . \quad (3.30)$$

The last step is to insert this result into Eq. (3.28) and to apply the replacements

$$d|\vec{p}_1| = \frac{p_1^0}{|\vec{p}_1|} dp_1^0 , \quad d|\vec{k}| = \frac{k^0}{|\vec{k}|} dk^0 \quad (3.31)$$

and

$$|\vec{p}_1| = \left(p_1^{0^2} - m_1^2 \right)^{\frac{1}{2}} , \quad (3.32)$$

$$|\vec{k}| = k^0 , \quad \text{since the gluon is on-shell} , \quad (3.33)$$

$$\sin^{d-4} \theta = \left(1 - \cos^2 \theta \right)^{\frac{d-4}{2}} . \quad (3.34)$$

Finally, the result is

$$\begin{aligned} d\Phi_3 = & \frac{1}{8} \frac{d\Omega_{d-1}}{(2\pi)^{d-1}} \frac{d\Omega_{d-2}}{(2\pi)^{d-2}} dp_1^0 dk^0 d\cos \theta \\ & \cdot \left[\left(p_1^{0^2} - m_1^2 \right) k^{0^2} (1 - \cos^2 \theta) \right]^{\frac{d-4}{2}} \delta(\cos \theta - \cos \theta_0) , \end{aligned} \quad (3.35)$$

with the condition

$$f(\cos \theta_0) = 0 . \quad (3.36)$$

In the case of $m_1 = 0$ it is

$$d\Phi_3 = \frac{1}{8} \frac{d\Omega_{d-1}}{(2\pi)^{d-1}} \frac{d\Omega_{d-2}}{(2\pi)^{d-2}} dp_1^0 dk^0 d\cos \theta \left[p_1^{0^2} k^{0^2} (1 - \cos^2 \theta) \right]^{\frac{d-4}{2}} \delta(\cos \theta - \cos \theta_0) . \quad (3.37)$$

3.1.3. Factorization of the $d\Phi_{2+1}$ Phase Space

The decay width at NLO can be written as

$$\Gamma_{\text{tot}} = \Gamma_{\text{tree}} + \Gamma_{\text{NLO}} \quad (3.38a)$$

$$= \int I_{\text{tree}} d\Phi_2 + \int I_{\text{virt}} d\Phi_2 + \int I_{\text{real}} d\Phi_{2+1} , \quad (3.38b)$$

where the I_{tree} , I_{virt} and I_{real} denote the integrands of the phase space integrals of the tree-level, the virtual and the real partial decay widths. After eliminating the UV divergences through renormalization, each of the latter two integrals is divergent due to the IR divergences. However, in the sum of the two these divergences cancel due to the KLN theorem, and the limit $\epsilon \rightarrow 0$ can then safely be taken.

In equation (3.38b) the partial width resulting from the NLO corrections is split into two separate integrals since the phase spaces are different for the virtual and real contributions. However, the notation of the three-particle phase space as $d\Phi_{2+1}$ already suggests that a two-particle phase space is contained therein. That this is indeed the case will be shown now for the general case of an $n + m$ phase space $d\Phi_{n+m}$.

The universal $n + m$ -particle phase space in d dimensions is given by

$$d\Phi_{n+m} = \left(\prod_{i=1}^{n+m} \frac{d^d p_i}{(2\pi)^d} \right) (2\pi)^d \delta^{(d)} \left(p - \sum_{i=1}^{n+m} p_i \right), \quad (3.39)$$

denoting the four-momentum of the decaying particle by p and the four-momenta of the decay products by p_i , $i = 1 \dots n + m$. We define a new four-momentum q by

$$q := \sum_{i=n}^{n+m} p_i \quad (3.40)$$

in order to insert a factor of 1 in Eq. (3.39) in three steps: replace the corresponding momenta by q , multiply by a delta function covering the definition (3.40) and finally integrate over q . Thus, the phase space reads

$$d\Phi_{n+m} = (2\pi)^d \delta^{(d)} \left(p - \sum_{i=1}^{n-1} p_i - q \right) (2\pi)^d \delta^{(d)} \left(q - \sum_{j=n}^{n+m} p_j \right) \frac{d^d q}{(2\pi)^d} \prod_{i=1}^{n+m} \frac{d^d p_i}{(2\pi)^d}. \quad (3.41)$$

Due to the independent integration bounds the order of integration can be exchanged arbitrarily. One explicit reformulation is

$$d\Phi_{n+m} = \underbrace{(2\pi)^d \delta^{(d)} \left(q - \sum_{j=n}^{n+m} p_j \right) \prod_{j=n}^{n+m} \frac{d^d p_j}{(2\pi)^d}}_{=: d\Phi_{\text{add}}} \cdot \underbrace{(2\pi)^d \delta^{(d)} \left(p - \sum_{i=1}^{n-1} p_i - q \right) \frac{d^d q}{(2\pi)^d} \prod_{i=1}^{n-1} \frac{d^d p_i}{(2\pi)^d}}_{=: d\Phi_n}, \quad (3.42)$$

which allows us to separate an n particle phase space $d\Phi_n$ with a hypothetical n th particle with four-momentum q and keep the remaining additional integrations denoted by $d\Phi_{\text{add}}$. This result is also known as phase space recursion formula. Now Eq. (3.38b) turns into

$$\Gamma = \int \left(I_{\text{tree}} + I_{\text{virt}} + \int I_{\text{real}} d\Phi_{\text{add}} \right) d\Phi_2, \quad (3.43)$$

revealing that the divergences must now cancel in the integrand in parenthesis. As the integrand is then regular the overall two-particle phase space integration can be performed in $d = 4$ dimensions. In this work initial state radiation (ISR) and final state radiation (FSR) of one gluon will be calculated, so the consequence of Eq. (3.42) for $n = 2$ and $m = 1$ is that the additional phase space $d\Phi_{\text{add}}$ contains six integrations, four of them covered by the delta function. Thus, in dimensional regularization, the two remaining integrations must reveal the divergences as poles in ϵ .

This fact is explicitly used in Section 3.3.2 in the calculation of ISR and FSR.

As a small annex one might think that the limit $\epsilon \rightarrow 0$ in the overall two-particle phase space integration can only be taken at the very end. Indeed for $d = 4 - 2\epsilon$ in the limit $\epsilon \rightarrow 0$ the phase space (3.21) results in an expansion series in ϵ . Taking the limit at the very end, all terms of $\mathcal{O}(\epsilon)$ drop out since the integrand is just a finite number. Factorizing the two-particle phase space and directly taking the limit $\epsilon \rightarrow 0$ draws a different picture: once the terms of $\mathcal{O}(\epsilon)$ or $\mathcal{O}(\epsilon^2)$ are multiplied with terms of opposite order in ϵ which are present in the integrand in dimensional regularization, finite terms are left over. However, the poles in ϵ in the virtual and real corrections cancel and so must the additional terms as well.

Therefore it is arbitrary when the limit $\epsilon \rightarrow 0$ is taken for the outer two-particle phase space and it is possible to directly use Eq. (3.23).

3.2. Renormalization

In this section the tree-level process and the vertex corrections to the decays $\tilde{u}_1 \rightarrow (c, u)\tilde{\chi}_1^0$ will be presented. As already mentioned in Section 3.1 the vertex corrections contain UV and IR divergences. The UV divergences will be canceled by renormalization as described in Section 3.2.2 which requires the calculation of self-energies of the outer legs in addition to the vertex corrections. The calculation of the self-energies will be presented in Section 3.2.3. The removal of the IR divergences by the real corrections is subject to Section 3.3.

3.2.1. Lagrangian and Vertex Corrections

The interaction of an up-type squark \tilde{u}_s with an up-type quark u_i and a neutralino $\tilde{\chi}_l^0$ is in general governed by two terms of the Lagrangian [38]

$$\mathcal{L}_{\tilde{u}\tilde{u}\tilde{\chi}^0} = \bar{u}_i G_{isl}^R \tilde{u}_s \mathcal{P}_R \tilde{\chi}_l^0 + \bar{u}_i G_{isl}^L \tilde{u}_s \mathcal{P}_L \tilde{\chi}_l^0 + \text{h.c.} . \quad (3.44)$$

The index $i = 1, 2, 3$ denotes the generation of the quark, $s = 1, \dots, 6$ numbers the mass eigenstates of the squarks and $l = 1, \dots, 4$ the mass eigenstates of the neutralinos and \mathcal{P}_R and \mathcal{P}_L are the left- and right-chiral projectors

$$\mathcal{P}_L = \frac{\mathbf{1} - \gamma_5}{2} , \quad \mathcal{P}_R = \frac{\mathbf{1} + \gamma_5}{2} . \quad (3.45)$$

Obviously, the generic structures of the left- and right-handed parts match, so in the following only the left-handed part is considered, the right-handed part is obtained analogously and the h.c., which stands for hermitian conjugated, will be omitted.

Replacing the coupling G_{isl}^L explicitly, the left-handed part of the Lagrangian in the interaction basis is given by

$$\mathcal{L}_{\tilde{u}\tilde{u}\tilde{\chi}^0, L} = -\bar{u}_i^{(0)} g e_{Rl}^{u_i} \tilde{u}_{iR}^{(0)} \mathcal{P}_L \tilde{\chi}_l^0 - \bar{u}_i^{(0)} \frac{g Z_{l4} m_{ij}^{\dagger(0)}}{\sqrt{2} m_W s_\beta} \tilde{u}_{jL}^{(0)} \mathcal{P}_L \tilde{\chi}_l^0 , \quad (3.46)$$

where the upper index '(0)' stands for unrenormalized fields and $m_{ij}^{\dagger(0)}$ is the hermitian conjugate of the unrenormalized quark mass matrix. In the interaction basis, only the three squark states corresponding to the correct chirality with respect to the interaction with the quark are used. Thus, the index s is not present in the above equation, but it is replaced by the indices $i, j = 1, 2, 3$ with an additional subscript L, R to indicate which of the six squark states are denoted by i and j . For better legibility it is convenient to define

$$Q_{1il}^L := -g e_{Rl}^{u_i} = g\sqrt{2} Q_{u_i} t_W Z_{l1} \quad \text{and} \quad Q_{2l}^L := -\frac{g Z_{l4}}{\sqrt{2} m_W s_\beta} , \quad (3.47)$$

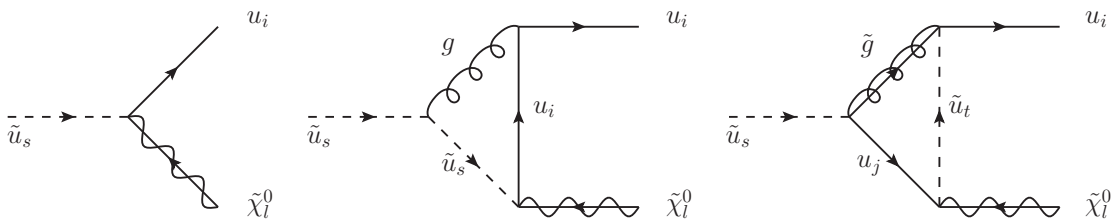


Figure 3.1: Tree-level diagram and vertex corrections in QCD/SQCD.

and for the right-handed term in the Lagrangian (not given here explicitly)

$$Q_{1il}^R := -ge_{Ll}^{u_i} = -g\sqrt{2}[Z_{l1}t_W(Q_{u_i} - I_{u_i}^3) + Z_{l2}I_{u_i}^3] \quad \text{and} \quad Q_{2l}^R := -\frac{gZ_{l4}}{\sqrt{2}m_W s_\beta}. \quad (3.48)$$

Here, g is the weak coupling constant, Z is the neutralino mixing matrix, m_W is the W boson mass, $s_\beta = \sin \beta$, $t_W = \tan \theta_W$ with θ_W being the Weinberg angle and Q_{u_i} and $I_{u_i}^3$ are the electric charge and the third component of the isospin of the quark, respectively. Then the Lagrangian (3.46) becomes

$$\mathcal{L}_{\bar{u}\tilde{u}\tilde{\chi}^0,L} = \underbrace{Q_{1il}^L \bar{u}_i^{(0)} \tilde{u}_{iR}^{(0)} \mathcal{P}_L \tilde{\chi}_l^0}_{\mathcal{L}_1} + \underbrace{Q_{2il}^L \bar{u}_i^{(0)} m_{ij}^{\dagger(0)} \tilde{u}_{jL}^{(0)} \mathcal{P}_L \tilde{\chi}_l^0}_{\mathcal{L}_2}. \quad (3.49)$$

In the following, the first term in Eq. (3.49) will be called \mathcal{L}_1 and the second term will be denoted by \mathcal{L}_2 . Note, that the couplings in Eqs. (3.47) and (3.48) are proportional to the weak coupling constant g , indicating that the tree-level process is mediated by the electroweak interaction. The QCD and SUSY-QCD one-loop corrections to the tree-level FCNC decay are expected to be important due to the large strong coupling constant and shall be calculated in the following. They are composed of the virtual and real corrections. In this section, the virtual corrections will be described. The Feynman diagrams for the tree-level process and the vertex corrections are depicted in Figure 3.1. The QCD and SQCD loops are mediated by a gluon and a gluino, respectively. The generation and mass eigenstate indices of the particles are chosen such that it can be read off at which vertices flavor changing is possible. In the QCD diagram, for example, the only flavor changing vertex is the squark-quark-neutralino vertex which is already present at tree-level. As mentioned before, the Lagrangian (3.49) has to be renormalized by introduction of appropriate counterterms. Due to the fact that only corrections proportional to the strong coupling constant are considered, all divergences must be proportional to the strong coupling constant as well. This allows to reduce the number of parameters in the Lagrangian which have to be renormalized. In detail, the couplings in Eqs. (3.47) and (3.48) do not have to be renormalized as they are weak couplings. The neutralino field $\tilde{\chi}_l^0$ does not need to be renormalized either, since the one-loop neutralino self-energies do not contain non-vanishing diagrams proportional to α_s (*cf.* Section 3.2.3). Also the neutralino mixing matrix Z needs not to be renormalized. This is already implied in the Lagrangian (3.49) where the upper index '(0)' is only present at the quark fields, the squark fields and the quark mass matrix.

To account for physical observables we rotate the fields from interaction eigenstates to mass eigenstates before introducing the renormalization constants. This is done by rotation with unitary matrices for the quark and the squark fields. In the case of quarks the mass eigenstates are also flavor eigenstates. This does not hold for the squarks due to the mixing of left- and

right-handed components within one flavor. At first, here the Super-CKM basis is chosen for the squark fields. Recapitulating Section 2.2.3, in this basis the left- and right-handed components of the squark field are rotated by the same unitary matrices $U^{uL,R}$ which rotate the quark fields from interaction to mass and thereby to flavor eigenstates. The benefit of this basis becomes apparent in models with MFV: at the scale μ_{MFV} both quarks and squarks are flavor diagonal after rotation with the quark mixing matrices $U^{uL,R}$. This means that at μ_{MFV} also the squark mass matrix is flavor diagonal. While the quarks are then already in their mass eigenstates, the squarks still have to be rotated with another matrix W to their mass eigenstates to account for the possible left-right mixing. If general flavor mixing is considered instead of MFV, the squark mass matrix can be flavor mixed in the Super-CKM basis.

The rotation of the fields can be incorporated in Eq. (3.49) by inserting unit matrices in terms of UU^\dagger and WW^\dagger leaving the Lagrangian invariant. From Eqs. (2.40) and (2.47) it follows, that the contributions of the left- and right-handed components of the squarks to the mass eigenstates are proportional to the first and second three columns of W , respectively. Since $\bar{u}\mathcal{P}_L = u^\dagger\mathcal{P}_R\gamma_0$ the projector \mathcal{P}_L projects out the right-handed component of the quark field. Thus, the quark rotation matrix U^{uR} together with components of W rotating the right-handed squarks are used to rotate the fields to their mass eigenstates in \mathcal{L}_1 . For \mathcal{L}_2 the components of W for the left-handed squarks and the quark rotation matrix U^{uL} are used for the squark. From now on the indices i, j, k, l, n, o, r will run from 1 to 3 whereas the indices s, t, v run from 1 to 6. Then, \mathcal{L}_1 and \mathcal{L}_2 are given by

$$\mathcal{L}_1 = Q_{1il}^L \underbrace{\bar{u}_i^{(0)} U_{ij}^{uR\dagger(0)}}_{=\bar{u}_j^{m(0)}} \underbrace{U_{jk}^{uR(0)} U_{kl}^{uR\dagger(0)}}_{=\delta_{jl}} W_{l+3,s}^{\dagger(0)} \underbrace{W_{s,n+3}^{(0)} U_{no}^{uR(0)} \tilde{u}_{oR}^{(0)}}_{=\tilde{u}_s^{m(0)}} \mathcal{P}_L \tilde{\chi}_l^0 \quad (3.50)$$

$$= Q_{1il}^L \bar{u}_i^{m(0)} W_{i+3,s}^{\dagger(0)} \tilde{u}_s^{m(0)} \mathcal{P}_L \tilde{\chi}_l^0 \quad (3.51)$$

$$\mathcal{L}_2 = Q_{2il}^L \underbrace{\bar{u}_i^{(0)} U_{ij}^{uR\dagger(0)}}_{=\bar{u}_j^{m(0)}} U_{jk}^{uR(0)} m_{kl}^{\dagger(0)} U_{ln}^{uL\dagger(0)} W_{ns}^{\dagger(0)} \underbrace{W_{so}^{(0)} U_{or}^{uL(0)} \tilde{u}_{rL}^{(0)}}_{=\tilde{u}_s^{m(0)}} \mathcal{P}_L \tilde{\chi}_l^0 \quad (3.52)$$

$$= Q_{2il}^L \bar{u}_i^{m(0)} U_{ij}^{uR(0)} m_{jk}^{\dagger(0)} U_{kl}^{uL\dagger(0)} W_{ls}^{\dagger(0)} \tilde{u}_s^{m(0)} \mathcal{P}_L \tilde{\chi}_l^0 . \quad (3.53)$$

The upper index m indicates that the fields are in their mass eigenstates. In Eqs. (3.51) and (3.53) the lower indices L, R for the squark fields are not needed any more as the correct components are implicitly selected by the rotation matrix W in front.

At this stage the bare fields and mixing matrices are replaced by the renormalized ones and the corresponding counterterms. Since in loop corrections the flavor of quarks and squarks can change, also their renormalization constants need to contain flavor off-diagonal elements. Consequently, the renormalization constants of the fields are 3×3 or 6×6 matrices. For the rotation matrices U and W the renormalization constants are matrices as well. The renormalization constants of the matrices will be chosen such that renormalized fields are rotated to mass eigenstates via renormalized matrices in the same manner as unrenormalized

fields are rotated with unrenormalized matrices [53, 68, 69]. The replacements are

$$\bar{u}_j^{m(0)} \rightarrow \bar{u}_i^m \left(\delta_{ij} + \frac{1}{2} \delta Z_{ij}^\dagger \right), \quad (3.54)$$

$$\tilde{u}_s^{m(0)} \rightarrow \left(\delta_{sv} + \frac{1}{2} \delta Z_{sv}^{\tilde{u}} \right) \tilde{u}_v^m, \quad (3.55)$$

$$U_{ik}^{uR(0)} \rightarrow \left(\delta_{ij} + \delta U_{ij}^R \right) U_{jk}^{uR}, \quad (3.56)$$

$$W_{i+3,v}^{\dagger(0)} \rightarrow W_{i+3,s}^\dagger \left(\delta_{sv} + \delta W_{sv}^\dagger \right), \quad (3.57)$$

$$m_{jk}^{\dagger(0)} \rightarrow m_{jk}^\dagger + \delta m_{jk}^\dagger, \quad (3.58)$$

and for the case of $W_{ls}^{\dagger(0)}$ correspondingly. So the two parts of the renormalized Lagrangian are

$$\mathcal{L}_1 = Q_{1il}^L \bar{u}_i^m \left(\delta_{ij} + \frac{1}{2} \delta Z_{ij}^{R\dagger} \right) W_{j+3,s}^\dagger \left(\delta_{st} + \delta W_{st}^\dagger \right) \left(\delta_{tv} + \frac{1}{2} \delta Z_{tv}^{\tilde{u}} \right) \tilde{u}_v^m \mathcal{P}_L \tilde{\chi}_l^0 \quad (3.59)$$

$$= Q_{1il}^L \bar{u}_i^m \left[W_{i+3,v}^\dagger + W_{i+3,s}^\dagger \delta W_{sv}^\dagger + W_{i+3,s}^\dagger \frac{1}{2} \delta Z_{sv}^{\tilde{u}} + \frac{1}{2} \delta Z_{ij}^{R\dagger} W_{j+3,v}^\dagger \right] \tilde{u}_v^m \mathcal{P}_L \tilde{\chi}_l^0 \quad (3.60)$$

and

$$\begin{aligned} \mathcal{L}_2 = & Q_{2il}^L \bar{u}_i^m \left(\delta_{ij} + \frac{1}{2} \delta Z_{ij}^{R\dagger} \right) \left(\delta_{jk} + \delta U_{jk}^R \right) U_{kl}^{uR} (m_{ln}^\dagger + \delta m_{ln}^\dagger) U_{no}^{uL\dagger} \left(\delta_{or} + \delta U_{or}^{L\dagger} \right) \\ & \cdot W_{rs}^\dagger \left(\delta_{st} + \delta W_{st}^\dagger \right) \left(\delta_{tv} + \frac{1}{2} \delta Z_{tv}^{\tilde{u}} \right) \tilde{u}_v^m \mathcal{P}_L \tilde{\chi}_l^0, \end{aligned} \quad (3.61)$$

where the quark renormalization constant δZ acquired an upper index R to indicate that it is the renormalization constant for the right handed part of the quark field. To simplify Eq. (3.61) as explained above the renormalized matrix U can be used to diagonalize the renormalized quark mass matrix m_{ln} . In detail, this leads to

$$\left(\delta_{jk} + \delta U_{jk}^R \right) U_{kl}^{uR} (m_{ln}^\dagger + \delta m_{ln}^\dagger) U_{no}^{uL\dagger} \left(\delta_{or} + \delta U_{or}^{L\dagger} \right) = \delta_{jr} (m_{uj} + \delta m_{uj}), \quad (3.62)$$

where on the right-hand side the ' \dagger ' can be omitted since the matrix is diagonal and has real entries. Thereby the second part of the Lagrangian \mathcal{L}_2 turns into

$$\mathcal{L}_2 = Q_{2il}^L \bar{u}_i^m \left(\delta_{ij} + \frac{1}{2} \delta Z_{ij}^{R\dagger} \right) \delta_{jo} (m_{uj} + \delta m_{uj}) W_{os}^\dagger \left(\delta_{sv} + \delta W_{sv}^\dagger + \frac{1}{2} \delta Z_{sv}^{\tilde{u}} \right) \tilde{u}_v^m \mathcal{P}_L \tilde{\chi}_l^0 \quad (3.63)$$

$$\begin{aligned} = & Q_{2il}^L \bar{u}_i^m \left[\delta_{ij} m_{uj} W_{jv}^\dagger + \delta_{ij} m_{uj} W_{js}^\dagger \delta W_{sv}^\dagger + \delta_{ij} m_{uj} W_{js}^\dagger \frac{1}{2} \delta Z_{sv}^{\tilde{u}} \right. \\ & \left. + \frac{1}{2} \delta Z_{ij}^{R\dagger} m_{uj} W_{jv}^\dagger + \delta_{ij} \delta m_{uj} W_{jv}^\dagger \right] \tilde{u}_v^m \mathcal{P}_L \tilde{\chi}_l^0 \end{aligned} \quad (3.64)$$

$$\begin{aligned} = & Q_{2il}^L \bar{u}_i^m \left[m_i W_{iv}^\dagger + m_i W_{is}^\dagger \delta W_{sv}^\dagger + m_i W_{is}^\dagger \frac{1}{2} \delta Z_{sv}^{\tilde{u}} \right. \\ & \left. + \frac{1}{2} \delta Z_{ij}^{R\dagger} m_j W_{jv}^\dagger + \delta m_i W_{iv}^\dagger \right] \tilde{u}_v^m \mathcal{P}_L \tilde{\chi}_l^0, \end{aligned} \quad (3.65)$$

where m_{u_i} is abbreviated by m_i . Here the squark rotation matrix from the Super-CKM basis to the mass eigenstate basis has been renormalized explicitly by Eq. (3.57) resulting in terms proportional to δW^\dagger in Eqs. (3.60) and (3.65). However, in anticipation of the explicit form of the renormalization constants in terms of self-energies (see Section 3.2.2) it is helpful to

change the δW^\dagger counterterm to a counterterm for the whole rotation matrix from interaction to mass eigenstates \widetilde{W} as defined in Eq. (2.47). As a counterterm for δW^\dagger is needed rather than for δW , we directly define the hermitian adjoint $\widetilde{W}^{\dagger(0)}$ of the unrenormalized matrix by

$$\widetilde{W}^{\dagger(0)} := U^{\dagger(0)} W^{\dagger(0)} . \quad (3.66)$$

This definition must hold for the renormalized matrices as well, leading to

$$\widetilde{W}^\dagger(1 + \delta\widetilde{W}^\dagger) = U^\dagger(1 + \delta U^\dagger)W^\dagger(1 + \delta W^\dagger) \quad (3.67)$$

$$\Leftrightarrow \delta\widetilde{W}^\dagger = \delta W^\dagger + W\delta U^\dagger W^\dagger . \quad (3.68)$$

As the renormalized quark mixing matrix has to be unitary, the counterterm δU is antihermitian. Then, the following term in \mathcal{L}_1 gives

$$W_{i+3,s}^\dagger \delta W_{sv}^\dagger = W_{i+3,s}^\dagger (\delta\widetilde{W}_{sv}^\dagger - W_{s,j+3} \delta U_{jk}^R W_{k+3,v}^\dagger) \quad (3.69)$$

$$= W_{i+3,s}^\dagger \delta\widetilde{W}_{sv}^\dagger + \delta U_{ij}^R W_{j+3,v}^\dagger \quad (3.70)$$

and the corresponding term in \mathcal{L}_2 reads

$$m_i W_{is}^\dagger \delta W_{sv}^\dagger = m_i W_{is}^\dagger (\delta\widetilde{W}_{sv}^\dagger - W_{sj} \delta U_{jk}^L W_{kv}^\dagger) \quad (3.71)$$

$$= m_i W_{is}^\dagger \delta\widetilde{W}_{sv}^\dagger + m_i \delta U_{ij}^L W_{jv}^\dagger , \quad (3.72)$$

where U^{uL} and U^{uR} have been chosen in accordance to the required rotation in Eqs. (3.60) and (3.65). Combining Eqs. (3.60) and (3.65) with Eqs. (3.70) and (3.72) the renormalized parts of the Lagrangian become

$$\begin{aligned} \mathcal{L}_1 = Q_{1il}^L \bar{u}_i^m & \left[W_{i+3,v}^\dagger + W_{i+3,s}^\dagger \delta\widetilde{W}_{sv}^\dagger + \delta U_{ij}^R W_{j+3,v}^\dagger + W_{i+3,s}^\dagger \frac{1}{2} \delta Z_{sv}^{\bar{u}} \right. \\ & \left. + \frac{1}{2} \delta Z_{ij}^{R\dagger} W_{j+3,v}^\dagger \right] \tilde{u}_v^m \mathcal{P}_L \tilde{\chi}_l^0 \end{aligned} \quad (3.73)$$

and

$$\begin{aligned} \mathcal{L}_2 = Q_{2il}^L \bar{u}_i^m & \left[m_i W_{iv}^\dagger + m_i W_{is}^\dagger \delta\widetilde{W}_{sv}^\dagger + m_i \delta U_{ij}^L W_{jv}^\dagger + m_i W_{is}^\dagger \frac{1}{2} \delta Z_{sv}^{\bar{u}} \right. \\ & \left. + \frac{1}{2} \delta Z_{ij}^{R\dagger} m_j W_{jv}^\dagger + \delta m_i W_{iv}^\dagger \right] \tilde{u}_v^m \mathcal{P}_L \tilde{\chi}_l^0 . \end{aligned} \quad (3.74)$$

In the derivation all terms of higher than linear order in the counterterms were tacitly neglected reflecting that only NLO corrections are calculated. Terms of $\mathcal{O}(\delta^n)$, $n \geq 2$ correspond to higher orders in perturbation theory. As explained at the beginning the \mathcal{P}_R part is obtained by substituting $R \leftrightarrow L$ everywhere.

3.2.2. The On-Shell Renormalization Scheme

In the previous section counterterms were introduced which will cancel the UV divergences. The finite contributions left over are determined by imposing requirements on the renormalized n -point functions. This is called renormalization scheme. Since the renormalization scheme is a matter of choice it is important to mention which renormalization scheme is used for the calculation as the result for the physical parameters can depend on the actual choice. Here, the on-shell (OS) scheme will be used. First, the matrix renormalization constants will be defined and afterwards all renormalization constants will be substituted by self-energies using the renormalization conditions of the OS scheme.

3.2.2.1. Matrix Renormalization

The renormalized Lagrangians (3.73) and (3.74) contain the following renormalization constants

$$\delta\widetilde{W}_{sv} , \quad \delta U_{ij}^R , \quad \delta U_{ij}^L , \quad \delta Z_{sv}^{\tilde{u}} , \quad \delta Z_{ij}^R , \quad \delta m_i . \quad (3.75)$$

As already mentioned in Section 3.2.1, the field renormalization constants δZ_{ij}^R and $\delta Z_{sv}^{\tilde{u}}$ are matrices to take into account the mixing between different flavors which is possible due to loop corrections to the propagators. The UV divergent part of the mixing matrix counterterms is determined such that it cancels the divergent part of the antihermitian part of the corresponding wave function renormalization matrix [68, 70, 71]

$$\delta U_{ij}^{R,L} = \frac{1}{4}(\delta Z_{ij}^{R,L} - \delta Z_{ij}^{R,L\dagger}) , \quad (3.76)$$

$$\delta\widetilde{W}_{sv} = \frac{1}{4}(\delta Z_{sv}^{\tilde{u}} - \delta Z_{sv}^{\tilde{u}\dagger}) . \quad (3.77)$$

Thus, by replacing δU^L in Eq. (3.74) another renormalization constant δZ^L is introduced for the left-handed part of the quark field. In Section 3.2.2.3 it will be shown that for the cancellation of artificial divergences occurring in the counterterms in special cases like $m_i = m_j$, this choice of the matrix renormalization constants is crucial [68]. Inserting Eqs. (3.76) and (3.77) into the two parts of the Lagrangian (3.73) and (3.74) leads to

$$\mathcal{L}_1 = Q_{1il}^L \bar{u}_i^m \left[W_{i+3,v}^\dagger + W_{i+3,s}^\dagger \frac{1}{4}(\delta Z_{sv}^{\tilde{u}\dagger} + \delta Z_{sv}^{\tilde{u}}) + \frac{1}{4}(\delta Z_{ij}^R + \delta Z_{ij}^{R\dagger}) W_{j+3,v}^\dagger \right] \tilde{u}_v^m \mathcal{P}_L \tilde{\chi}_l^0 \quad (3.78)$$

and

$$\begin{aligned} \mathcal{L}_2 = Q_{2il}^L \bar{u}_i^m & \left[m_i W_{iv}^\dagger + \delta m_i W_{iv}^\dagger + m_i W_{is}^\dagger \frac{1}{4}(\delta Z_{sv}^{\tilde{u}\dagger} + \delta Z_{sv}^{\tilde{u}}) \right. \\ & \left. + \left(\frac{1}{2} \delta Z_{ij}^{R\dagger} m_j + \frac{1}{4} m_i (\delta Z_{ij}^L - \delta Z_{ij}^{L\dagger}) \right) W_{jv}^\dagger \right] \tilde{u}_v^m \mathcal{P}_L \tilde{\chi}_l^0 . \end{aligned} \quad (3.79)$$

In the following, the renormalization scheme will be specified.

3.2.2.2. Renormalization Constants in the On-Shell Scheme

In the OS scheme the renormalized masses of the particles are required to be equal to their physical values. This imposes conditions on the renormalized two-point functions Γ^{SS} and $\Gamma^{f\bar{f}}$ of scalars s and fermions f , namely that they must vanish at the physical masses m_s and $m_{f_i} = m_i$ and that the residues of the two-point functions are equal to one. In momentum space this means (see for example [72, 73])

$$\widetilde{\text{Re}}\Gamma_{R,st}^{SS}(p) \Big|_{p^2=m_s^2} = 0 , \quad (3.80a)$$

$$\widetilde{\text{Re}}\Gamma_{R,st}^{SS}(p) \Big|_{p^2=m_t^2} = 0 , \quad (3.80b)$$

$$\lim_{p^2 \rightarrow m_s^2} \frac{1}{p^2 - m_s^2} \widetilde{\text{Re}}\Gamma_{R,ss}^{SS}(p) = 1 \quad (3.80c)$$

for the scalar two-point function and

$$\widetilde{\text{Re}}\Gamma_{R,ij}^{f\bar{f}}(p) u_j(p) \Big|_{p^2=m_j^2} = 0 , \quad (3.81a)$$

$$\lim_{p^2 \rightarrow m_i^2} \frac{\not{p} + m_i}{p^2 - m_i^2} \widetilde{\text{Re}}\Gamma_{R,ii}^{f\bar{f}}(p) u_i(p) = u_i(p) \quad (3.81b)$$

for the fermionic one. In addition to the fermion generation indices i and j also scalar indices s, t for the scalar superpartners of the fermions are introduced in the above equations. The subscript R stands for renormalized and the \Re indicates, that the real part is only to be taken of the loop integrals but not of the mixing matrices. The fermion two-point function can be decomposed into left- and right-chiral parts and the respective scalar parts, denoted by the upper indices L, R and SL, SR , respectively [72]

$$\Gamma_{R,ij}^{f\bar{f}}(p) = \not{p}\mathcal{P}_L\Gamma_{R,ij}^{f\bar{f},L}(p^2) + \not{p}\mathcal{P}_R\Gamma_{R,ij}^{f\bar{f},R}(p^2) + \mathcal{P}_L\Gamma_{R,ij}^{f\bar{f},SL}(p^2) + \mathcal{P}_R\Gamma_{R,ij}^{f\bar{f},SR}(p^2) , \quad (3.82)$$

with p denoting the momentum of the corresponding particle. The renormalized two-point functions on which the conditions (3.80) and (3.81) are applied, consist of the unrenormalized tree-level terms, the unrenormalized self-energies Σ and the counterterms. In detail they are given by [72, 73]

$$\begin{aligned} \Gamma_{R,st}^{SS}(p) &= (p^2 - m_s^2)\delta_{st} + \Sigma_{st}^{SS}(p^2) \\ &\quad + \frac{1}{2}(p^2 - m_s^2)\delta Z_{st}^S + \frac{1}{2}(p^2 - m_t^2)\delta Z_{st}^{S\dagger} - \delta_{st}\delta m_s^2 , \end{aligned} \quad (3.83)$$

$$\Gamma_{R,ij}^{f\bar{f},L}(p^2) = \delta_{ij} + \Sigma_{ij}^L(p^2) + \frac{1}{2}(\delta Z_{ij}^L + \delta Z_{ij}^{L\dagger}) , \quad (3.84)$$

$$\Gamma_{R,ij}^{f\bar{f},R}(p^2) = \delta_{ij} + \Sigma_{ij}^R(p^2) + \frac{1}{2}(\delta Z_{ij}^R + \delta Z_{ij}^{R\dagger}) , \quad (3.85)$$

$$\Gamma_{R,ij}^{f\bar{f},SL}(p^2) = -m_i\delta_{ij} + \Sigma_{ij}^{SL}(p^2) - \frac{1}{2}(m_i\delta Z_{ij}^L + m_j\delta Z_{ij}^{R\dagger}) - \delta_{ij}\delta m_i , \quad (3.86)$$

$$\Gamma_{R,ij}^{f\bar{f},SR}(p^2) = -m_i\delta_{ij} + \Sigma_{ij}^{SR}(p^2) - \frac{1}{2}(m_i\delta Z_{ij}^R + m_j\delta Z_{ij}^{L\dagger}) - \delta_{ij}\delta m_i , \quad (3.87)$$

where δ_{ij} and δ_{st} are Kronecker deltas. The left- and right-chiral and scalar parts of the fermion self-energy are defined by the decomposition of the fermion self-energy in accordance with [68, 72]

$$\Sigma_{ij}^f(p) = \not{p}\mathcal{P}_L\Sigma_{ij}^L(p^2) + \not{p}\mathcal{P}_R\Sigma_{ij}^R(p^2) + \mathcal{P}_L\Sigma_{ij}^{SL}(p^2) + \mathcal{P}_R\Sigma_{ij}^{SR}(p^2) , \quad (3.88)$$

with $\not{p} = p^\mu\gamma_\mu$. This is needed to explicitly evaluate the renormalization conditions for the fermions (3.81) in order to replace the renormalization constants $\delta Z_{ij}^{R,L}$ by self-energies. The validity of this decomposition follows from the fact that the leading order unrenormalized two-point function of a fermion in momentum space is $\Gamma^{f\bar{f}} = \not{p} - m$ in combination with the observation that the Lorentz tensor structure of a vertex function cannot change in any order of perturbation theory. This is a consequence of the different types of underlying symmetries: the Lorentz structure corresponds to the space-time symmetry whereas the perturbation expansion corresponds to a gauge symmetry.

Note that here, in contrast to other definitions of the decomposition [69, 74], no factor of m_i or m_j is extracted out of the scalar parts of the self-energies $\Sigma_{ij}^{SR}, \Sigma_{ij}^{SL}$ in Eq. (3.88) since flavor mixing in the quark sector is possible, mediated by a gluino. Thus, it can happen that there is neither a quark i with mass m_i nor a quark j with mass m_j in the loop but any other quark. This will also affect the explicit form of the renormalization constants $\delta Z^{R,L}$ in terms of the self-energies later on.

Due to hermiticity of the Lagrangian the following relations hold for the fermion self-energy [68, 72]

$$\Sigma_{ji}^{L*}(p^2) = \Sigma_{ij}^L(p^2) , \quad \Sigma_{ji}^{R*}(p^2) = \Sigma_{ij}^R(p^2) , \quad \Sigma_{ij}^{SR}(p^2) = \Sigma_{ji}^{SL*}(p^2) , \quad (3.89)$$

and the squark self energy has to be hermitian. In view of the last relation of Eq. (3.89) it is clear that the fermion self-energy is not necessarily symmetric in i and j . As a consequence

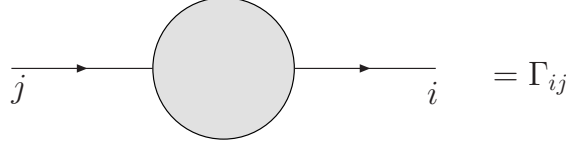


Figure 3.2: Fermion two-point function.

it is important to which side of the two-point function the indices i and j correspond. The correct definition is depicted in Figure 3.2 in consistency with the Feynman rules used.

Now the OS renormalization conditions (3.80) and (3.81) can be applied on the two-point functions which finally leads to the explicit form of the renormalization constants in terms of unrenormalized self-energies [53, 68, 72, 73]

$$\delta m_i = \frac{1}{2} \widetilde{\text{Re}} \left(m_i (\Sigma_{ii}^L(m_i^2) + \Sigma_{ii}^R(m_i^2)) + \Sigma_{ii}^{SL}(m_i^2) + \Sigma_{ii}^{SR}(m_i^2) \right), \quad (3.90)$$

$$\delta m_s^2 = \widetilde{\text{Re}} \Sigma_{ss}^{\tilde{u}}(m_s^2), \quad (3.91)$$

$$\delta Z_{st}^{\tilde{u}} = \frac{2}{m_s^2 - m_t^2} \widetilde{\text{Re}} \Sigma_{st}^{\tilde{u}}(m_t^2), \quad s \neq t, \quad (3.92)$$

$$\delta Z_{ss}^{\tilde{u}} = -\widetilde{\text{Re}} \left. \frac{\partial \Sigma_{ss}^{\tilde{u}}(p^2)}{\partial p^2} \right|_{p^2=m_s^2}, \quad (3.93)$$

$$\delta Z_{ij}^L = \frac{2}{m_i^2 - m_j^2} \widetilde{\text{Re}} \left[m_j^2 \Sigma_{ij}^L(m_j^2) + m_i m_j \Sigma_{ij}^R(m_j^2) + m_i \Sigma_{ij}^{SL}(m_j^2) + m_j \Sigma_{ij}^{SR}(m_j^2) \right], \quad i \neq j, \quad (3.94)$$

$$\delta Z_{ij}^R = \frac{2}{m_i^2 - m_j^2} \widetilde{\text{Re}} \left[m_j^2 \Sigma_{ij}^R(m_j^2) + m_i m_j \Sigma_{ij}^L(m_j^2) + m_j \Sigma_{ij}^{SL}(m_j^2) + m_i \Sigma_{ij}^{SR}(m_j^2) \right], \quad i \neq j, \quad (3.95)$$

$$\delta Z_{ii}^L = -\widetilde{\text{Re}} \Sigma_{ii}^L(m_i^2) - m_i \left. \frac{\partial}{\partial p^2} \widetilde{\text{Re}} \left[m_i (\Sigma_{ii}^L(p^2) + \Sigma_{ii}^R(p^2)) + \Sigma_{ii}^{SL}(p^2) + \Sigma_{ii}^{SR}(p^2) \right] \right|_{p^2=m_i^2}, \quad (3.96)$$

$$\delta Z_{ii}^R = -\widetilde{\text{Re}} \Sigma_{ii}^R(m_i^2) - m_i \left. \frac{\partial}{\partial p^2} \widetilde{\text{Re}} \left[m_i (\Sigma_{ii}^L(p^2) + \Sigma_{ii}^R(p^2)) + \Sigma_{ii}^{SL}(p^2) + \Sigma_{ii}^{SR}(p^2) \right] \right|_{p^2=m_i^2}. \quad (3.97)$$

Here, the upper index S for the self-energy and renormalization constant of the scalar particle in Eq. (3.83) is replaced by \tilde{u} as in this work the scalar particle will be an up-type squark. This can now be applied to \mathcal{L}_1 and \mathcal{L}_2 of (3.78) and (3.79), respectively. From now on the $\widetilde{\text{Re}}$ will be omitted for easier reading.

Regarding the squark counterterms there is only one linear combination appearing in both \mathcal{L}_1 and \mathcal{L}_2 . Using Eqs. (3.92) and (3.93) leads to

$$\frac{1}{4} \left(\delta Z_{sv}^{\tilde{u}\dagger} + \delta Z_{sv}^{\tilde{u}} \right) = -\frac{1}{2} \frac{1}{m_s^2 - m_v^2} \left(\Sigma_{sv}^{\tilde{u}}(m_s^2) - \Sigma_{sv}^{\tilde{u}}(m_v^2) \right), \quad s \neq v, \quad (3.98)$$

and for the diagonal terms

$$\frac{1}{4} \left(\delta Z_{ss}^{\tilde{u}\dagger} + \delta Z_{ss}^{\tilde{u}} \right) = -\frac{1}{2} \left. \frac{\partial \Sigma_{ss}^{\tilde{u}}(p^2)}{\partial p^2} \right|_{p^2=m_s^2}. \quad (3.99)$$

If the squark masses are degenerate Eq. (3.98) turns into the derivative in Eq. (3.99) with the subscripts ss replaced by sv . This is different for the fermion counterterms, as the quark masses are very small compared to the squark masses and thereby to the relevant scale of our process. Therefore the masses of the quarks of the first and the second generation can be set to zero for simplicity. For $m_i = m_j$ and in particular $m_i = m_j = 0$ the renormalization constants (3.94) and (3.95) then diverge due to the prefactor

$$\frac{2}{m_i^2 - m_j^2} . \quad (3.100)$$

Note that this is the case for $i \neq j$. However, these divergences can be removed from the counterterms by appropriate linear combinations of the renormalization constants $\delta Z^{R,L}$ [68]. This can be achieved by choosing the renormalization constants for the mixing matrices exactly as proposed in Section 3.2.2.1.

In detail, there are two different linear combinations of counterterms $\delta Z^{R,L}$ appearing in \mathcal{L}_1 and \mathcal{L}_2 (*cf.* Eqs. (3.78) and (3.79)). To write them in a way where it is possible to discern that the divergences are in fact removed, two helpful relations are

$$m_j^2 \Sigma(m_j^2) - m_i^2 \Sigma(m_i^2) = \frac{1}{2} \left[-(m_i^2 + m_j^2)(\Sigma(m_i^2) - \Sigma(m_j^2)) - (m_i^2 - m_j^2)(\Sigma(m_i^2) + \Sigma(m_j^2)) \right] \quad (3.101)$$

and

$$m_i^2 \Sigma(m_j^2) - m_j^2 \Sigma(m_i^2) = (m_i^2 - m_j^2)(\Sigma(m_i^2) + \Sigma(m_j^2)) + m_j^2 \Sigma(m_j^2) - m_i^2 \Sigma(m_i^2) , \quad (3.102)$$

where the generation indices i, j and superscripts R, L, SR, SL have been ignored for the self-energies. Note that in Eq. (3.102) the last two terms can be replaced using Eq. (3.101). Then the final results for the linear combinations of the fermion counterterms in the Lagrangians (3.78) and (3.79) with use of Eqs. (3.94)-(3.97) are given by

$$\begin{aligned} \frac{1}{4}(\delta Z_{ij}^R + \delta Z_{ij}^{R\dagger}) &= \frac{1}{2} \frac{1}{m_i^2 - m_j^2} \left[-m_j(\Sigma_{ij}^{SL}(m_i^2) - \Sigma_{ij}^{SL}(m_j^2)) \right. \\ &\quad - m_i(\Sigma_{ij}^{SR}(m_i^2) - \Sigma_{ij}^{SR}(m_j^2)) \\ &\quad - m_i m_j (\Sigma_{ij}^L(m_i^2) - \Sigma_{ij}^L(m_j^2)) \\ &\quad - \frac{1}{2}(m_i^2 + m_j^2)(\Sigma_{ij}^R(m_i^2) - \Sigma_{ij}^R(m_j^2)) \\ &\quad \left. - \frac{1}{2}(m_i^2 - m_j^2)(\Sigma_{ij}^R(m_i^2) + \Sigma_{ij}^R(m_j^2)) \right] \end{aligned} \quad (3.103)$$

and

$$\begin{aligned}
\frac{1}{2}\delta Z_{ij}^{R\dagger}m_j + \frac{1}{4}m_i(\delta Z_{ij}^L - \delta Z_{ij}^{L\dagger}) &= \frac{1}{2}\frac{1}{m_i^2 - m_j^2} \left[(m_i^2 - m_j^2)\Sigma_{ij}^{SL}(m_i^2) \right. \\
&\quad + (m_i^2 - m_j^2)m_i\Sigma_{ij}^L(m_i^2) \\
&\quad - m_im_j(\Sigma_{ij}^{SR}(m_i^2) - \Sigma_{ij}^{SR}(m_j^2)) \\
&\quad - m_im_j^2(\Sigma_{ij}^L(m_i^2) - \Sigma_{ij}^L(m_j^2)) \\
&\quad - m_i^2m_j(\Sigma_{ij}^R(m_i^2) - \Sigma_{ij}^R(m_j^2)) \\
&\quad + (m_i^2 - m_j^2)(\Sigma_{ij}^{SL}(m_i^2) + \Sigma_{ij}^{SL}(m_j^2)) \\
&\quad - \frac{1}{2}(m_i^2 + m_j^2)(\Sigma_{ij}^{SL}(m_i^2) - \Sigma_{ij}^{SL}(m_j^2)) \\
&\quad \left. - \frac{1}{2}(m_i^2 - m_j^2)(\Sigma_{ij}^{SL}(m_i^2) + \Sigma_{ij}^{SL}(m_j^2)) \right], \tag{3.104}
\end{aligned}$$

which hold for $i \neq j$. For the diagonal counterterms the results are

$$\begin{aligned}
\frac{1}{4}(\delta Z_{ii}^R + \delta Z_{ii}^{R\dagger}) &= \frac{1}{2} \left[-\Sigma_{ii}^R(m_i^2) \right. \\
&\quad \left. - m_i \frac{\partial}{\partial p^2} \left(m_i(\Sigma_{ii}^R(p^2) + \Sigma_{ii}^L(p^2)) + \Sigma_{ii}^{SR}(p^2) + \Sigma_{ii}^{SL}(p^2) \right) \Big|_{p^2=m_i^2} \right] \tag{3.105}
\end{aligned}$$

and

$$\begin{aligned}
\frac{1}{2}\delta Z_{ii}^{R\dagger}m_i + \frac{1}{4}m_i(\delta Z_{ii}^L - \delta Z_{ii}^{L\dagger}) &= -\frac{1}{2}m_i \left[\Sigma_{ii}^R(m_i^2) \right. \\
&\quad \left. + m_i \frac{\partial}{\partial p^2} \left(m_i(\Sigma_{ii}^R(p^2) + \Sigma_{ii}^L(p^2)) + \Sigma_{ii}^{SR}(p^2) + \Sigma_{ii}^{SL}(p^2) \right) \Big|_{p^2=m_i^2} \right]. \tag{3.106}
\end{aligned}$$

3.2.2.3. Limits and Special Cases

The derivative of a function $f(x)$ can be defined by the differential quotient

$$\lim_{b \rightarrow a} \frac{f(a) - f(b)}{a - b} = \frac{\partial f(x)}{\partial x} \Big|_{x=a}. \tag{3.107}$$

The preceding formulation of the linear combinations of the counterterms appearing in the Lagrangian is chosen such that either the divergent global denominator

$$\frac{1}{m_i^2 - m_j^2} \tag{3.108}$$

is canceled or that the derivative of a self-energy is recovered in the limit $m_j \rightarrow m_i$. In both cases the divergence for $m_i = m_j$ is removed. It is now clear that the choice for the renormalization of the mixing matrix is vital here, since it is exactly this linear combination of field renormalization constants which leads either to derivatives or to the cancellation of the denominator. Taking the limit $m_j \rightarrow m_i$ leads to

$$\begin{aligned}
\lim_{m_j \rightarrow m_i} \left(\frac{1}{4}(\delta Z_{ij}^R + \delta Z_{ij}^{R\dagger}) \right) &= \\
\frac{1}{2} \left[-\Sigma_{ij}^R(m_i^2) - m_i \frac{\partial}{\partial p^2} \left(m_i(\Sigma_{ij}^R(p^2) + \Sigma_{ij}^L(p^2)) + \Sigma_{ij}^{SR}(p^2) + \Sigma_{ij}^{SL}(p^2) \right) \Big|_{p^2=m_i^2} \right] \tag{3.109}
\end{aligned}$$

and

$$\begin{aligned} \lim_{m_j \rightarrow m_i} \left(\frac{1}{2} \delta Z_{ij}^{R\dagger} m_i + \frac{1}{4} m_i (\delta Z_{ij}^L - \delta Z_{ij}^{L\dagger}) \right) &= \Sigma_{ij}^{SL}(m_i^2) + \frac{1}{2} m_i \Sigma_{ij}^L(m_i^2) \\ &- \frac{1}{2} m_i^2 \frac{\partial}{\partial p^2} \left(m_i (\Sigma_{ij}^R(p^2) + \Sigma_{ij}^L(p^2)) + \Sigma_{ij}^{SR}(p^2) + \Sigma_{ij}^{SL}(p^2) \right) \Big|_{p^2=m_i^2}. \end{aligned} \quad (3.110)$$

As a numerical cancellation is impossible due to the divergent prefactor (3.108) the divergence has to be canceled analytically by taking the limit $m_j \rightarrow m_i$ and this case has to be implemented in addition to the case $i \neq j$. Further it may be convenient to set

$$|m_i - m_j| < \epsilon, \quad \epsilon > 0 \quad (3.111)$$

as condition to switch to the limit $m_j \rightarrow m_i$. In this way possible numerical instabilities due to the finite precision of data types can be avoided.

In the massless case the expressions (3.109) and (3.110) simplify further to

$$\lim_{m_i \rightarrow 0} \left(\lim_{m_j \rightarrow m_i} \left(\frac{1}{4} (\delta Z_{ij}^R + \delta Z_{ij}^{R\dagger}) \right) \right) = -\frac{1}{2} \Sigma_{ij}^R(0) \quad (3.112)$$

$$\lim_{m_i \rightarrow 0} \left(\lim_{m_j \rightarrow m_i} \left(\frac{1}{2} \delta Z_{ij}^{R\dagger} m_i + \frac{1}{4} m_i (\delta Z_{ij}^L - \delta Z_{ij}^{L\dagger}) \right) \right) = \Sigma_{ij}^{SL}(0). \quad (3.113)$$

Although the limits (3.112) and (3.113) are already covered by Eqs. (3.109) and (3.110) they are stated here as it can be useful to implement these cases separately for numerical evaluations of the counterterms since only one self-energy has to be evaluated in comparison to five or six evaluations, respectively.

Note again that the divergence in the fermion counterterm is not related to the divergences appearing in Feynman graphs. Motivated by the fact that quarks of different generations only differ in mass the question arises whether the two cases $i = j$ and $m_i = m_j$ are the same. For the first linear combination

$$\frac{1}{4} (\delta Z_{ij}^R + \delta Z_{ij}^{R\dagger}) \quad (3.114)$$

this is indeed the case. However, for the second one

$$\frac{1}{2} \delta Z_{ij}^{R\dagger} m_i + \frac{1}{4} m_i (\delta Z_{ij}^L - \delta Z_{ij}^{L\dagger}) \quad (3.115)$$

it is not (compare Eqs. (3.105) and (3.106) to Eqs. (3.109) and (3.110)). The difference ensues from the two distinct renormalization conditions imposed for $i = j$ and $i \neq j$ in Eq. (3.81). In addition it is not possible to set $m_i = m_j$ directly in each renormalization constant $\delta Z^{R,L}$ but only in the linear combinations stated above.

3.2.3. Self-Energies

In Section 3.2.2.2 explicit formulas for the linear combinations of renormalization constants of the fields were derived. For the quark fields these are given in Eqs. (3.103) to (3.106) and for the squark fields the formulas are given by (3.98) and (3.99). Additionally, the mass renormalization constants (3.90) and (3.91) have to be used. As already explained, self-energies with respect to the strong interaction are required for the cancellation of the UV divergences.

At one-loop level there are two diagrams contributing to the quark self-energies at $\mathcal{O}(\alpha_s)$. One diagram due to the exchange of a gluon and a quark and the other one due to a squark

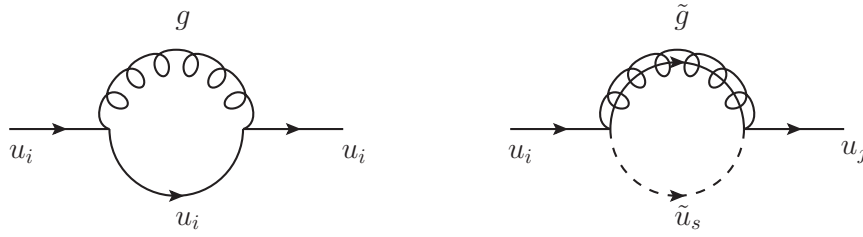


Figure 3.3: One-loop contributions to the quark self-energy in QCD and SQCD.

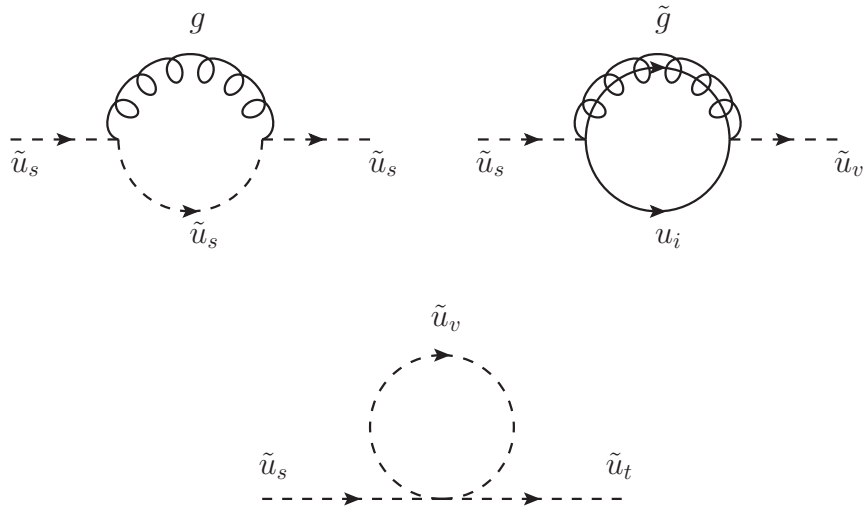


Figure 3.4: One-loop contributions to the squark self-energy in QCD and SQCD.

and gluino loop as depicted in Figure 3.3. While in the first diagram the flavor of the quark remains unchanged, it can change in the second diagram at the squark-quark-gluino vertices. For the squarks only the three diagrams shown in Figure 3.4 give non-vanishing contributions. The diagrams in the first line of Fig. 3.4 are similar to the diagrams for the quark self-energy shown before, but with quarks and squarks interchanged. This reflects the fact that the gauge quantum numbers of the SM particles and their superpartners are the same. The gluon and gluino carry isospin zero. Therefore at the vertices with a gluon or gluino the other two particles must carry the same isospin. In our case the initial particles are up-type quarks or squarks respectively, so the particles in the loops must be up-type, too.

As squarks are scalar particles there are interactions possible which are not present for the corresponding SM particles, leading to new contributions to the squark self-energy. Precisely, a four sfermion interaction is possible.

The Feynman rules for the different combinations of sfermions at the four sfermion vertex can be found in [38], for example. Only diagrams with an up-type or down-type squark in the loop result in α_s -contributions. Two different color connections of the squarks at the vertex are possible for the diagram with a down-type squark in the loop. In one case the particle in the loop carries the same color as the incoming particle and thereby the same as the outgoing one and in the other case the color of the incoming particle is directly connected to that of the outgoing particle and the color of the particle in the loop is arbitrary. Thus, in the sum

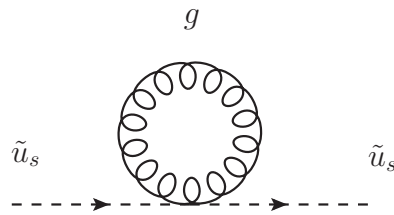


Figure 3.5: Diagram for the interaction of two squarks with two gluons.

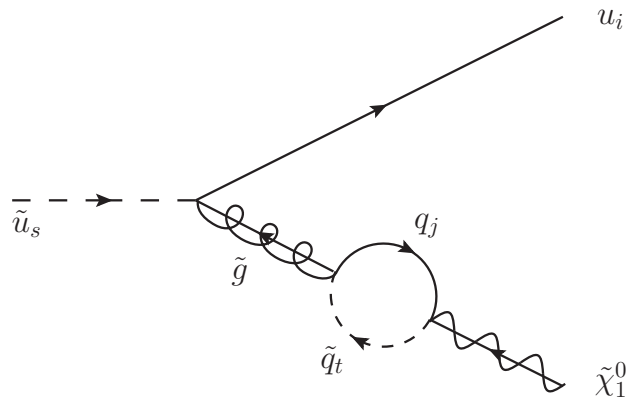


Figure 3.6: Possible diagram with a loop in the neutralino leg.

over the colors the latter contribution will acquire a relative factor of three regarding the first case. This is the reason why then, if the particles are correctly assigned to the legs of the vertex, the contributions of the two different color connections for a down-type squark in the loop cancel in the sum over the colors. So in total, only the diagram with an up-type squark in the loop as shown in Figure 3.4 will contribute to the self-energy of the squark.

Another vertex, which is not present in the Standard Model, is the interaction of two gluons with two squarks, leading to the diagram shown in Fig. 3.5. The amplitude of this diagram is proportional to the integral of the gluon propagator over the loop momentum. So in dimensional regularization we have

$$\mathcal{M} \propto \int d^d k \frac{1}{k^2} \propto A_0(0) , \quad (3.116)$$

where $A_0(0)$ is the scalar one-point function [75]. But since

$$A_0(0) = 0 , \quad (3.117)$$

the amplitude is zero. Therefore the amplitude for the diagram in Figure 3.5 vanishes due to the gluon being massless.

The only diagram with a loop in the neutralino leg leading to an amplitude proportional to the strong coupling constant α_s is shown in Figure 3.6. As the gluino is part of a color octet whereas the neutralino is a color singlet, the amplitude for the diagram vanishes, however. This can be understood by inspection of the two vertices in the loop: the squark-quark-gluino coupling contributes an $SU(3)_C$ generator $T_{\alpha\beta}^a$ with the color indices α and β of the quark

and the squark in the loop and a denoting the gluino index. By contrast, the squark-quark-neutralino vertex is color-diagonal which means that the vertex contains a factor $\delta_{\alpha\beta}$. Thus, the amplitude is proportional to the trace of the $SU(3)_C$ generator. As the T^a are traceless, the amplitude vanishes. Therefore there are no neutralino self-energies which contribute at $\mathcal{O}(\alpha_s)$. This is why the neutralino field was not renormalized in the discussion of the renormalization procedure in Sec. 3.2.1.

3.2.4. Kinematics of the Decay

In this section it will be shown by general considerations that the kinematic structure of the transition amplitude is independent of the choice of the reference frame.

Using the Feynman rules according to the Lagrangian (3.44) the generic structure of the transition amplitude for the decay of the squark into a quark and a neutralino reads

$$\mathcal{M} = \bar{u}_i(p_1, \lambda_1)(C_R \mathcal{P}_R + C_L \mathcal{P}_L)_{ij} v_j(p_2, \lambda_2) , \quad (3.118)$$

with u and v being the spinors of the quark and the neutralino, respectively, with momenta p_1 and p_2 and helicities λ_1 and λ_2 . The couplings are denoted by C_L and C_R and the indices $i, j = 1, \dots, 4$ are spinor indices and the Einstein sum convention is employed. The constant factor resulting from the Feynman rules for the squark is absorbed in C_L and C_R . Higher-order corrections modify C_L and C_R but not the kinematic structure of the decay amplitude investigated here.

The absolute value of Eq. (3.118) squared is

$$|\mathcal{M}|^2 = \bar{u}_i(p_1, \lambda_1)(C_R \mathcal{P}_R + C_L \mathcal{P}_L)_{ij} v_j(p_2, \lambda_2) \cdot v_k^\dagger(p_2, \lambda_2)(C_R \mathcal{P}_R + C_L \mathcal{P}_L)_{kl}^\dagger (\bar{u}_l(p_1, \lambda_1))^\dagger , \quad (3.119)$$

where k and l are two additional spinor indices. In this notation the order of the factors is arbitrary. Using $\bar{u} = u^\dagger \gamma_0$, $\gamma_0 \mathcal{P}_R = \mathcal{P}_L \gamma_0$ and $\gamma_0 \gamma_0 = \mathbf{1}$, Eq. (3.119) becomes

$$|\mathcal{M}|^2 = u_l(p_1, \lambda_1) \bar{u}_i(p_1, \lambda_1)(C_R \mathcal{P}_R + C_L \mathcal{P}_L)_{ij} v_j(p_2, \lambda_2) \bar{v}_k(p_2, \lambda_2)(C_R^* \mathcal{P}_L + C_L^* \mathcal{P}_R)_{kl} . \quad (3.120)$$

To derive the unpolarized transition amplitude the sum rules

$$\sum_{\lambda} u_i(p, \lambda) \bar{u}_j(p, \lambda) = (\not{p} + m)_{ij} \quad (3.121a)$$

$$\sum_{\lambda} v_i(p, \lambda) \bar{v}_j(p, \lambda) = (\not{p} - m)_{ij} , \quad (3.121b)$$

are used, where m denotes the mass of the particle. Then, the square of the transition amplitude is

$$\sum_{\lambda_1, \lambda_2} |\mathcal{M}|^2 = (\not{p}_1 + m_1)_{li} (C_R \mathcal{P}_R + C_L \mathcal{P}_L)_{ij} (\not{p}_2 - m_2)_{jk} (C_R^* \mathcal{P}_L + C_L^* \mathcal{P}_R)_{kl} \quad (3.122)$$

$$= \text{Tr} \{ (\not{p}_1 + m_1)(C_R \mathcal{P}_R + C_L \mathcal{P}_L)(\not{p}_2 - m_2)(C_R^* \mathcal{P}_L + C_L^* \mathcal{P}_R) \} . \quad (3.123)$$

Using the relations for the Dirac γ matrices (see Appendix B) this results in

$$\sum_{\lambda_1, \lambda_2} |\mathcal{M}|^2 = \text{Tr} \left\{ |C_R|^2 \frac{\mathbf{1} - \gamma_5}{2} \not{p}_1 \not{p}_2 + |C_L|^2 \frac{\mathbf{1} + \gamma_5}{2} \not{p}_1 \not{p}_2 - m_1 m_2 C_R^* C_L \frac{\mathbf{1} - \gamma_5}{2} - m_1 m_2 C_L^* C_R \frac{\mathbf{1} + \gamma_5}{2} \right\} \quad (3.124a)$$

$$= \frac{1}{2} (|C_R|^2 + |C_L|^2) \text{Tr} \{ \not{p}_1 \not{p}_2 \} - \frac{1}{2} m_1 m_2 \text{Tr} \{ \mathbf{1} \} (C_R^* C_L + C_L^* C_R) \quad (3.124b)$$

$$= (|C_R|^2 + |C_L|^2) [m_{\tilde{q}}^2 - m_1^2 - m_2^2] - 2m_1 m_2 (C_R^* C_L + C_L^* C_R) . \quad (3.124c)$$

In the last step

$$\text{Tr} \{ \not{p}_1 \not{p}_2 \} = 4p_1^\mu p_{2\mu} \quad (3.125a)$$

$$= 2 \left[(p_{1\mu} + p_{2\mu})^2 - p_1^2 - p_2^2 \right] \quad (3.125b)$$

$$= 2 \left[s - m_1^2 - m_2^2 \right] \quad (3.125c)$$

was used together with the Mandelstam variable $s = m_{\tilde{q}}^2$ for the decay of a squark \tilde{q} with mass $m_{\tilde{q}}$. In the special case of the decay $\tilde{u}_1 \rightarrow (c, u)\tilde{\chi}_1^0$ with vanishing charm- or up-quark mass and $r^2 = m_{\tilde{\chi}_1^0}^2/m_{\tilde{u}_1}^2$ with $m_{\tilde{\chi}_1^0}$ denoting the mass of the neutralino it is

$$\sum_{\lambda_1, \lambda_2} |\mathcal{M}|^2 = (|C_R|^2 + |C_L|^2) m_{\tilde{u}_1}^2 (1 - r^2). \quad (3.126)$$

The results (3.124c) and (3.126) show that the squared amplitude consists of the couplings and constant factors in terms of masses, independently of the reference frame. For the process $\tilde{u}_1 \rightarrow (c, u)\tilde{\chi}_1^0$ at tree-level this means, that for the calculation of the decay width (3.7) for a massless charm- or up-quark one only has to replace the integral by Eqs. (3.126) and (3.23) and insert the couplings (3.47) and (3.48).

3.3. Real Corrections: Gluon Radiation

In this section the real corrections at NLO to the decay $\tilde{u}_1 \rightarrow (c, u)\tilde{\chi}_1^0$ will be calculated. First, the relevant Feynman diagrams and transition amplitudes are given in Section 3.3.1. Then in Section 3.3.2, the three-particle phase space and the amplitudes will be reparametrized to make use of dimensional regularization in order to extract the IR divergences. As explained above they will cancel with the ones coming from the virtual corrections. The final result is given in Section 3.3.3.

3.3.1. Feynman Diagrams and Amplitudes

The partial decay width containing the real corrections in Eq. (3.38b) reads

$$\Gamma_{\text{real}} = \frac{1}{2m_{\tilde{q}}} \int |\overline{\mathcal{M}_{\text{real}}}|^2 d\Phi_3, \quad (3.127)$$

where $m_{\tilde{q}}$ is the mass of the decaying squark and \mathcal{M} is the transition amplitude. As only NLO corrections with respect to the strong interaction are considered in this thesis there are only two diagrams contributing to the transition amplitude in Eq. (3.127). Namely, a gluon can be radiated either from the final state (FSR) or from the initial state (ISR), as depicted in Figure 3.7. The transition amplitude for FSR will be denoted by \mathcal{M}_1 and the one for ISR will be called \mathcal{M}_2 . The final states of the two diagrams shown in Figure 3.7 are indistinguishable so that $|\overline{\mathcal{M}_{\text{real}}}|^2$ is given by

$$|\overline{\mathcal{M}_{\text{real}}}|^2 = |\mathcal{M}_1 + \mathcal{M}_2|^2 \quad (3.128a)$$

$$= |\mathcal{M}_1|^2 + |\mathcal{M}_2|^2 + 2\text{Re}\{\mathcal{M}_1 \mathcal{M}_2^\dagger\}. \quad (3.128b)$$

In the following, p is the four-momentum of the decaying squark and $p_1, \lambda_1, p_2, \lambda_2$ and k, r are the four-momenta and polarizations of the quark, the neutralino and the gluon, respectively.

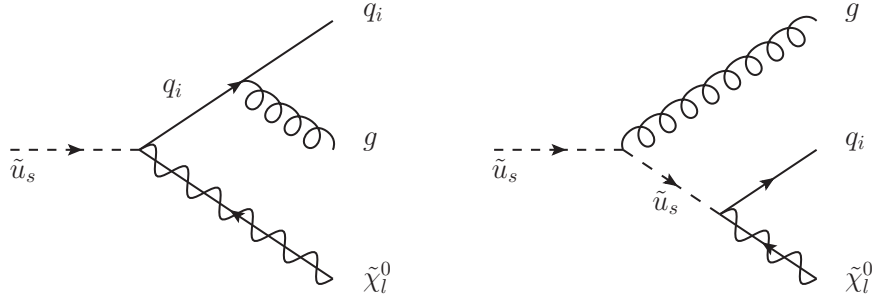


Figure 3.7: Final state radiation (left) and initial state radiation (right) of a gluon.

Accordingly, the mass of the quark will now be denoted by m_1 and the mass of the neutralino by m_2 . Applying the Feynman rules the two amplitudes read

$$i\mathcal{M}_1 = g_s T^a \bar{u}(p_1, \lambda_1) \gamma_\mu \epsilon_r^{\mu*}(k) \frac{(\not{p}_1 + \not{k} + m_1)}{2(p_1 k)} \cdot [C_L \mathcal{P}_L + C_R \mathcal{P}_R] v(p_2, \lambda_2) \delta(p - p_1 - p_2 - k), \quad (3.129)$$

$$i\mathcal{M}_2 = g_s T^a \bar{u}(p_1, \lambda_1) [C_L \mathcal{P}_L + C_R \mathcal{P}_R] v(p_2, \lambda_2) \frac{-1}{2(pk)} \cdot \epsilon_r^{\mu*}(k) (2p_\mu - k_\mu) \delta(p - p_1 - p_2 - k), \quad (3.130)$$

where g_s is the strong gauge coupling constant, T^a the $SU(3)_C$ generator, u and v are the spinors for the quark and the neutralino and ϵ^μ is the polarization vector of the gluon. In accordance with Section 3.2.4 the coupling of squark, quark and neutralino is written as $[C_L \mathcal{P}_L + C_R \mathcal{P}_R]$. Note, that in Eqs. (3.129) and (3.130) momentum conservation at each vertex is directly used to determine the momentum of the internal particle. Since the gluon is on-shell only transverse components will take part, so that $\epsilon^\mu k_\mu$ is equal to zero and the polarization sum for the gluons is given by [10]

$$\sum_r \epsilon_r^{\mu*}(k) \epsilon_r^\nu(k) = -g^{\mu\nu}. \quad (3.131)$$

Squaring Eqs. (3.129) and (3.130) and suppressing the arguments of the spinors and the polarization vectors leads to

$$|\mathcal{M}_1|^2 = \frac{g_s^2 C_F}{4(p_1 k)^2} \text{Tr} \left\{ u \bar{u} \gamma^\mu (\not{p}_1 + \not{k} + m_1) [C_L \mathcal{P}_L + C_R \mathcal{P}_R] v \bar{v} \cdot [C_L^* \mathcal{P}_R + C_R^* \mathcal{P}_L] \gamma_0 (\not{p}_1^\dagger + \not{k}^\dagger + m_1) \gamma^{\nu\dagger} \gamma_0 \epsilon_\mu^* \epsilon_\nu \right\}, \quad (3.132)$$

$$|\mathcal{M}_2|^2 = \frac{g_s^2 C_F}{(pk)^2} \text{Tr} \left\{ u \bar{u} [C_L \mathcal{P}_L + C_R \mathcal{P}_R] p_\mu \epsilon^{\mu*} \epsilon^\nu p_\nu v \bar{v} [C_L^* \mathcal{P}_R + C_R^* \mathcal{P}_L] \right\}. \quad (3.133)$$

Here, the color structure of the amplitudes has already been evaluated using [76]

$$\sum_a T_{bc}^a T_{cd}^a = C_F \delta_{bd} \quad \text{with} \quad C_F = \frac{N^2 - 1}{2N} \quad (3.134)$$

for the generators T_{bc}^a of a group $SU(N)$. Applying the polarization sums (3.121) and (3.131) and using the relations for the gamma matrices (see Appendix B) we arrive at

$$\begin{aligned} |\overline{\mathcal{M}_1}|^2 &= \frac{-g_s^2 C_F}{4(p_1 k)^2} \text{Tr} \left\{ 4(m_1^3 + m_1(p_1 k) + m_1^2 \not{p}_1 + (m_1^2 - (p_1 k)) \not{k}) \right. \\ &\quad \cdot \frac{1}{2} \left(\not{p}_2 (|C_L|^2 + |C_R|^2) + \not{p}_2 \gamma_5 (|C_L|^2 - |C_R|^2) \right. \\ &\quad \left. \left. - m_2 (C_L C_R^* + C_R C_L^*) + m_2 \gamma_5 (C_L C_R^* - C_R C_L^*) \right) \right\}, \end{aligned} \quad (3.135)$$

$$\begin{aligned} |\overline{\mathcal{M}_2}|^2 &= \frac{-g_s^2 C_F m_q^2}{2(pk)^2} \text{Tr} \left\{ (\not{p}_1 + m_1) \left(\not{p}_2 (|C_L|^2 + |C_R|^2) + \not{p}_2 \gamma_5 (|C_L|^2 - |C_R|^2) \right. \right. \\ &\quad \left. \left. - m_2 (C_L C_R^* + C_R C_L^*) + m_2 \gamma_5 (C_L C_R^* - C_R C_L^*) \right) \right\}. \end{aligned} \quad (3.136)$$

Evaluation of the traces (note, that all terms proportional to γ_5 drop out) leads to the final result

$$\begin{aligned} |\overline{\mathcal{M}_1}|^2 &= \frac{-2g_s^2 C_F}{(p_1 k)^2} \left[(m_1^2(p_1 p_2) + (p_2 k)(m_1^2 - (p_1 k))) (|C_L|^2 + |C_R|^2) \right. \\ &\quad \left. - m_2 (m_1^3 + m_1(p_1 k)) (C_L C_R^* + C_R C_L^*) \right], \end{aligned} \quad (3.137)$$

$$|\overline{\mathcal{M}_2}|^2 = \frac{-2g_s^2 C_F m_q^2}{(pk)^2} \left[(p_1 p_2) (|C_L|^2 + |C_R|^2) - m_1 m_2 (C_L C_R^* + C_R C_L^*) \right]. \quad (3.138)$$

The interference term in Eq. (3.128b) is calculated in analogy to the two terms already shown. Therefore only important intermediate results are presented here. Using Eqs. (3.129) and (3.130) we arrive at

$$\begin{aligned} \mathcal{M}_1 \mathcal{M}_2^\dagger &= 2g_s^2 C_F \bar{u} \not{\ell} \frac{(\not{p}_1 + \not{k} + m_1)}{2(p_1 k)} [C_L \mathcal{P}_L + C_R \mathcal{P}_R] v \\ &\quad \cdot p_\mu \epsilon^\mu \frac{-1}{2(pk)} \bar{v} \gamma_0 [C_L^* \mathcal{P}_L + C_R^* \mathcal{P}_R] \gamma_0 u. \end{aligned} \quad (3.139)$$

The spin summed mixed term then reads

$$\begin{aligned} \overline{\mathcal{M}_1 \mathcal{M}_2^\dagger} &= \frac{g_s^2 C_F}{4(pk)(p_1 k)} \text{Tr} \left\{ (\not{p}_1 + m_1) (2(m_1^2 + (p_1 k) + (p_1 p_2) + (p_2 k)) + m_1 \not{k} - \not{k} \not{p}_2) \right. \\ &\quad \left(\not{p}_2 (|C_L|^2 + |C_R|^2) + \not{p}_2 \gamma_5 (|C_L|^2 - |C_R|^2) \right. \\ &\quad \left. \left. - m_2 (C_L C_R^* + C_R C_L^*) + m_2 \gamma_5 (C_L C_R^* - C_R C_L^*) \right) \right\} \end{aligned} \quad (3.140)$$

and after evaluating the trace the final result is

$$\begin{aligned} \text{Re} \{ \overline{\mathcal{M}_1 \mathcal{M}_2^\dagger} \} &= \frac{g_s^2 C_F}{2(pk)(p_1 k)} \left[(|C_L|^2 + |C_R|^2) (2m_1^2(p_2 k) - 2m_2^2(p_1 k)) \right. \\ &\quad + 4(p_1 p_2) (m_1^2 + (p_1 k) + (p_1 p_2) + (p_2 k)) \\ &\quad \left. + (C_L C_R^* + C_R C_L^*) (-m_1 m_2 (m_1^2 + 3(p_1 k) + (p_1 p_2) - (p_2 k))) \right]. \end{aligned} \quad (3.141)$$

3.3.2. Re-Parametrization of the Phase Space and the Amplitudes

In Section 3.1.3 it was shown that the three-particle phase space needed for the real corrections contains a two-particle phase space and remaining integrations which will reveal the

IR divergences. The integrals needed for this calculation were already calculated in [77], for example. In order to use the results derived in that work, the phase space integral and the amplitudes have to be adopted to the notation employed there.

First of all, the new integration variables are defined by

$$y = \frac{2(p_1 k)}{m_{\bar{q}}^2(1-r)^2}, \quad (3.142)$$

$$z = \frac{2(p_1 p_2)}{m_{\bar{q}}^2(1-r^2)}, \quad (3.143)$$

with

$$r^2 = \frac{m_2^2}{m_{\bar{q}}^2} \quad (3.144)$$

as before. From Eqs. (3.142) and (3.143) it is possible to derive all other dot products of four-momenta needed for the amplitudes of Section 3.3.1. They are given by

$$(p_1 k) = \frac{m_{\bar{q}}^2}{2}(1-r)^2 y, \quad (3.145a)$$

$$(p_1 p_2) = \frac{m_{\bar{q}}^2}{2}(1-r^2)z, \quad (3.145b)$$

$$(p_1 p) = \frac{m_{\bar{q}}^2}{2}(1-r)^2 y + \frac{m_{\bar{q}}^2}{2}(1-r^2)z + m_1^2, \quad (3.145c)$$

$$(k p) = \frac{m_{\bar{q}}^2}{2}(1-r^2)(1-z) - \frac{m_1^2}{2}, \quad (3.145d)$$

$$(p_2 k) = \frac{m_{\bar{q}}^2}{2}(1-r^2)(1-z) - \frac{m_{\bar{q}}^2}{2}(1-r)^2 y - \frac{m_1^2}{2}, \quad (3.145e)$$

$$(p_2 p) = \frac{m_{\bar{q}}^2}{2}(1+r^2) - \frac{m_{\bar{q}}^2}{2}(1-r)^2 y - \frac{m_1^2}{2}. \quad (3.145f)$$

In the following transformation of the integral m_1 is set to zero for simplicity as it is the mass of a quark which is light in comparison to the mass of the decaying squark. The three-particle phase space has been given in Eq. (3.37) and is here repeated for convenience,

$$d\Phi_3 = \frac{1}{8} \frac{d\Omega_{d-1}}{(2\pi)^{d-1}} \frac{d\Omega_{d-2}}{(2\pi)^{d-2}} dp_1^0 dk^0 d\cos\theta \left[p_1^0 k^0 (1 - \cos^2\theta) \right]^{-\epsilon} \delta(\cos\theta - \cos\theta_0). \quad (3.146)$$

From Eqs. (3.145) p_1^0 and k^0 can be extracted in the rest frame of the decaying particle as

$$(pk) = p^0 k^0 - \vec{p}\vec{k} = m_{\bar{q}} k^0 \quad (3.147a)$$

$$\Leftrightarrow k^0 = \frac{m_{\bar{q}}}{2}(1-r^2)(1-z) \quad (3.147b)$$

and

$$(pp_1) = p^0 p_1^0 - \vec{p}\vec{p}_1 = m_{\bar{q}} p_1^0 \quad (3.148a)$$

$$\Leftrightarrow p_1^0 = \frac{m_{\bar{q}}}{2}(1-r)^2 y + \frac{m_{\bar{q}}}{2}(1-r^2)z. \quad (3.148b)$$

Variable transformation of the integrand in Eq. (3.146) leads to

$$f(p_1^0, k^0) dp_1^0 dk^0 = g(y, z) |\det \mathcal{J}| dy dz, \quad (3.149)$$

where \mathcal{J} is the Jacobi matrix of the variable transformation $(p_1^0, k^0) \rightarrow (y, z)$ which can be obtained from the definitions of p_1^0 and k^0 in Eqs. (3.147) and (3.148). The absolute value of its determinant is then given by

$$|\det \mathcal{J}| = \frac{m_{\bar{q}}^2}{4} (1-r)^2 (1-r^2), \quad (3.150)$$

and we obtain

$$f(p_1^0, k^0) dp_1^0 dk^0 = g(y, z) \frac{m_{\bar{q}}^2}{4} (1-r)^2 (1-r^2) dy dz. \quad (3.151)$$

The transformed integrand $g(y, z)$ as well as the integration bounds for y and z will be determined in the following.

3.3.2.1. Integration Bounds

The integration bounds for y and z can be derived using the properties of the dot products of Section 3.3.2. In addition, the following properties of $r^2 = m_2^2/m_{\bar{q}}^2$ are implicitly used:

$$m_{\bar{q}} > 0 \quad \text{and} \quad 0 \leq m_2^2 < m_{\bar{q}}^2 \quad (3.152a)$$

$$\Rightarrow r^2 \in [0, 1) \quad \text{and} \quad r \in [0, 1) \quad (3.152b)$$

$$\Rightarrow 1-r > 0 \quad \text{and} \quad 1-r^2 > 0. \quad (3.152c)$$

Bounds for the z -Integration

The upper bound in the rest frame of the decaying particle is found to be

$$(kp) = p^0 k^0 - \vec{p} \vec{k} = p^0 k^0 \geq 0 \quad (3.153a)$$

$$\Leftrightarrow \frac{m_{\bar{q}}^2}{2} (1-r^2)(1-z) \geq 0 \quad (3.153b)$$

$$\Leftrightarrow 1-z \geq 0 \quad (3.153c)$$

$$\Leftrightarrow z \leq 1. \quad (3.153d)$$

For the lower bound, we first show that

$$(p_1 p_2) = p_1^0 p_2^0 - \sqrt{p_1^{02} - m_1^2} \sqrt{p_2^{02} - m_2^2} \cos \varphi \geq 0 \quad (3.154)$$

with φ denoting the angle between the momenta \vec{p}_1 and \vec{p}_2 . Consider

1. Case $\cos \varphi > 0$:

Since $p_i^{02} - m_i^2 \leq p_i^{02}$, $i = 1, 2$ holds

$$(p_1 p_2) \geq p_1^0 p_2^0 (1 - \cos \varphi) \geq p_1^0 p_2^0 (1 - 1) = 0. \quad (3.155)$$

2. Case $\cos \varphi < 0$:

It is $(p_1 p_2) = p_1^0 p_2^0 + \sqrt{p_1^{02} - m_1^2} \sqrt{p_2^{02} - m_2^2} |\cos \varphi|$.

Since $p_i^{02} = m_i^2 + |\vec{p}_i|^2 \geq m_i^2$ it is $\sqrt{p_i^{02} - m_i^2} \geq 0$ for $i = 1, 2$ and thus $(p_1 p_2) \geq 0$.

Now Eq. (3.145b) can be applied to get the lower bound for z by

$$(p_1 p_2) \geq 0 \quad (3.156a)$$

$$\Leftrightarrow \frac{m_{\bar{q}}^2}{2} (1-r^2) z \geq 0 \quad (3.156b)$$

$$\Leftrightarrow z \geq 0. \quad (3.156c)$$

So the result is

$$z \in [0, 1] . \quad (3.157)$$

Bounds for the y -Integration

The lower bound is directly obtained from (3.145a). Recall, that θ is the angle between \vec{p}_1 and \vec{k} . Then, since $\cos \theta \leq 1$ holds

$$(p_1 k) = p_1^0 k^0 (1 - \cos \theta) \geq 0 \quad (3.158a)$$

$$\Leftrightarrow \frac{m_q^2}{2} (1 - r)^2 y \geq 0 \quad (3.158b)$$

$$\Leftrightarrow y \geq 0 . \quad (3.158c)$$

For the upper bound denoted by \hat{y} consider again (3.145a) but with $\cos \theta = -1$:

$$\frac{m_q^2}{2} (1 - r)^2 \hat{y} = 2p_1^0 k^0 \Big|_{y=\hat{y}} \quad (3.159a)$$

$$\Leftrightarrow (1 - r)^2 \hat{y} = (1 - r)^2 \hat{y} (1 - r^2) (1 - z) + (1 - r^2)^2 z (1 - z) \quad (3.159b)$$

$$\Leftrightarrow \hat{y} (1 - (1 - r^2) (1 - z)) = (1 + r)^2 z (1 - z) \quad (3.159c)$$

$$\Leftrightarrow \hat{y} = \frac{(1 + r)^2 z (1 - z)}{z + r^2 (1 - z)} , \quad (3.159d)$$

where k^0 and p_1^0 were replaced by Eqs. (3.147b) and (3.148b), respectively. We therefore have

$$y \in [0, \hat{y}] \quad \text{with} \quad \hat{y} = \frac{(1 + r)^2 z (1 - z)}{z + r^2 (1 - z)} . \quad (3.160)$$

Note that the upper bound for y depends on z so that the order of integration is not arbitrary any more.

3.3.2.2. Transformation of the Integrand

The integrand consists of the three-particle phase space of Eq. (3.146) and the amplitudes squared of Section 3.3.1.

Phase Space

Comparison of Eq. (3.149) with Eq. (3.146) yields

$$f(p_1^0, k^0) = \left[p_1^{02} k^{02} (1 - \cos^2 \theta) \right]^{-\epsilon} . \quad (3.161)$$

For the case of $m_1 = 0$ with $(p_1 k) = p_1^0 k^0 (1 - \cos \theta)$ we have

$$(p_1^0 k^0)^2 = \frac{(p_1 k)^2}{(1 - \cos \theta)^2} . \quad (3.162)$$

Inserting this into Eq. (3.161) and replacing the dot product using Eq. (3.145a) leads to

$$g(y, z) = \left[\frac{m_q^4}{4} (1 - r)^4 y^2 \frac{1 + \cos \theta}{1 - \cos \theta} \right]^{-\epsilon} . \quad (3.163)$$

The remaining step is to determine $\cos \theta_0$ in terms of y and z since carrying out the $\cos \theta$ integration returns a factor $(1 + \cos \theta_0)/(1 - \cos \theta_0)$ in the integrand. Starting with the initial condition

$$p_1^0 + \sqrt{(\vec{p} - \vec{p}_1 - \vec{k})^2 + m_{\bar{q}}^2} + k^0 - m_{\bar{q}} = 0, \quad (3.164)$$

the extraction of $\cos \theta_0$ is straight forward. By introducing r and the dot products of Eqs. (3.145) the result is

$$\cos \theta_0 = \frac{m_{\bar{q}}^2(1 - r^2) - 2(pp_1) - 2(pk) + 2p_1^0 k^0}{2p_1^0 k^0}, \quad (3.165)$$

and therefore the factor in the integrand becomes

$$\frac{1 + \cos \theta_0}{1 - \cos \theta_0} = \frac{4p_1^0 k^0 + m_{\bar{q}}^2(1 - r^2) - 2((pp_1) + (pk))}{-m_{\bar{q}}^2(1 - r^2) + 2((pp_1) + (pk))}. \quad (3.166)$$

Using dot products of Eqs. (3.145) again, yields

$$2((pp_1) + (pk)) = 2m_{\bar{q}}^2 - 2(pp_2) \quad (3.167a)$$

$$= m_{\bar{q}}^2(1 - r^2) + m_{\bar{q}}^2(1 - r)^2 y \quad (3.167b)$$

and Eq. (3.166) simplifies to

$$\frac{1 + \cos \theta_0}{1 - \cos \theta_0} = \frac{4p_1^0 k^0 - m_{\bar{q}}^2(1 - r)^2 y}{m_{\bar{q}}^2(1 - r)^2 y}. \quad (3.168)$$

By further replacing p_1^0 and k^0 through Eqs. (3.147) and (3.148) we get

$$\frac{1 + \cos \theta_0}{1 - \cos \theta_0} = y^{-1} \left[(1 + r)^2 z(1 - z) - y(z + r^2(1 - z)) \right] \quad (3.169a)$$

$$= y^{-1}(\hat{y} - y)(z + r^2(1 - z)) \quad (3.169b)$$

with \hat{y} from Eq. (3.160). The result for the term in the integrand coming from the phase space is then given by

$$g(y, z) = \left[\frac{m_{\bar{q}}^4}{4} (1 - r)^4 y^2 \right]^{-\epsilon} \left[y^{-1}(\hat{y} - y)(z + r^2(1 - z)) \right]^{-\epsilon}. \quad (3.170)$$

Now everything can be put together and the three-particle phase space in $d = 4 - 2\epsilon$ dimensions using Eq. (3.37) reads

$$\begin{aligned} d\Phi_3 &= \frac{1 - r^2}{32(2\pi)^4 \Gamma(1 - \epsilon)} (m_{\bar{q}}^2)^{1-2\epsilon} (1 - r)^{2-4\epsilon} (4\pi)^{3\epsilon} \\ &\cdot \int_0^1 \int_0^{\hat{y}} y^{-\epsilon} (\hat{y} - y)^{-\epsilon} (z + r^2(1 - z))^{-\epsilon} dy dz. \end{aligned} \quad (3.171)$$

The corresponding result for the two-particle phase space as derived in Section 3.1.2.1 is

$$d\Phi_2 = \frac{d\Omega_{d-1}}{8(2\pi)^2} \frac{1}{(m_{\bar{q}}^2)^\epsilon} (1 - r^2)^{1-2\epsilon} (4\pi)^{2\epsilon} \quad (3.172)$$

and therefore

$$\begin{aligned} d\Phi_3 = d\Phi_2 \frac{1}{4(2\pi)^2} (4\pi)^\epsilon (m_q^2)^{1-\epsilon} (1-r)^2 \frac{1}{\Gamma(1-\epsilon)} \left(\frac{1+r}{1-r} \right)^{2\epsilon} \\ \cdot \int_0^1 \int_0^{\hat{y}} y^{-\epsilon} (\hat{y}-y)^{-\epsilon} (z+r^2(1-z))^{-\epsilon} dy dz . \end{aligned} \quad (3.173)$$

The factorization shown for the general case in Section 3.1.3 is demonstrated here explicitly by Eq. (3.173). Both Eq. (3.171) and (3.173) are in agreement with Ref. [77].

Amplitudes

The amplitudes have been given in terms of dot products of four-momenta in Section 3.3.1. The latter are now replaced using Eqs. (3.145) and the amplitudes are then written such that the integrals given in Table I of Ref. [77] can be identified directly. Setting $m_1 = 0$ and defining

$$C := 2g_s^2 C_F (|C_L|^2 + |C_R|^2) , \quad (3.174)$$

the amplitudes become

$$\overline{|\mathcal{M}_1|^2} = C \left[\frac{-1}{(1-r)^2} (1-r)^2 + \frac{1+r}{1-r} \left(\frac{1}{y} \right) - \frac{1+r}{1-r} \left(\frac{z}{y} \right) \right] , \quad (3.175)$$

$$\overline{|\mathcal{M}_2|^2} = C \frac{2(1+r)^2}{1-r^2} \left[\left(\frac{1}{(1+r)^2(1-z)} \right) + \frac{1}{2} \left(\frac{-2}{(1+r)^2(1-z)^2} \right) \right] , \quad (3.176)$$

and

$$2\text{Re}\{\overline{\mathcal{M}_1 \mathcal{M}_2^\dagger}\} = C \frac{1+r}{1-r} \left[-2 \left(\frac{1}{y} \right) + \left(\frac{2}{(1-z)y} \right) - 2r^2 \left(\frac{1}{(1+r)^2(1-z)} \right) \right] . \quad (3.177)$$

3.3.3. Divergences and Finite Terms

To complete the calculation of the partial decay width resulting from FSR and ISR in Eq. (3.127) the integrals over y and z have to be evaluated. The remaining two-particle phase space in Eq. (3.173) only contributes a factor

$$d\Phi_2 = \frac{1}{8\pi} (1-r^2) , \quad (3.178)$$

as shown in Section 3.1.2.1. It is not necessary to keep the two-particle phase space in $d = 4 - 2\epsilon$ dimensions due to the arguments given at the end of Section 3.1.3. The same factor for the phase space also applies for the decay width at tree-level and for the virtual corrections in Eq. (3.38b).

Using the results for the integrals given in Ref. [77], the singular terms coming from the

amplitudes in Eqs. (3.175) to (3.177) appear as poles in ϵ

$$\overline{|\mathcal{M}_1|^2}\Big|_{yz} = C \frac{1+r}{1-r} \left[-\frac{1}{2\epsilon} - \frac{5}{4} - \frac{1}{2(1-r^2)} - \frac{r^4}{2(1-r^2)^2} \ln r^2 + \ln(1-r^2) \right], \quad (3.179)$$

$$\overline{|\mathcal{M}_2|^2}\Big|_{yz} = C \frac{1+r}{1-r} \left[\frac{1}{\epsilon} + \frac{4-2r^2}{1-r^2} + \frac{2r^4}{(1-r^2)^2} \ln r^2 - 2 \ln(1-r^2) \right], \quad (3.180)$$

$$\begin{aligned} 2\text{Re}\{\overline{\mathcal{M}_1\mathcal{M}_2^\dagger}\}\Big|_{yz} &= C \frac{1+r}{1-r} \left[\frac{1}{\epsilon^2} + \frac{2}{\epsilon}(1 - \ln(1-r^2)) + 6 - \frac{5\pi^2}{6} \right. \\ &\quad \left. - \frac{2r^2}{1-r^2} - 4 \ln(1-r^2) + 2 \ln^2(1-r^2) \right. \\ &\quad \left. - \frac{2r^2}{(1-r^2)^2} \ln r^2 + 2\text{Li}_2(1-r^2) \right]. \end{aligned} \quad (3.181)$$

The sum of all contributions then reads

$$\begin{aligned} \overline{|\mathcal{M}_{\text{real}}|^2}\Big|_{yz} &= C \frac{1+r}{1-r} \left[\frac{1}{\epsilon^2} + \frac{1}{\epsilon} \left(\frac{5}{2} - 2 \ln(1-r^2) \right) + \frac{35}{4} - \frac{5\pi^2}{6} \right. \\ &\quad \left. - \frac{1}{2(1-r^2)} - 5 \ln(1-r^2) + 2 \ln^2(1-r^2) \right. \\ &\quad \left. + \frac{r^2(3r^2-4)}{2(1-r^2)^2} \ln r^2 + 2\text{Li}_2(1-r^2) \right]. \end{aligned} \quad (3.182)$$

In terms of Eq. (3.43) now the total decay width with renormalized quantities in the amplitudes can be written as

$$\Gamma = \frac{1}{2m_{\tilde{q}}} \int \left(\overline{|\mathcal{M}_{\text{tree}}|^2} + \overline{|\mathcal{M}_{\text{virt}}|^2} + \overline{|\mathcal{M}_{\text{real}}|^2}\Big|_{yz} \right) d\Phi_2 \quad (3.183)$$

and the IR divergences will cancel in the integrand. This is not checked analytically here since the virtual corrections which contain the counterpart to the IR divergences of the real corrections are not calculated by hand. However, a numerical check was performed with the use of Eq. (3.182) proving that all divergences are canceled in Eq. (3.183). Terms of $\mathcal{O}(\epsilon^0)$ are the finite contributions to the decay width coming from ISR and FSR.

3.4. Four-Body Decay

As explained in Section 2.2.4, once the mass difference between the lightest up-type squark and the neutralino becomes small and in particular smaller than the mass of the W boson, the four-body decay of the squark is a competing process to the flavor changing two-body decay into a charm- or an up-quark and a neutralino. The calculation of the decay width for the four-body decay is not part of this work, but was performed by other members of our research group. Here, only some basic facts shall be mentioned.

There are many different diagrams contributing to the four-body decay of the squark. Exemplarily, two Feynman diagrams are shown in Figure 3.8. The left one shows the decay with an internal top-quark and a W boson. Thus, there is no suppression due to FCNC couplings at the squark-quark-neutralino vertex. Then the off-shell top decays via its dominant decay mode into a bottom-quark and an off-shell W boson which subsequently decays into a fermion-anti-fermion pair. The final state is hence given by $\tilde{\chi}_1^0 b f f'$. The fermion-anti-fermion

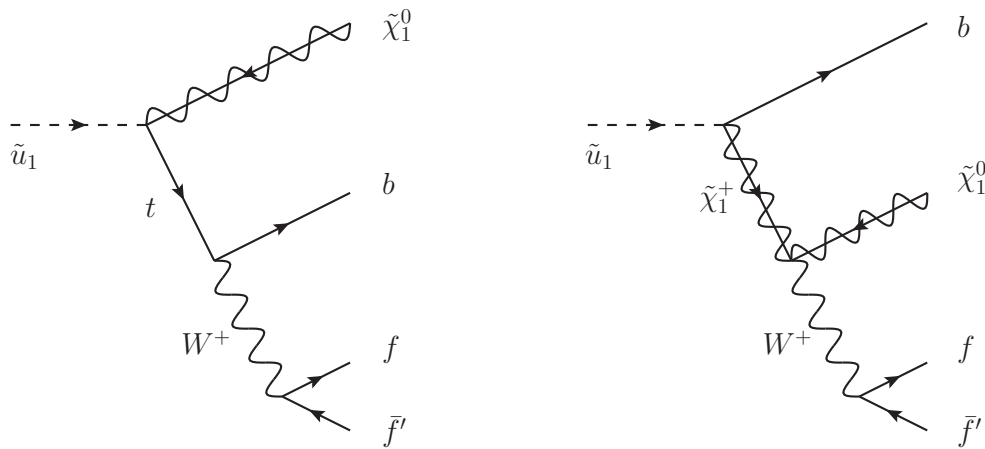


Figure 3.8: Examples for contributions to the four-body decay.

pair $f\bar{f}'$ consists of leptons in about a third, and of quarks in about two third of the cases, corresponding to the branching ratios of the leptonic and hadronic decay modes of the W boson.

The same final state can be reached in the diagram on the right of Figure 3.8, where the internal particles are a chargino $\tilde{\chi}_1^+$ and a W boson. Also other diagrams are possible involving charged Higgs bosons, squarks and gluinos. However, all internal particles in these diagrams are heavier than the top-quark and the W boson. Additionally, in the amplitude for the left diagram the first two vertex factors are proportional to the dominant elements of the squark rotation matrix and the CKM matrix. Thus, the diagram on the left is expected to give the largest contribution to the four-body decay.

This has been confirmed by explicit calculation. Results and consequences for the detection of the lightest up-type squark \tilde{u}_1 are presented in Chapter 5.

This chapter aims at describing the implementation of the calculation shown in Chapter 3 and on the procedure of deriving the numerical results. This includes the calculation itself, the generation of the particle spectrum (see Section 4.2) and the check whether all constraints coming from experiments are satisfied (Section 4.3).

4.1. Implementation of the Calculation

In Chapter 3 all components needed for the analytical expression for the decay width were derived. For the numerical calculation of the decay width, basically Eq. (3.183) needs to be implemented. The two-particle phase space in $d = 4$ dimensions is given by Eq. (3.178) and the transition amplitude resulting from the real corrections is given by Eq. (3.182). The tree-level part and the virtual contributions are given in Eq. (3.126), where the couplings C_L and C_R are given by the expressions within the brackets in Eqs. (3.78) and (3.79) with the renormalization constants replaced by the formulas given in Section 3.2.2.2.

All these formulas have been implemented in a Fortran program. The analytic formulas for the real corrections have been derived by hand, as well as the renormalization procedure and the counterterms. The transition amplitudes for the leading order, the vertex corrections and the self-energies have been generated using `FeynArts` [78] and `FormCalc` [79] and the resulting formulas have been exported to a Fortran code which has then been implemented in the Fortran program. To check that the divergences are canceled, the UV divergent parts of the amplitudes have been extracted using built-in functions of `FormCalc` and it has been verified that the UV divergent parts of the counterterms and the vertex corrections cancel. For the IR divergences the option, provided by `LoopTools` [79], to isolate the contributions proportional to ϵ^{-1} or ϵ^{-2} in the loop integrals, together with the implementation of the divergent parts in Eq. (3.182) has been used to check the cancellation of the IR divergences numerically. The Fortran program features the SUSY Les Houches Accord 2 (SLHA2) [51], which means that all parameters like masses, couplings and mixing angles have to be provided in the SLHA2 format. The calculation and the program have been checked against an independent calculation and implementation by another member of our research group [60].

One feature concerning the implementation of the real corrections shall be highlighted here. The transition amplitude for the real contributions in Eq. (3.182) contains a term proportional to a dilogarithm, which cannot be decomposed into ordinary logarithms any further. As no

built-in function for the dilogarithm is available in Fortran, an own implementation of the expansions series [80]

$$\text{Li}_2(z) = \sum_{k=1}^{\infty} \frac{z^k}{k^2}; \quad |z| < 1 \quad (4.1)$$

has been used. In the case of Eq. (3.182) the argument z is given by $1 - r^2$. Recalling that $r^2 = m_2^2/m_{\tilde{q}}^2$ and $m_2 < m_{\tilde{q}}$ the condition $|z| < 1$ is fulfilled for $m_2 \neq 0$.

4.2. Spectrum Generator

In order to calculate the particle spectrum, the couplings and the mixing matrices, a spectrum generator is used. The spectrum generator itself requires inputs, containing information about the physical model which shall be used, input parameters of the Standard Model (SM) and inputs related to the model of interest. In this work **SPheno** [81, 82] is used for this purpose. Both input and output of the spectrum generator are in the SLHA format.

As explained in Sections 2.2.2 and 2.2.3, the MSSM with a general flavor structure is used here. Therefore the SLHA2 [51] format is chosen for both the input and output files. The model used in this work and the model specific parameters have been explained in Section 2.2.2. For convenience they are stated here again,

$$m_{\tilde{L}_1} = m_{\tilde{L}_2}, \quad m_{\tilde{L}_3}, \quad (4.2)$$

$$m_{\tilde{E}_1} = m_{\tilde{E}_2}, \quad m_{\tilde{E}_3}, \quad (4.3)$$

$$m_{\tilde{Q}_1} = m_{\tilde{Q}_2}, \quad m_{\tilde{Q}_3}, \quad (4.4)$$

$$m_{\tilde{U}_1} = m_{\tilde{U}_2}, \quad m_{\tilde{U}_3}, \quad (4.5)$$

$$m_{\tilde{D}_1} = m_{\tilde{D}_2}, \quad m_{\tilde{D}_3}, \quad (4.6)$$

$$M_1, \quad M_2, \quad M_3 \quad (4.7)$$

are the flavor-diagonal soft SUSY breaking masses,

$$\mu, \quad m_A, \quad \tan \beta \quad (4.8)$$

are the higgsino mass parameter, the pseudoscalar mass and the ratio of the two vevs of the two Higgs doublets and

$$A_t, \quad A_b, \quad A_\tau \quad (4.9)$$

are the trilinear couplings for the particles of the third generation. Other inputs are the SM parameters

$$G_F, \quad \alpha_s^{\overline{\text{MS}}}(M_Z), \quad m_{Z,\text{pole}}, \quad m_b^{\overline{\text{MS}}}(m_b), \quad m_{t,\text{pole}}, \quad m_{\tau,\text{pole}}, \quad V_{\text{CKM}}, \quad (4.10)$$

where G_F is the Fermi constant, $m_{Z,\text{pole}}$ the pole mass of the Z -boson, $\alpha_s^{\overline{\text{MS}}}(M_Z)$ the strong coupling constant in the $\overline{\text{MS}}$ scheme at the scale M_Z , $m_b^{\overline{\text{MS}}}(m_b)$ the running mass of the b -quark in the $\overline{\text{MS}}$ scheme at the scale m_b , $m_{t,\text{pole}}$ and $m_{\tau,\text{pole}}$ the pole masses of the top-quark and the τ -lepton and V_{CKM} is the CKM-matrix. Both input and output parameters of the spectrum are evaluated at the scale $Q = 300$ GeV. The spectrum generator reads in the input values and determines via RGE running the particle spectrum, the couplings and mixing matrices iteratively and provides the resulting spectrum at the desired scale Q . More information can be found in Refs. [81, 82].

Some general features concerning the relevant parameters for the decay $\tilde{u}_1 \rightarrow (c, u)\tilde{\chi}_1^0$ can be understood by neglecting the general flavor structure and thus assuming the lightest up-type

squark to be the lightest stop \tilde{t}_1 . The masses of the stop mass eigenstates \tilde{t}_1 and \tilde{t}_2 are given by (see [59], for example)

$$m_{\tilde{t}_{1,2}}^2 = \frac{1}{2}(m_{\tilde{U}_3}^2 + m_{\tilde{Q}_3}^2) + \frac{1}{4}m_Z^2 \cos 2\beta + m_t^2 \mp \left\{ \left[\frac{1}{2}(m_{\tilde{Q}_3}^2 - m_{\tilde{U}_3}^2) + m_Z^2 \cos 2\beta \left(\frac{1}{4} - \frac{2}{3} \sin^2 \theta_W \right) \right]^2 + m_t^2 (\mu \cot \beta - A_t)^2 \right\}^{\frac{1}{2}}. \quad (4.11)$$

In the case of general mixing the strongest influence comes from $m_{\tilde{U}_3}$, $m_{\tilde{Q}_3}$, A_t and $\tan \beta$, although the other soft SUSY-breaking parameters also play a role. In particular for the mixing matrices, all soft SUSY-breaking masses are relevant. The neutralino mass matrix reads [38]

$$\mathcal{M}_{\text{neut}} = \begin{pmatrix} M_1 & 0 & -M_Z c_\beta s_W & M_Z s_\beta s_W \\ 0 & M_2 & M_Z c_\beta c_W & -M_Z s_\beta c_W \\ -M_Z c_\beta s_W & M_Z c_\beta c_W & 0 & -\mu \\ M_Z s_\beta s_W & -M_Z s_\beta c_W & -\mu & 0 \end{pmatrix}, \quad (4.12)$$

where the upper two rows correspond to the bino and wino states and the lower two rows to the higgsino states. Thus, the mixing of gauginos and higgsinos is given by the upper right and lower left 2×2 matrices and is of $\mathcal{O}(M_Z)$. Assuming that $M_1, M_2, |\mu| \gg M_Z$ the masses of the four neutralinos are dominated by M_1 , M_2 and $|\mu|$. In order to understand which parameters are important for a light neutralino, also the chargino masses have to be considered. They are given by [38]

$$M_{\tilde{\chi}_{2,1}^\pm} = \frac{1}{2} \left[|M_2^2| + |\mu^2| + 2M_W^2 \pm \left\{ (|M_2^2| - |\mu^2|)^2 + 4M_W^4 \cos^2 2\beta + 4M_W^2 (|M_2^2| + |\mu^2| + 2\text{Re}(M_2\mu) \sin 2\beta) \right\}^{\frac{1}{2}} \right]. \quad (4.13)$$

From Eq. (4.13) it can be inferred that if either M_2 or $|\mu|$ is much smaller than the other one, respectively, the mass of the light chargino $M_{\tilde{\chi}_1^\pm}$ is dominated by the lighter parameter of M_2 and $|\mu|$. Thus, if the light neutralino is obtained by taking low values for M_2 or $|\mu|$, also at least one chargino has a small mass. In order to see to what extent this is possible the lower limits for chargino masses have to be considered [83]. A light neutralino can always be obtained for a small value of M_1 , which already implies that presumably the lightest neutralino will be bino-like. A way to enlarge the higgsino component of the lightest neutralino is given by $\tan \beta$ which governs the mixing of gauginos and higgsinos.

The leading terms for the mass squared of the lightest CP -even Higgs boson h^0 with $m_A \gg m_Z$ are [84–86]

$$m_{h^0}^2 = m_Z^2 \cos^2 2\beta + \frac{3g^2 m_t^4}{8\pi^2 m_W^2} \left[\log \left(\frac{m_S^2}{m_t^2} \right) + X_t^2 \left(1 - \frac{X_t^2}{12} \right) \right] + \dots, \quad (4.14)$$

where y_t and m_t are the Yukawa coupling and the mass of the top-quark, $m_S^2 = m_{\tilde{t}_1} m_{\tilde{t}_2}$ and $X_t = (A_t + \mu \cot \beta)/m_S$. As can be inferred from Eq. (4.14), the Higgs boson mass can be raised to the measured value of ~ 125 GeV through large stop masses and/or large mixing. The impact of these parameters on the masses of the particles and thereby on the decay widths and branching ratios will be studied in Chapter 5.

4.3. Experimental Constraints

No SUSY particle has been observed so far. Nevertheless, exclusion limits for these particles have been deduced from their non-observation. In the numerical analysis these limits are taken into account. In addition it is checked whether the spectrum used is compatible with the LHC Higgs data, with the measured relic density and with the limits on the strengths of flavor changing neutral currents. In Section 4.3.1 the constraints coming from the Higgs discovery will be presented, followed by the constraints from the Dark Matter measurement in Section 4.3.2. Afterwards the effects on flavor observables at low energy will be checked (Section 4.3.3) and finally the current mass exclusion limits for SUSY particles will be discussed.

4.3.1. Higgs

As explained in Section 2.2.2, in the MSSM there are five Higgs bosons and it is possible that one of them has properties similar to the SM Higgs boson such that the discovered Higgs boson could also be a SUSY Higgs boson. This means that the Higgs sector of the SUSY spectrum must be compatible with the measurement of one SM-like Higgs boson and the non-observation of the remaining four Higgs particles.

The compatibility with the experimental Higgs data is checked with the programs `HiggsBounds` and `HiggsSignals` [87–89]. `HiggsBounds` takes as inputs the effective couplings of the considered model normalized to the SM values, the masses and the widths of the Higgs bosons and checks their compatibility with the non-observation of the SUSY Higgs bosons. The result is the information, whether the spectrum is excluded at 95% CL with respect to measurements at Tevatron and LHC or not. `HiggsSignals`, on the other hand, which takes the same input, validates the compatibility of the Higgs sector of the spectrum with the data from the observation of a Higgs boson. Here, the result is given as a p -value. To be consistent, in this work a p -value of at least 0.05 is demanded for a positive result, corresponding to a non-exclusion at 95% CL.

In order to perform these checks, the effective couplings and the widths which serve as inputs for the above programs have to be calculated. To this end, the program `HDECAY` [90] is used here in a modified version both for the SUSY Higgs bosons and for the SM Higgs particle. The original version of `HDECAY` features the SLHA1 format, where only left- and right-mixing in the squark and slepton sector is taken into account. In this work, also the mixing of different generations is considered, and therefore the spectrum is given in the SLHA2 format. In order to avoid rewriting the program to account for the SLHA2, a transformation of the SLHA2 format to the SLHA1 format is used. More precisely, the 2×2 matrices mixing the left- and right-handed states of the third generation sfermions have to be extracted from the 6×6 matrix mixing both the left- and right-handed components and the flavors. Moreover, the dominating flavors of all sfermions have to be identified among the mass-ordered states \tilde{f}_s , $s = 1 \dots 6$.

To retrieve the 2×2 matrices for the mixing of the left- and right-handed components of the third generation sfermions, consider the definitions of the mixing matrices of the SLHA1 [91]

$$\begin{pmatrix} \tilde{f}_1 \\ \tilde{f}_2 \end{pmatrix} = \begin{pmatrix} F_{11} & F_{12} \\ F_{21} & F_{22} \end{pmatrix} \begin{pmatrix} \tilde{f}_L \\ \tilde{f}_R \end{pmatrix}, \quad (4.15)$$

and of the SLHA2 [51]

$$\begin{pmatrix} \tilde{f}_1 \\ \tilde{f}_2 \\ \tilde{f}_3 \\ \tilde{f}_4 \\ \tilde{f}_5 \\ \tilde{f}_6 \end{pmatrix} = \begin{pmatrix} F_{11} & \dots & \dots & \dots & \dots & F_{16} \\ \vdots & \ddots & & & & \vdots \\ \vdots & & \ddots & & & \vdots \\ \vdots & & & \ddots & & \vdots \\ \vdots & & & & \ddots & \vdots \\ F_{61} & \dots & \dots & \dots & \dots & F_{66} \end{pmatrix} \begin{pmatrix} \tilde{f}_{1L} \\ \tilde{f}_{2L} \\ \tilde{f}_{3L} \\ \tilde{f}_{1R} \\ \tilde{f}_{2R} \\ \tilde{f}_{3R} \end{pmatrix}, \quad (4.16)$$

where \tilde{f} stands for either up-type squarks or down-type squarks or sleptons. Here, the focus is on squarks. It is possible to identify the dominating flavors of the mass ordered states by inspection of the matrix. The main contribution to the mass ordered states on the left-hand side comes from one single flavor as usually the flavor off-diagonal elements are small, in order to account for the restrictions due to flavor observables. Thus, it is possible to search for the column with the largest element in each row of the 6×6 matrix in Eq. (4.16) and determine the flavor origin of the mass state \tilde{f}_s according to the flavor ordered states on the right-hand side. The third generation sfermion mixing matrices for the SLHA1 format are then determined by the third and sixth element of the rows, where the largest contribution comes from either the third or the sixth element. Due to mass ordered states and flavor mixing, the rows where this is the case, can change. Hence, a scan over all rows is necessary. Note, that the order in mass of the identified states is already correct by scanning from row one to row six as both in the SLHA1 and the SLHA2, the states on the left-hand side are mass ordered.

The absolute value of the determinant of the extracted 2×2 matrix can serve as a check whether the correct elements are extracted and whether the assumption that flavor-changing effects are small, is reasonable. If the flavor off-diagonal elements are small, the absolute value of the determinant of the 2×2 matrices will be close to one. Not affecting the mixing angle, the sign of the determinant is unimportant. If the absolute value of the determinant significantly deviates from one, either the wrong elements are taken from the 6×6 matrix, or flavor-changing effects are important. An additional check is provided by ensuring that exactly two states are found with the largest contribution coming from a particular third generation sfermion.

In the SLHA1 format the squark states are flavor ordered, whereas in the SLHA2 format they are mass ordered. Therefore the squark masses given in the SLHA2 spectrum have to be assigned to a certain flavor to account for the SLHA1 format. In order to achieve this, the mass of the mass eigenstate is associated with the flavor and left- or right-handed component according to the position of the largest element in the 6×6 matrix of Eq. (4.16). This means that the reordering scheme is again based on the 6×6 mixing matrices and the assumption that the largest element in each row determines the flavor origin. For the correct mapping of the masses, see Tables 4.1 and 4.2. A possible procedure for the reordering is

1. Find the largest contribution for each row in the 6×6 matrices.
2. Determine the flavor and left/right origin of the mass state according to the right-hand side of Eq. (4.16).
3. Determine the position where the mass of this state is stored according to the SLHA-numbering (Table 4.1).
4. Relocate this mass to the position corresponding to the appropriate flavor and left/right

state found in step 2 using Table 4.2.

Mass Ordered States			
SLHA2 numbering	mass state	matrix row	position in array
1000001	\tilde{d}_1	1	6
1000003	\tilde{d}_2	2	10
1000005	\tilde{d}_3	3	14
2000001	\tilde{d}_4	4	7
2000003	\tilde{d}_5	5	11
2000005	\tilde{d}_6	6	15
1000002	\tilde{u}_1	1	8
1000004	\tilde{u}_2	2	12
1000006	\tilde{u}_3	3	16
2000002	\tilde{u}_4	4	9
2000004	\tilde{u}_5	5	13
2000006	\tilde{u}_6	6	17

Table 4.1: Table with the SLHA2 numbering for the reordering scheme from SLHA2 to SLHA1.

As an example, consider the SLHA particle identification number 1000002. According to Table 4.1 the mass assigned to this number corresponds to the mass of the \tilde{u}_1 in the SLHA2 format. If now the spectrum is interpreted in the SLHA1 format, the mass is associated with the left-handed up-squark (Table 4.1), regardless of the contribution of the up-flavor to the mass eigenstate \tilde{u}_1 . In this thesis, the largest contribution to the \tilde{u}_1 comes from the top-squarks so the mass of the \tilde{u}_1 should rather be assigned to the lightest stop with the particle number 1000006 in the SLHA1 format (see Table 4.2). The reordering scheme proposed above provides a general method for the correct mapping.

Note, that the masses now assigned to the flavor states are not exact but only approximate. The smaller the mixing, the better the approximation. The assumption that the mixing of different generations has negligible effects on the result, has to be checked in the individual case. For the cases considered in this thesis, typically, the absolute values of the determinants of the extracted 2×2 matrices were in the range of 0.995 to 1. For the determination of the Higgs decays, the described transformation is needed in the calculation of Higgs decays into gauge bosons and fermions. In these decays and the involved couplings, no flavor changing occurs at leading order. Moreover, the flavor off-diagonal elements of the matrix in Eq. (4.16) are small. Thus, the impact on the results is expected to be negligible.

4.3.2. Dark Matter

One of the motivations to investigate theories beyond the Standard Model is the observation of Dark Matter (DM). By accurate measurements of the cosmic microwave background (CMB) it is possible to draw conclusions regarding the density of DM in space. These measurements were performed by the space telescopes Planck and WMAP. Planck reported a cold dark

Flavor Ordered States		
SLHA1 numbering	flavor state	position in array
1000001	\tilde{d}_L	6
2000001	\tilde{d}_R	7
1000002	\tilde{u}_L	8
2000002	\tilde{u}_R	9
1000003	\tilde{s}_L	10
2000003	\tilde{s}_R	11
1000004	\tilde{c}_L	12
2000004	\tilde{c}_R	13
1000005	\tilde{b}_1	14
2000005	\tilde{b}_2	15
1000006	\tilde{t}_1	16
2000006	\tilde{t}_2	17

Table 4.2: Table with the SLHA1 numbering for the reordering scheme from SLHA2 to SLHA1.

matter density of [33]

$$\Omega_c h^2 = 0.1199 \pm 0.0027 . \quad (4.17)$$

As explained in Section 2.2.2 the lightest SUSY particle can be a candidate for DM. In this work the lightest neutralino is taken to be the LSP. The density for neutralino DM can be calculated and compared to the Planck measurement, which is done here with the program `SuperIso Relic` [92, 93]. Reading in the SUSY spectrum in terms of an SLHA file the program calculates the relic density. More details can be found in Refs. [92, 93]. We impose a constraint of

$$\Omega_c h^2 < 0.12 , \quad (4.18)$$

on the relic density resulting from neutralinos, which is compatible with the Planck measurement. By imposing only an upper bound, the neutralinos are not assumed to be the only source contributing to the measured relic density. However, the neutralino relic density should not exceed the measured limit.

It turns out that the parameter space for a light bino-like neutralino as LSP which satisfies the constraint in Eq. (4.18) is quite limited. This changes, if the mass of at least one neutral Higgs boson is about twice as heavy as the neutralino. In that case the resonant production of the Higgs boson is possible by the annihilation of two neutralinos and the Higgs boson can further decay into SM particles as shown in Figure 4.1. Candidates for such Higgs bosons could be the heavier CP -even Higgs boson H^0 or the pseudoscalar Higgs boson A^0 . In addition to the decay into massive fermions denoted by f and \bar{f} in Figure 4.1 both Higgs particles could also decay into other massive particles. As in the final state there are less LSPs than in the initial state, this process can lower the relic density.

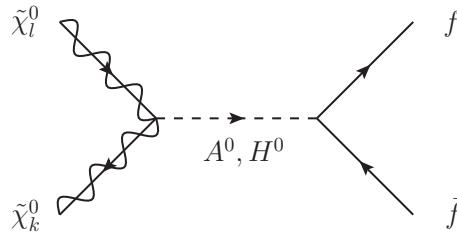


Figure 4.1: Annihilation of two neutralinos into SM particles with intermediate Higgs bosons.

4.3.3. Low Energy Flavor Observables

Loop-mediated decays can be affected by new particles running in the loops. In particular, in models where FCNCs are possible at tree-level the new particles can have significant impact on rare decays of mesons. Many of these rare decays have been measured precisely and therefore the experimental results can rule out points or regions in the parameter space of the model, where the predictions for the corresponding decays are not compatible with the measured values. In this thesis, the predictions for these rare decays are calculated with `SuperIso` [94, 95]. The program gives out the needed branching ratios. The experimental values for the branching ratios used to check for compatibility are

$$\text{BR}(B_s^0 \rightarrow \mu^+ \mu^-) = (2.9_{-0.7}^{+0.7}) \times 10^{-9} \quad [96], \quad (4.19)$$

$$\text{BR}(B^0 \rightarrow \mu^+ \mu^-) < 8.1 \times 10^{-10} \quad [97], \quad (4.20)$$

$$\text{BR}(B^- \rightarrow \tau^- \bar{\nu}_\tau) = (0.96_{-0.35}^{+0.35}) \times 10^{-4} \quad [98], \quad (4.21)$$

$$\text{BR}(B^+ \rightarrow \tau^+ \nu_\tau) = (1.83_{-0.73}^{+0.77}) \times 10^{-4} \quad [99], \quad (4.22)$$

$$\text{BR}(B \rightarrow X_s \gamma) = (3.21_{-0.52}^{+0.52}) \times 10^{-4} \quad [100], \quad (4.23)$$

where the errors are upper and lower one sigma bounds. A parameter point is ruled out if at least one BR deviates more than two standard deviations from the values given in Eqs. (4.19) to (4.23).

Supersymmetric particles can also alter the anomalous magnetic moment of the muon. The measured value is

$$\frac{g_\mu - 2}{2} = (11659209_{-6}^{+6}) \times 10^{-10} \quad [86]. \quad (4.24)$$

The SUSY contribution to the anomalous magnetic moment is demanded to be smaller than the experimental error given in Eq. (4.24). That way, the contribution is small enough that it is not possible to exclude the parameter point by this measurement. The SUSY contribution to the anomalous magnetic moment is also calculated with `SuperIso`.

4.3.4. Mass Exclusion Bounds

With the experimental exclusion limits on the sparticle masses it is possible to exclude regions of the parameter space of the specific model.

We demand the mass of the light CP-even Higgs boson to be

$$m_{h^0} = 125.5_{-3.0}^{+3.0} \text{GeV}. \quad (4.25)$$

This limit is compatible with the measured mass of the Higgs boson discovered by ATLAS and CMS [1, 2]. The large allowed interval for the Higgs boson mass accounts for the uncertainties of the spectrum generator [101]. In Section 4.3.1 the program `HiggsSignals` was used to check the compatibility of the Higgs sector of the scenario with the experimental data. The result of the check with `HiggsSignals` complies with the cut on the mass in Eq. (4.25) in most cases. Nevertheless, both tests are conducted as the latter is a pure cut on the mass of the Higgs boson while in `HiggsSignals` also its width and effective couplings are used.

Other lower bounds on the masses of the SUSY particles, which are employed in this thesis, are

$$m_{\tilde{g}} > 1.45 \text{ TeV} \quad [102] , \quad (4.26)$$

$$m_{\tilde{\chi}_1^0} > 200 \text{ GeV} \quad [57] , \quad (4.27)$$

$$m_{\tilde{u}_1} > 245 \text{ GeV} \quad [57] , \quad (4.28)$$

The limits for the lightest up-type squark and the neutralino in Eqs. (4.27) and (4.28) in combination ensure that the current experimental exclusion bound given in Ref. [57] is respected in any case. The parameter space is further constrained by requiring that

$$(m_{\tilde{u}_1} - m_{\tilde{\chi}_1^0}) \in [5, 75] \text{ GeV} . \quad (4.29)$$

Also the exclusion bounds derived in the references of Eqs. (4.26) to (4.28) are given at 95% CL. Thus, the constraints shown in the sections above altogether assure that the scenarios used for the numerical analysis in the next chapter are not excluded at at least 95% CL with respect to the observables which are considered.

As explained in Section 3.4 the four-body decay of the \tilde{u}_1 is a competing process to the two-body decay into a quark and the lightest neutralino. The four-body decay and the two-body decay were both implemented in the program `SUSY-HIT` [103] by another member of our research group. Since both decay modes are important and have to be calculated, `SUSY-HIT` has been used to derive the numerical results presented in the next Chapter instead of the own stand-alone program only covering the two-body decay. It has been checked that the results for the two-body decay in both implementations are consistent. As both the spectrum generator and `HDECAY` are launched separately, only `SDECAY` [104] has been invoked within `SUSY-HIT` in order to calculate the decay widths for the two decay modes explained before.

Little changes had to be made in all programs listed in the above sections in order to link them.

As already stated in Chapter 3, the two- and the four-body decay of the lightest up-type squark \tilde{u}_1 are competing processes in the parameter region where the mass difference of the \tilde{u}_1 and the $\tilde{\chi}_1^0$ is smaller than the W mass. Therefore in this section results for both the calculation of the FCNC two-body decay shown in Chapter 3 and the calculation of the four-body decay which was performed by other members of our research group [60] will be shown. Starting with a random scan over parameters which are relevant for these processes in Section 5.1, properties of both decay modes will be discussed, followed by an analysis of the impact of symmetries of the soft SUSY breaking parameters (Sec. 5.2).

5.1. Random Scan

In Section 4.2 it was briefly derived which input parameters of the model dominantly affect the two- and four-body decays. Consequently a random scan over the parameters

$$m_{\tilde{Q}_3}, \quad m_{\tilde{U}_3}, \quad A_t, \quad M_1, \quad m_A \quad \text{and} \quad \tan\beta \quad (5.1)$$

was performed. The scan ranges for these parameters are

$$m_{\tilde{Q}_3} \in [1000, 1500] \text{ GeV}, \quad (5.2)$$

$$m_{\tilde{U}_3} \in [300, 600] \text{ GeV}, \quad (5.3)$$

$$A_t \in [1000, 2000] \text{ GeV}, \quad (5.4)$$

$$M_1 \in [220, 500] \text{ GeV}, \quad (5.5)$$

$$m_A \in [400, 1000] \text{ GeV}, \quad (5.6)$$

$$\tan\beta \in [1, 15]. \quad (5.7)$$

All other parameters are fixed to

$$\begin{aligned} M_2 &= 650 \text{ GeV}, \\ M_3 &= 1530 \text{ GeV}, \\ \mu &= 900 \text{ GeV}, \end{aligned} \quad (5.8)$$

and

$$A_q = A_l = 0 , \quad (5.9)$$

with $q = u, d, c, s, b$ and $l = e, \mu, \tau$. The soft SUSY breaking masses for the sleptons are chosen to be

$$m_{\tilde{L}, \tilde{E}} = 1000 \text{ GeV} , \quad (5.10)$$

and the ones for the squarks are set to

$$m_{\tilde{Q}_i} = m_{\tilde{U}_i} = 1500 \text{ GeV} , \quad i = 1, 2 \quad (5.11)$$

and

$$m_{\tilde{D}} = 1500 \text{ GeV} . \quad (5.12)$$

The SM parameters were set to

$$G_F = 1.16637 \cdot 10^{-5} , \quad (5.13)$$

$$\alpha_s^{\overline{\text{MS}}}(M_Z) = 0.1184 , \quad (5.14)$$

$$m_{Z, \text{pole}} = 91.1876 \text{ GeV} , \quad (5.15)$$

$$m_b^{\overline{\text{MS}}}(m_b) = 4.25 \text{ GeV} , \quad (5.16)$$

$$m_{t, \text{pole}} = 173.3 \text{ GeV} , \quad (5.17)$$

$$m_{\tau, \text{pole}} = 1.777 \text{ GeV} , \quad (5.18)$$

and

$$\lambda = 0.2257 , \quad A = 0.814 , \quad \bar{\rho} = 0.135 , \quad \bar{\eta} = 0.349 \quad (5.19)$$

for the CKM matrix in the Wolfenstein parametrization, as given by the Particle Data Group [105]. Moreover, the masses of the first and second generation of quarks and leptons are set to zero. Note that $m_{\tilde{U}_3}$ is chosen to be small to get a light up-type squark and not $m_{\tilde{Q}_3}$ since a low $m_{\tilde{Q}_3}$ would also lead to a rather light down-type squark. At the beginning of Section 2.2.4 it was emphasized that the mass difference of \tilde{u}_1 and $\tilde{\chi}_1^0$

$$\Delta m = m_{\tilde{u}_1} - m_{\tilde{\chi}_1^0} \quad (5.20)$$

is an important quantity for the phenomenology of the decay of the \tilde{u}_1 which is why the results will be presented with respect to this mass difference Δm . To avoid threshold effects when the difference is close to the charm-quark mass or the W boson mass, the results are restricted to a range of

$$\Delta m \in [5, 75] \text{ GeV} , \quad (5.21)$$

and all parameter points shown in the following plots pass all constraints explained in Section 4.3. First, we will focus on the two-body decay $\tilde{u}_1 \rightarrow (c, u)\tilde{\chi}_1^0$. The scatter plot in Fig. 5.1 shows the partial decay width of the two-body decay with Δm on the horizontal axis, taking into account both the up- and the charm-quark final state. There is a considerable spreading of the results for a fixed mass difference of the \tilde{u}_1 and the $\tilde{\chi}_1^0$ over up to six orders of magnitude. For example at $\Delta m \approx 5 \text{ GeV}$ the decay width attains values reaching from about 10^{-14} GeV to 10^{-8} GeV . The \tilde{u}_1 is dominantly composed of stop flavor states (Sec. 2.2.4 and 4.2), so that the two-body decay into a charm- or an up-quark is mediated by the flavor off-diagonal elements in the mixing matrix for the squarks. These elements can vary over several orders of magnitude, depending on the choice of the input parameters of the model. Hence, it is possible that different combinations of input parameters yield the same mass difference of

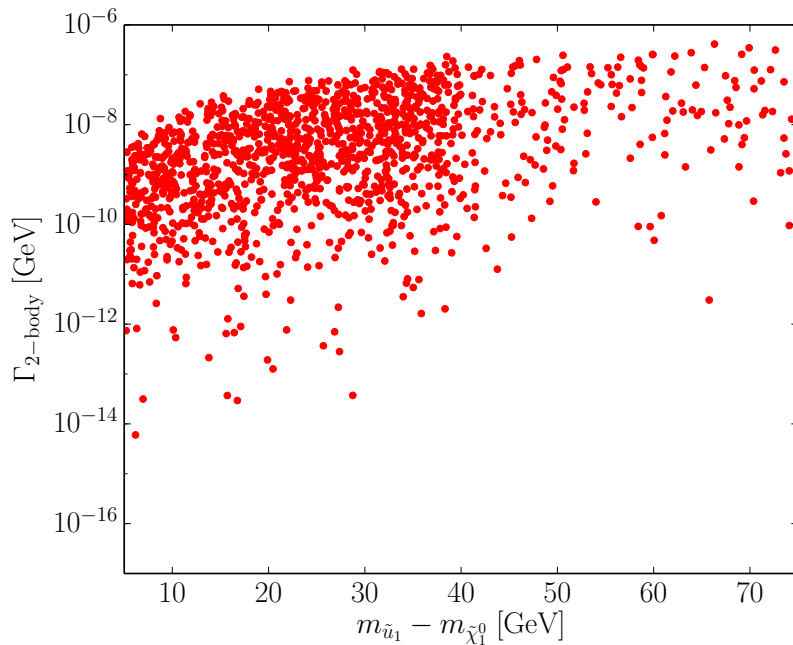


Figure 5.1: Partial decay width of the two-body decay $\tilde{u}_1 \rightarrow (c, u)\tilde{\chi}_1^0$ for the scan over the parameter range of Eqs. (5.2) to (5.7).

the \tilde{u}_1 and the $\tilde{\chi}_1^0$, but result in considerably different mixing matrix elements. This is the reason for the large spreading in Fig. 5.1.

In Ref. [106] it was already shown that if the mass difference of the LSP and the NLSP is sufficiently small, the relic density is low enough to be compatible with experimental data. However, if the mass difference is too high, the relic density becomes too high as well. The points in Fig. 5.1 fulfill the upper bound on the relic density also for larger mass differences, because in this case the described resonant annihilation of two neutralinos into the heavier CP -even Higgs boson or the pseudoscalar Higgs boson reduces the relic density to values compatible with the measured value. This can take place if

$$2m_{\tilde{\chi}_1^0} \approx m_{H^0, A^0} . \quad (5.22)$$

In the region with $\Delta m \lesssim 40$ GeV the density of possible parameter points is much higher than for $\Delta m \gtrsim 40$ GeV. In the scan over the parameter space m_A and M_1 were varied. These parameters influence the masses of the the two Higgs bosons and the neutralino in Eq. (5.22). Thus the condition (5.22) is only fulfilled by accident and it becomes clear that in the range of the mass difference where the resonant annihilation is necessary to acquire the correct relic density, less scenarios satisfy all constraints.

In order to investigate the relative strength of the decay into the up-quark compared to the decay into the charm-quark, the ratio of the partial decay widths R_{uc} is calculated as

$$R_{uc} = \frac{\Gamma_{u\tilde{\chi}_1^0}}{\Gamma_{c\tilde{\chi}_1^0}} , \quad (5.23)$$

with $\Gamma_{u\tilde{\chi}_1^0}$ and $\Gamma_{c\tilde{\chi}_1^0}$ being the partial decay widths of the decays into up- and charm-quark, respectively. The result is depicted in Figure 5.2(a) and shows that the contribution of the

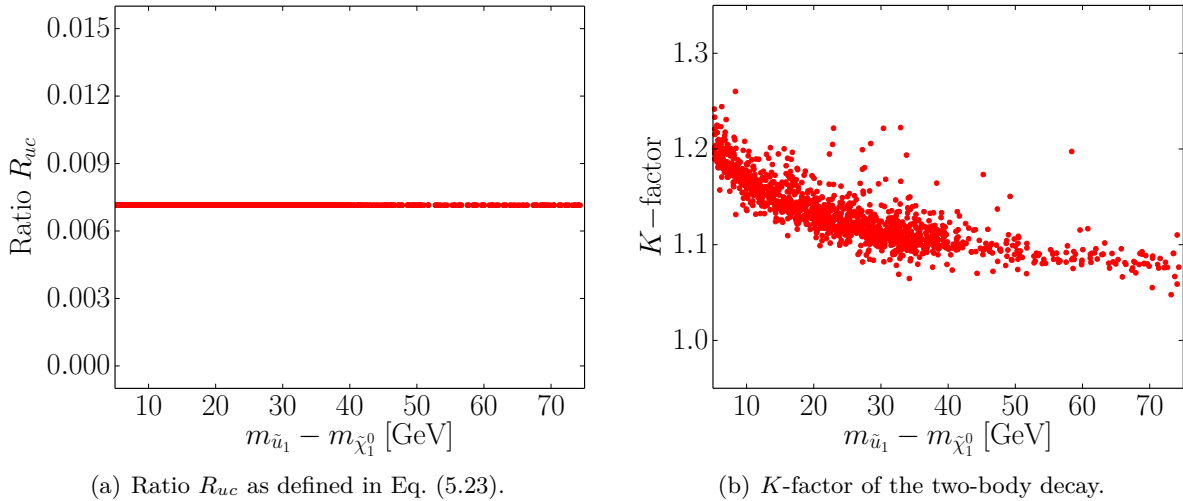


Figure 5.2: Results for the two-body-decay.

decay into the up-quark amounts to less than one percent in comparison to the decay into the charm-quark. Furthermore, the ratio remains constant for all parameter points and the complete range of the mass difference. This can be understood, knowing that the amplitudes of the two decays only differ by the corresponding element of the squark mixing matrix. As the flavor off-diagonal elements are generated through RGE running involving loop processes with CKM matrix elements, the ratio R_{uc} can be estimated by the relative size of the respective CKM matrix elements [53]

$$\left| \frac{V_{ub}}{V_{cb}} \right|^2 \approx 0.0075, \quad (5.24)$$

being in good agreement with the results in Figure 5.2(a). Although the absolute values of the two flavor off-diagonal mixing matrix elements involved in the two decay widths can vary over a wide range, *cf.* Fig. 5.1, their relative strength remains constant.

Next, the impact of the NLO corrections presented in Chapter 3 on the decay width is analyzed. A measure for the contribution of the NLO corrections is given by the K -factor defined as

$$K = \frac{\Gamma_{\text{NLO}}}{\Gamma_{\text{LO}}}, \quad (5.25)$$

where Γ_{NLO} is the NLO SUSY-QCD decay width and Γ_{LO} denotes the LO decay width. The K -factor for all parameter points of the random scan is shown in Figure 5.2(b). The NLO corrections become more important for lower values of the mass difference between the \tilde{u}_1 and the $\tilde{\chi}_1^0$ and roughly amount to 5 to 25 %.

In the following, results for the four-body decay $\tilde{u}_1 \rightarrow \tilde{\chi}_1^0 d_i f \bar{f}'$ are shown. Here, d_i , $i = 1, 2, 3$ denotes a down-type quark and the fermion-anti-fermion pair $f \bar{f}'$ stands for either a quark-anti-quark pair or a charged lepton with the corresponding neutrino. In Figure 5.3 the partial decay widths of both the two- and the four-body decay are presented, taking into account all final states for each of the two decay modes. The results for the four-body decay exhibit a fundamentally different behavior than the ones for the two-body decay: While the results for the two-body decay are distributed over a wide region all points for the four-body decay are concentrated on a small band, implying that the four-body decay essentially depends on the mass difference. This is only possible, if it only weakly depends on the strength of the flavor

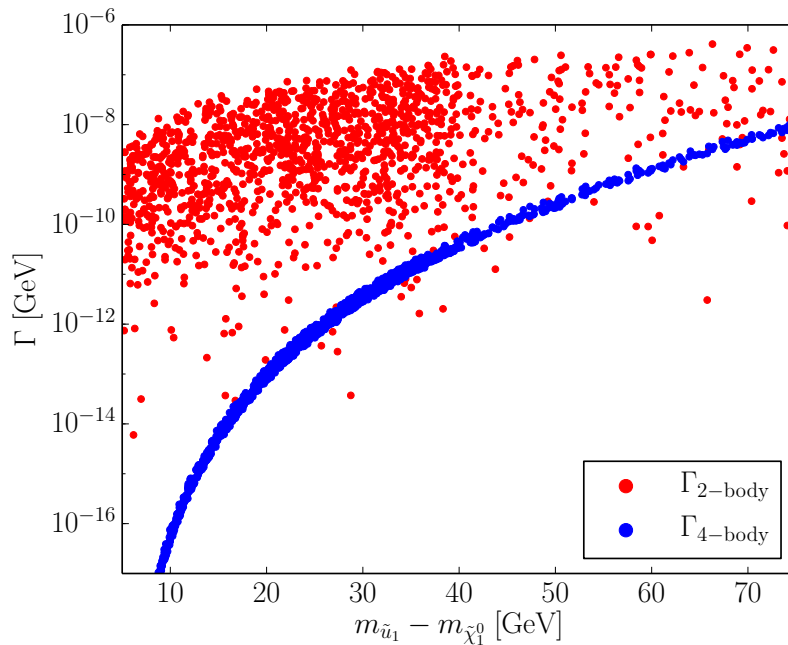


Figure 5.3: Partial decay widths.

off-diagonal elements in the squark mixing matrix, since the results for the two-body decay have shown that they vary over several orders of magnitude. Consequently, the Feynman diagrams where only the dominant elements of the mixing matrices are involved must give the largest contribution to the decay width. An example for such a diagram is given in Figure 3.8 (left). At the first vertex the squark mixing matrix element between the \tilde{u}_1 and the top flavor is picked, which is the largest one as the \tilde{u}_1 is mostly a stop. The second vertex involves the element V_{tb} of the CKM-matrix, again being the dominant one. The intermediate top quark could also be replaced by a charm- or an up-quark since the \tilde{u}_1 is not a flavor eigenstate. But if these diagrams gave a considerable contribution, a spreading of the partial decay width of the four-body decay would be expected, similar to the case of the two-body decay. With the two-body and four-body decay widths the total decay width of the \tilde{u}_1 can be calculated by

$$\Gamma_{\text{tot}} = \Gamma_{2\text{-body}} + \Gamma_{4\text{-body}} . \quad (5.26)$$

The total decay width is shown in Fig. 5.4(a) and dominated by the two-body decay width which is in most cases at least two orders of magnitude larger than the four-body decay width (see Fig. 5.3). Supposing a distance of $50 \mu\text{m}$ is sufficient to detect a particle decay as displaced vertex [107] the life-time τ of the particle must be

$$\tau \gtrsim \frac{50 \mu\text{m}}{c} = 1.67 \cdot 10^{-13} \text{ s} , \quad (5.27)$$

assuming that the speed of the particle is approximately given by $c \approx 3 \cdot 10^8 \text{ m/s}$ [86]. In terms of the decay law (3.2) the life-time of a particle is defined as the time when the number of particles in the probe has decreased to $N_0 e^{-1}$. The decay width is related to the lifetime through

$$\Gamma = \frac{\hbar}{\tau} . \quad (5.28)$$

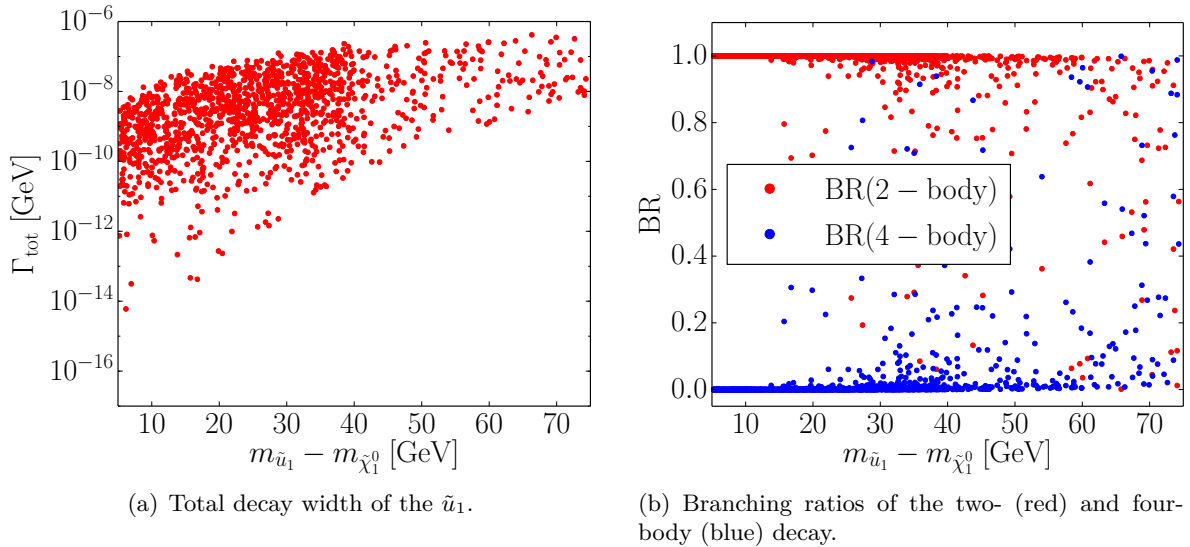


Figure 5.4: The \tilde{u}_1 total decay width (left) and two- and four-body decay branching ratios (right).

With $\hbar \approx 6.582 \cdot 10^{-25}$ GeVs [86] the threshold for observing a displaced vertex is

$$\Gamma_{\text{disp}} \lesssim 3.95 \cdot 10^{-12} \text{ GeV} . \quad (5.29)$$

If the resolution of the detector is higher than assumed in Eq. (5.27) the upper bound for a displaced vertex will increase accordingly. Applying this to the total decay width reveals that for most of the scenarios in this scan it is not possible to detect the decay of the \tilde{u}_1 as displaced vertex. The only exceptions are a few points at the lower end of the mass difference.

Taking a travel distance of $d = 1 \cdot 10^{-15}$ m for a color charged particle to hadronize [108] the upper bound for hadronization is found to be

$$\Gamma_{\text{had}} \lesssim 0.20 \text{ GeV} . \quad (5.30)$$

Thus the \tilde{u}_1 will hadronize in all scenarios found in the random scan. Naturally, the question arises if the hadronization will influence the decay of the \tilde{u}_1 and thereby its signature. This problem is known in flavor physics and a heavy-mass expansion can be used to calculate inclusive decay rates of hadrons which contain a heavy and a light quark [109]. Then the dominant contribution is given by the perturbative calculation at parton level and long-distance bound state effects are suppressed by inverse powers of the mass of the heavy parton. In Ref. [109] this expansion is used to calculate decays of B mesons. As the mass of the \tilde{u}_1 is much higher than the mass of the b quark, the heavy-mass expansion can be expected to hold here as well, resulting in the fact that the hadronization will not have a strong impact on the decay of the \tilde{u}_1 .

The branching ratios depicted in Fig. 5.4(b) illustrate once again that the two-body decay is dominant for most of the parameter points. In these cases, the assumption made for the experimental analysis that the branching ratio into a charm-quark and the neutralino in the parameter region $\Delta m < m_W$ is one, can be confirmed (see Sec. 2.2.4 and Ref. [57]). However, inferring from Figure 5.4(b) our calculations also show that there are parameter points where the assumption does not hold any more and the four-body decay dominates. The analysis of these points is subject to the next section.

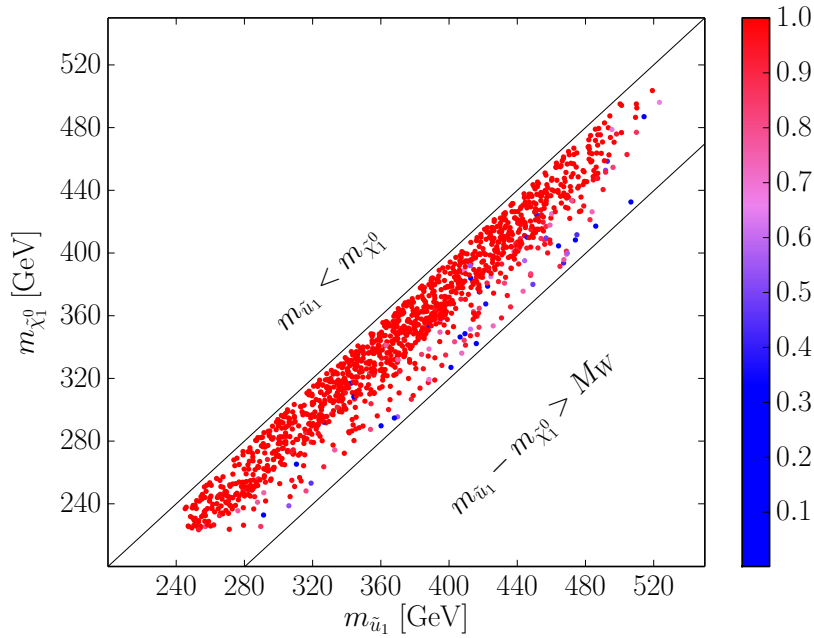


Figure 5.5: Parameter points of the random scan in the $(m_{\tilde{u}_1}, m_{\tilde{\chi}_1^0})$ -plane. The color code indicates the value of the branching ratio of the two-body decay. All final states of each of the two decay modes are included.

Figure 5.5 displays all scenarios of the random scan in the $(m_{\tilde{u}_1}, m_{\tilde{\chi}_1^0})$ -plane and the color is determined according to the branching ratio of the two-body decay: red corresponds to a large branching ratio and blue to a small branching ratio. While so far all results have been presented with respect to the mass difference of the \tilde{u}_1 and the $\tilde{\chi}_1^0$, here the values of the two masses are shown on the horizontal and vertical axis, respectively. The upper skewed line corresponds to $\Delta m = 0$ and the lower one to $\Delta m = m_W$, so that the region studied in this thesis is located in between. It is apparent that there are scenarios which are not excluded by the constraints applied and described in Section 4.3 over a wide range of the masses of the two particles. It is not possible to recognize a substantial difference of the coloring and the distribution of the points for low and high values of masses. This confirms that the effects described above depend on the mass difference and not on the absolute values themselves. The allowed masses are bounded from below by the constraints described in Chapter 4, the upper limits, on the other hand, reflect the limited scan range of the parameters in Eqs. (5.2) to (5.7).

As there are parameter points all over the mass range of the lightest up-type squark and the neutralino which are passing the constraints applied, and the branching ratio of the decay into a charm-quark and the neutralino is close to one in many cases, the search for the \tilde{u}_1 in this decay channel should be continued.

5.2. Random Scan with a $U(3) \times U(2) \times U(3)$ Symmetry

In the random scan of the previous section some scenarios were found where the four-body decay has a branching ratio close to one and the two-body decay is negligible. As this is the

opposite of the assumption made for the experimental analysis [57], now the conditions which have to be fulfilled to make the four-body decay important will be investigated.

It was already stated that the two-body decay strongly depends on the size of the flavor off-diagonal elements in the squark mixing matrix. By contrast, the four-body decay is nearly independent of these elements. Hence, reducing the size of the flavor mixing elements in the mixing matrix will change the relative strength of the two decay modes in favor of the four-body decay. As explained in Section 2.2.3 the flavor off-diagonal elements in the squark mixing matrix are generated via RGE running. With respect to the gauge quantum the three generations of quarks and squarks are identical. If in addition all particles had the same mass the RGEs would be the same for all generations and the mixing of different generations would remain fixed at all scales. However, in reality the masses of quarks of different generations are not equal resulting in distinct RGEs for each generation and thereby the generation mixing can vary depending on the energy scale. In this sense in SUSY models of course the soft SUSY breaking masses of the squarks are important for the mixing of different generations. For example in the concept of MFV, usually universal soft SUSY breaking masses are chosen for all generations, resulting in a

$$U(3)_{\tilde{Q}} \times U(3)_{\tilde{U}} \times U(3)_{\tilde{D}} \quad (5.31)$$

symmetry, with $U(3)_{\tilde{Q}}$ standing for the symmetry of the soft SUSY breaking masses for the left-handed isospin doublets and $U(3)_{\tilde{U}}$ and $U(3)_{\tilde{D}}$ for the ones of the up- and down-type right-handed isospin singlets [110]. These flavor symmetries provide a method to reduce the mixing of different generations. Inspecting Eqs. (5.2), (5.3), (5.11) and (5.12) shows that the full symmetry of Eq. (5.31) is not respected in the random scan of the previous section. Thus, a possibility to diminish the flavor mixing is to extend the symmetries of the soft SUSY breaking masses.

Here, this is done in a new, modified random scan. In detail, all input parameters of the model agree with the ones of the random scan in the previous section, with the exception of $m_{\tilde{Q}_i}$, $i = 1, 2, 3$. In the random scan above, $m_{\tilde{Q}_1}$ and $m_{\tilde{Q}_2}$ were fixed and only $m_{\tilde{Q}_3}$ was varied in the scan. A closer look on the scenarios of the previous random scan where the four-body decay has a rather large branching ratio reveals, that in these cases the soft SUSY breaking mass $m_{\tilde{Q}_3}$ is approximately the same as $m_{\tilde{Q}_1}$ and $m_{\tilde{Q}_2}$. Inspired by this observation, now all three soft SUSY breaking masses will be modified at the same time with

$$m_{\tilde{Q}_1} = m_{\tilde{Q}_2} = m_{\tilde{Q}_3} . \quad (5.32)$$

As a consequence the flavor symmetry of the soft SUSY breaking parameters is enhanced to

$$U(2)_{\tilde{Q}} \times U(2)_{\tilde{U}} \times U(3)_{\tilde{D}} \longrightarrow U(3)_{\tilde{Q}} \times U(2)_{\tilde{U}} \times U(3)_{\tilde{D}} . \quad (5.33)$$

The same analysis as in the previous section is performed, skipping the separate consideration of the results for the two-body decay since here the focus is on the four-body decay.

The partial decay widths of the two- and four-body decay for the modified random scan are displayed in Figure 5.6. Here, the partial decay width of the two-body decay is much smaller compared to the random scan of Section 5.1, whereas the four-body decay width remains nearly unchanged. This means that extending the symmetry of the left-handed soft SUSY breaking masses significantly reduced the size of the flavor off-diagonal elements of the squark mixing matrix. That the size of the four-body decay is basically the same, again confirms the observation made in Section 5.1 that flavor-changing elements do not have a large impact on this decay mode. The major difference with respect to the results obtained in Section 5.1 is, that now already at a mass difference of $\Delta m \approx 20$ GeV the partial

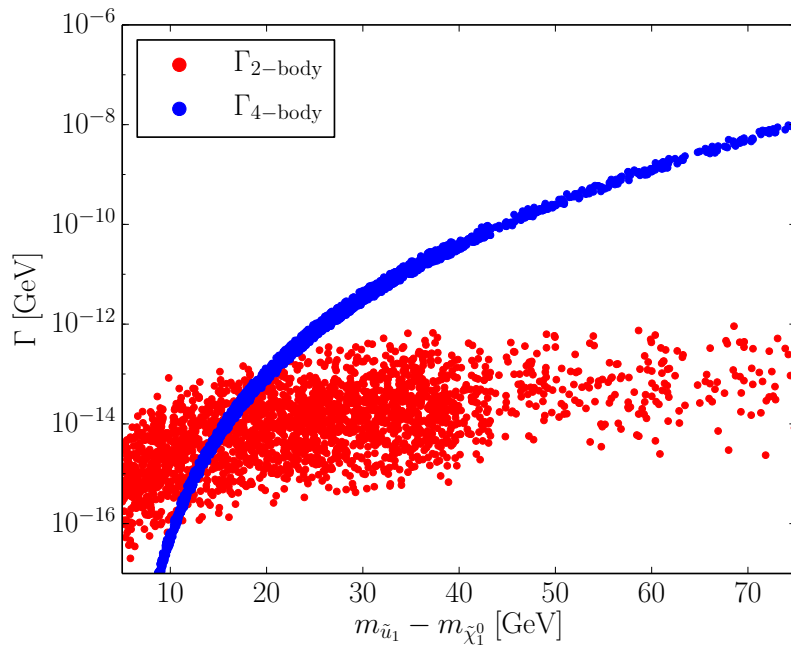


Figure 5.6: Two-body (red) and four-body (blue) partial decay widths in the modified random scan with a larger symmetry group for the soft SUSY breaking masses (Eq. (5.33)).

decay width of the four-body decay is higher than the one of the two-body decay, without exception. Furthermore, the spreading of the two-body decay is reduced to about two orders of magnitude. As in the previous section the lower density of possible parameter points for mass differences $\Delta m \gtrsim 40$ GeV arises from the fact that a Higgs boson must have a mass of around two times the neutralino mass by accident in order to fulfill the constraint for the relic density.

Thus, the total decay width of the \tilde{u}_1 depicted in Figure 5.7(a) is governed by the four-body decay over a wide range of the mass difference of the \tilde{u}_1 and the lightest neutralino. As before, the \tilde{u}_1 will hadronize before decaying. However, according to the bound of Eq. (5.29) now displaced vertices are possible if the mass difference is lower than about 25 GeV.

From the partial and the total decay widths, the branching ratios of the two modes are calculated and shown in Figure 5.7(b), taking into account all final states for each of the two decay modes. Clearly, the four-body decay dominates for mass differences of $\Delta m \gtrsim 15$ GeV. Comparing this to Fig. 5.4(b) demonstrates that the phenomenology of the decay has completely changed. Only for very low mass differences of NLSP and LSP the two-body decay is still important which can be understood from the fact that the phase space is then very limited and the internal, off-shell particles in the four-body decay lead to further suppression.

As now the four-body decay is the dominant decay mode of the \tilde{u}_1 it is natural to analyze the strength of different final states as proposed in Section 3.4. In Figure 5.8 the branching ratios of four selected final states which give the largest contribution to the four-body decay are presented. The sum of the branching ratios of the \tilde{u}_1 into the lightest neutralino, a bottom-quark and a quark-anti-quark pair $q\bar{q}'$ where $q = u, d, s, c$, is marked in red, and the branching ratios into the neutralino, a bottom-quark and a lepton with the corresponding

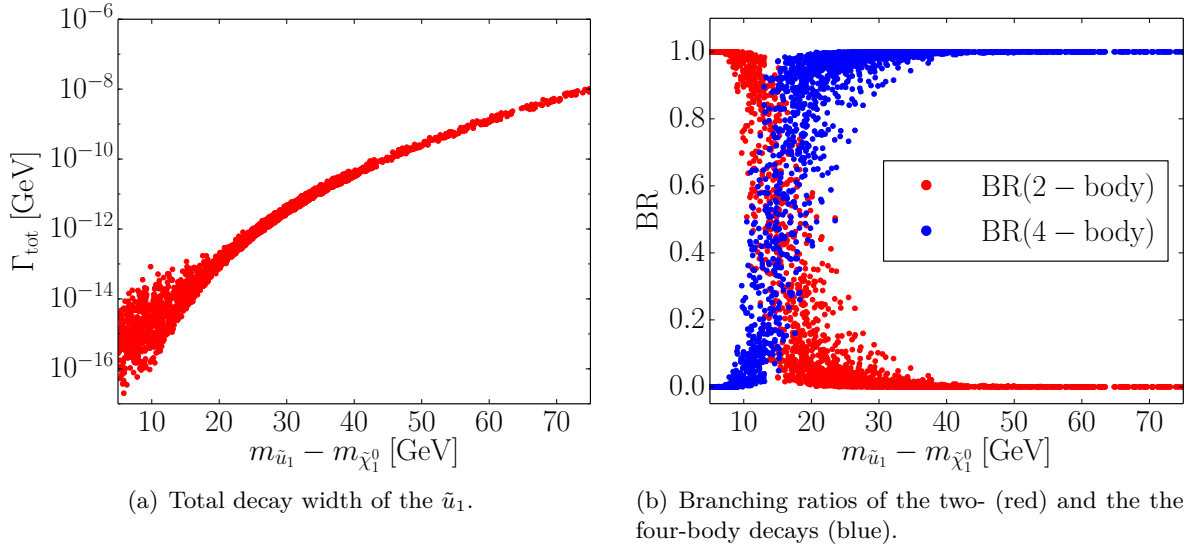


Figure 5.7: Total decay width (left) and branching ratios (right) in the modified random scan with a $U(3)_{\tilde{Q}} \times U(2)_{\tilde{U}} \times U(3)_{\tilde{D}}$ symmetry for the soft SUSY breaking masses.

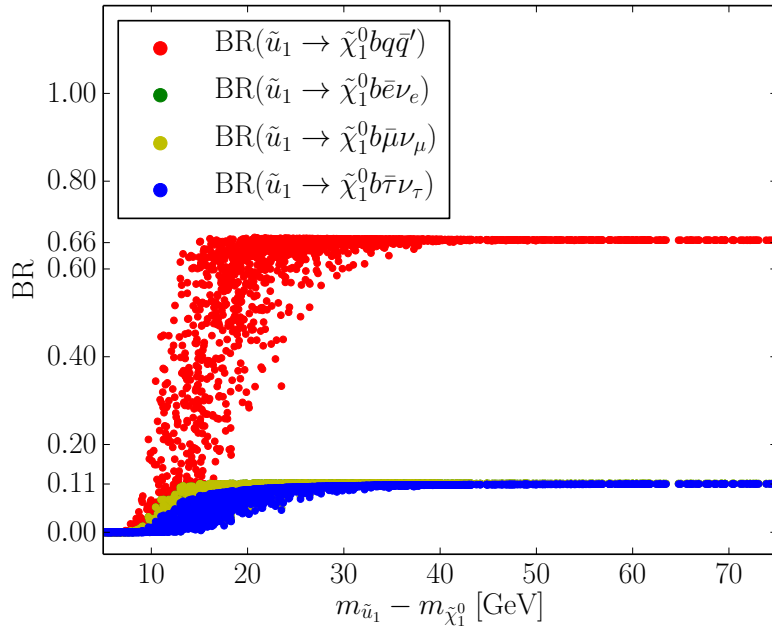


Figure 5.8: Branching ratios of the four-body decay into the four most important final states.

neutrino $\bar{l}\nu_l$, $l = e, \mu, \tau$ are colored green, yellow and blue, respectively. First, we focus on low Δm . From $\Delta m \approx 10$ GeV the branching ratios for all final states rise, as was already seen in Fig. 5.7(b). Neglecting the masses of the leptons, due to lepton universality the same growth of the branching ratios for all three lepton final states is expected. For the electron and the muon this is confirmed as the points of these two final states lie on top of each other, so only the yellow points are visible in Figure 5.8. As stated in Section 2.2.4 the mass of the τ -lepton is taken into account. This causes the branching ratio of the τ final state to increase more slowly than the other two branching ratios, but the same values are reached once the mass difference is high enough so that the mass of the τ has only negligible effects on the phase space. For $\Delta m \gtrsim 35$ GeV the branching ratios approach constant values of about 0.66 for the sum of the final states with a quark-anti-quark pair and of about 0.11 for each of the lepton final states. These are about the same branching ratios of leptonic and hadronic decays which would be expected for the decay of a W boson. In combination with the b quark this forms a top-quark decay signature. Thus, if the four-body decay is dominant, the process signature of the \tilde{u}_1 decay looks like the one of a top-quark decay with missing transverse energy caused by the neutralino leaving the detector. The detailed analysis of the four-body decay shows, that the diagram with an intermediate top-quark and a W boson (left diagram of Fig. 3.8) gives the largest contribution to these final states [60]. However, a difficulty for the reconstruction of the event, i.e. the determination of the origin of the decay products, is that it will not be possible to reconstruct the W boson or the top-quark directly by forming the invariant mass of the decay products as neither the top-quark nor the W boson are on-shell.

The region $\Delta m \in [15, 30]$ GeV may offer another interesting signature: combining the results from Figure 5.7(a) and 5.7(b) reveals, that here the lifetime of the \tilde{u}_1 is long enough to have a displaced vertex from the \tilde{u}_1 decay and that the four-body decay can already be the dominant decay mode. In this case there can be two separate displaced vertices, one from the \tilde{u}_1 decay and one from the b -quark in the final state. Again, for better detector resolutions than assumed in Eq. (5.27) this region is extended.

To conclude, in Figure 5.9 the scenarios found in the random scan with the soft SUSY breaking masses obeying a $U(3)_{\tilde{Q}} \times U(2)_{\tilde{U}} \times U(3)_{\tilde{D}}$ symmetry are plotted in the $(m_{\tilde{u}_1}, m_{\tilde{\chi}_1^0})$ -plane. Again, the \tilde{u}_1 mass is indicated on the horizontal axis, the $\tilde{\chi}_1^0$ mass on the vertical axis, and the value of the branching ratio of the sum of the two-body decays $\tilde{u}_1 \rightarrow (u, c)\tilde{\chi}_1^0$ is shown by the color code. The results from the previous section hold here as well. Possible parameter points are located all over the studied range of the masses of the two particles and the phenomenology essentially depends on the mass difference, not on the absolute mass values. The difference to the result of the previous random scan in Fig. 5.5 is as obvious as in Figures 5.6 to 5.8. The two-body decay is only important for a narrow band corresponding to mass differences of $\Delta m \in [0, 20]$ GeV, otherwise the four-body decay is dominant.

The results presented in this Section show that in contrast to the case of the first random scan in the previous section it is also possible that the four-body decay is the dominant decay mode of the \tilde{u}_1 over a wide range of the mass difference Δm . Then, the assumption of a branching ratio equal to one for the two-body decay into a charm-quark and the lightest neutralino in Ref. [57] does not hold any more. For that reason we emphasize that a complementary search for the \tilde{u}_1 should be conducted in the four-body decay channel.

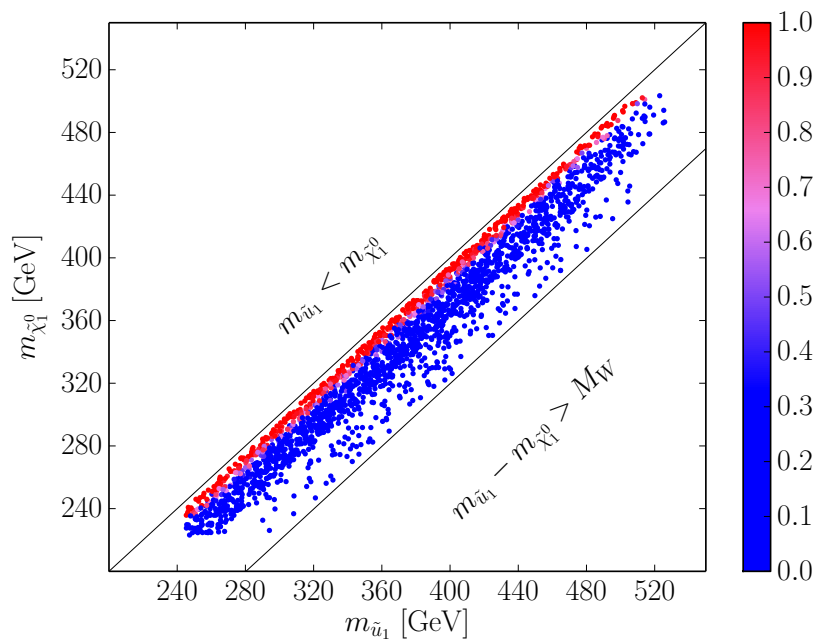


Figure 5.9: Parameter points of the modified random scan in the $(m_{\tilde{u}_1}, m_{\tilde{\chi}_1^0})$ -plane. The color code indicates the value of the branching ratio of the two-body decay, including both the up-quark and the charm-quark final state.

In this thesis the FCNC two-body decay of the lightest up-type squark \tilde{u}_1 into a charm- or an up-quark and the lightest neutralino $\tilde{\chi}_1^0$ has been calculated in the MSSM using a general flavor structure. In this model the FCNC decay is possible at tree-level and the dominant NLO corrections result from the strong interaction. In Chapter 3 the decay width of the \tilde{u}_1 has been calculated, for the first time including SUSY-QCD NLO corrections. In order to cancel the UV divergences occurring in the loop diagrams the Lagrangian was renormalized in the on-shell scheme. The remaining IR divergences are cancelled by the corresponding divergences in the real corrections. The implementation of these calculations in a stand-alone Fortran program has been checked against an independent calculation and implementation by another member of our research group [60]. The competing four-body decay of the \tilde{u}_1 into the neutralino, a down-type quark and two additional SM fermions has been calculated by other members as well [60], taking into account the general flavor structure explained in Section 2.2.3 and the masses of the third generation fermions in the final state. For the numerical analysis a scan was performed in the MSSM parameter space. Only those points were retained, that are compatible with the Higgs data, the DM measurement, the flavor observables and the current exclusion limits for SUSY particles (Chapter 4). For valid parameter points results were presented for the two-body and the four-body decay in the parameter region where the mass difference of the \tilde{u}_1 and the neutralino is $\Delta m \in [5, 75]$ GeV, since in this regime these decays are important.

The results in Chapter 5 demonstrate that the two-body decay strongly depends on the size of the flavor-changing elements in the squark mixing matrix whereas the four-body decay is nearly independent of them. Depending on the mass difference of the \tilde{u}_1 and the neutralino, the NLO corrections for the two-body decay amount to 5 to 25%. It has been shown that the size of the flavor off-diagonal elements in the squark mixing matrix is affected by assumptions on the soft SUSY breaking masses. If the flavor changing elements are rather large, the two-body decay with a charm-quark and the neutralino in the final state is dominant. By contrast, if the elements are rather small, the four-body decay is dominant and the final state is given by $\tilde{\chi}_1^0 b q \bar{q}'$ with $q = u, d, s, c$ in about two third of the cases and by $\tilde{\chi}_1^0 b \bar{l} \nu_l$ with $l = e, \mu, \tau$ in about one third of the cases, affecting the experimental analysis exclusively based on the two-body decay into a charm quark and the lightest neutralino [57].

As long as the results are compatible with experimental data, there is no preferred range of the flavor off-diagonal elements from the theoretical point of view. It is therefore important

to search for the \tilde{u}_1 in both the two-body and the four-body decay channel, since depending on the size of the mixing elements either the former or the latter decay can have a branching ratio close to one over a wide range of the mass difference between the \tilde{u}_1 and the $\tilde{\chi}_1^0$.

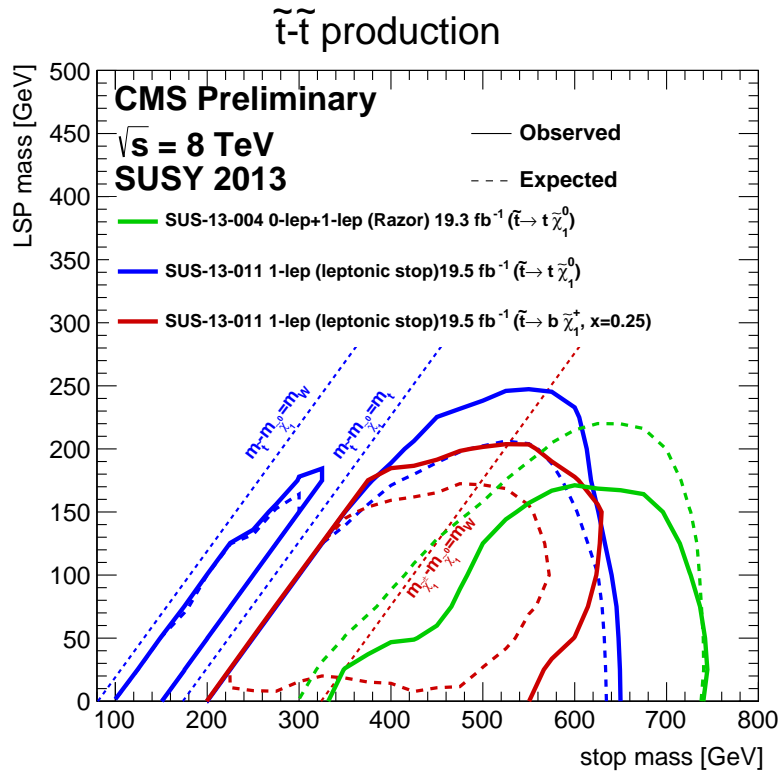
In order to further narrow down the viable parameter space, we currently investigate the possibility to add more flavor observables to the analysis. In detail, the contributions to Kaon or B meson mixing due to SUSY particles in loops can impose more constraints on the parameter space of the MSSM. These observables are expected to favor small flavor off-diagonal elements in the squark mixing matrix, which will then cause an enhancement of the four-body decay in comparison to the two-body decay.

The search for SUSY particles and in particular squarks is an ongoing task for the current experiments. As explained in Section 2.2.4 at present the only search for up-type squarks in the parameter region where the mass difference of the lightest up-type squark and the lightest neutralino is smaller than the mass of the W boson, focuses on the FCNC two-body decay. The calculation and the results presented in this thesis show, that the assumption of a branching ratio of one for the two-body decay made in the experimental analysis is not necessarily true and that the competing four-body decay can be dominant instead. In this thesis, results on the decay width of the \tilde{u}_1 and possible signatures of the relevant decay modes have been presented for both cases.

With this work we hope to provide the experiments with more precise information for their analysis and we further encourage the search for light up-type squarks, not only in the two-body but also in the four-body decay final states, to take another step to find supersymmetry!

A. CMS Limits on Stop Pair-Production

The current summary plot based on [61, 62] for all exclusion limits on stop pair production published by the CMS collaboration is shown in Figure A.1. The stop mass is plotted on



the horizontal and the neutralino mass on the vertical axis, respectively. Here, the left blue dashed line corresponds to $\Delta m = m_W$ and the right blue dashed line indicates $\Delta m = m_t$.

Hence, no exclusion limits are available yet for $\Delta m < m_W$.

B. Dirac Gamma-Matrices

This is a collection of relations for Dirac matrices in the notation adopted from [111]. The γ -matrices are defined as

$$\gamma_0 = \beta, \quad \gamma_i = \beta\alpha_i \quad \text{with } i = 1, 2, 3, \quad (7.1)$$

where β and α_i are hermitian and satisfy

$$\alpha_i^2 = \beta^2 = 1, \quad \{\alpha_i, \beta\} = 0, \quad \{\alpha_i, \alpha_j\} = 2\delta_{ij}. \quad (7.2)$$

This implies that

$$\gamma_0^\dagger = \gamma_0 \quad \text{and} \quad \gamma_i^\dagger = -\gamma_i \quad (7.3)$$

and one can show that the γ -matrices obey the Clifford Algebra

$$\{\gamma^\mu, \gamma^\nu\} = 2g^{\mu\nu} \quad (7.4)$$

and similarly

$$\{\gamma^{\mu\dagger}, \gamma^{\nu\dagger}\} = 2g^{\mu\nu}. \quad (7.5)$$

In four dimensions γ_5 is defined as

$$\gamma_5 = i\gamma_0\gamma_1\gamma_2\gamma_3, \quad (7.6)$$

$$\{\gamma^\mu, \gamma_5\} = 0, \quad (7.7)$$

$$\gamma_5^2 = \mathbf{1}_4. \quad (7.8)$$

Then, the following relations hold in four dimensions:

$$\gamma_0(\gamma_\mu)^\dagger\gamma_0 = \gamma_\mu, \quad (7.9)$$

$$\gamma_0(\gamma_5)^\dagger\gamma_0 = -\gamma_5, \quad (7.10)$$

$$\gamma_0(\gamma_\mu\gamma_\nu)^\dagger\gamma_0 = \gamma_\nu\gamma_\mu, \quad (7.11)$$

$$\gamma_0(\gamma_5\gamma_\mu)^\dagger\gamma_0 = \gamma_\mu(-\gamma_5) = \gamma_5\gamma_\mu, \quad (7.12)$$

$$\gamma_0(\not{a}\not{b}\dots\not{c})^\dagger\gamma_0 = \not{c}\dots\not{b}\not{a}. \quad (7.13)$$

In order to simplify traces it is often convenient to use

$$\gamma_\mu\not{a} = -\not{a}\gamma_\mu + 2a_\mu, \quad (7.14)$$

$$\not{a}\not{b} = -\not{b}\not{a} + 2a \cdot b \mathbf{1}_4, \quad (7.15)$$

$$\gamma^\mu\gamma_\mu = 4 \mathbf{1}_4, \quad (7.16)$$

$$\gamma^\mu\not{a}\not{b}\gamma_\mu = 4a \cdot b \mathbf{1}_4, \quad (7.17)$$

$$\text{Tr}\{\not{a}\not{b}\} = 4a \cdot b, \quad (7.18)$$

$$\text{Tr}\{\not{a}_1\not{a}_2\dots\not{a}_{2n+1}\} = 0, \quad (7.19)$$

$$\text{Tr}\{\gamma_5\gamma_\mu\} = 0, \quad (7.20)$$

$$\text{Tr}\{\gamma_5\gamma_\mu\gamma_\nu\} = 0, \quad (7.21)$$

with $n \in \mathbb{N}$ by exploiting the anticommutator relations above. Some special cases are

$$\{\gamma^0, \gamma^\nu\} = g^0_\mu \{\gamma^{\mu\dagger}, \gamma^{\nu\dagger}\} \quad (7.22)$$

$$= g^0_\mu \cdot 2g^{\mu\nu} \quad (7.23)$$

$$= 2g^{0\nu}, \quad (7.24)$$

$$\gamma^0 \not{p} = -\not{p} \gamma^0 + 2p^0. \quad (7.25)$$

In $d \neq 4$ dimensions the following relations hold (taken from [67])

$$\{\gamma^\mu, \gamma^\nu\} = 2g^{\mu\nu}, \quad (7.26)$$

$$\gamma^\mu \gamma_\mu = d \mathbf{1}_d, \quad (7.27)$$

$$\gamma^\mu \gamma_\nu \gamma_\mu = (2 - d) \gamma_\nu, \quad (7.28)$$

and

$$\{\gamma_5, \gamma_\mu\} = 0, \quad \text{for } \mu = 0, 1, 2, 3, \quad (7.29)$$

$$[\gamma_5, \gamma_\mu] = 0, \quad \text{otherwise}, \quad (7.30)$$

$$(\gamma_5)^2 = \mathbf{1}_d, \quad (7.31)$$

$$(\gamma_5)^\dagger = \gamma_5. \quad (7.32)$$

- [1] **ATLAS** Collaboration, G. Aad *et al.*, “Observation of a new particle in the search for the Standard Model Higgs boson with the ATLAS detector at the LHC,” *Phys.Lett.* **B716** (2012) 1–29, [arXiv:1207.7214](#) [hep-ex].
- [2] **CMS** Collaboration, S. Chatrchyan *et al.*, “Observation of a new boson at a mass of 125 GeV with the CMS experiment at the LHC,” *Phys.Lett.* **B716** (2012) 30–61, [arXiv:1207.7235](#) [hep-ex].
- [3] A. Djouadi, “The Anatomy of electro-weak symmetry breaking. I: The Higgs boson in the standard model,” *Phys.Rept.* **457** (2008) 1–216, [arXiv:hep-ph/0503172](#) [hep-ph].
- [4] A. Djouadi, “The Anatomy of electro-weak symmetry breaking. II. The Higgs bosons in the minimal supersymmetric model,” *Phys.Rept.* **459** (2008) 1–241, [arXiv:hep-ph/0503173](#) [hep-ph].
- [5] J. F. Gunion *et al.*, *The Higgs hunters guide*. Frontiers in physics ; 80. Westview Press, 2003.
- [6] Nobelprize.org, “The nobel prize in physics 2013,” 2013.
http://www.nobelprize.org/nobel_prizes/physics/laureates/2013/.
- [7] S. L. Glashow, “Partial-symmetries of weak interactions,” *Nuclear Physics* **22** no. 4, (1961) 579 – 588.
- [8] A. Salam, “Weak and Electromagnetic Interactions,” *Conf.Proc.* **C680519** (1968) 367–377.
- [9] S. Weinberg, “A Model of Leptons,” *Phys. Rev. Lett.* **19** (Nov, 1967) 1264–1266.
- [10] M. Peskin and D. Schroeder, *An Introduction to Quantum Field Theory*. Westview Press, 1995.
- [11] M. Goldhaber, L. Grodzins, and A. W. Sunyar, “Helicity of Neutrinos,” *Phys. Rev.* **109** (Feb, 1958) 1015–1017.

- [12] K. Nishijima, “Charge Independence Theory of V Particles,” *Progress of Theoretical Physics* **13** no. 3, (1955) 285–304.
- [13] T. Nakano and K. Nishijima, “Charge Independence for V-particles,” *Progress of Theoretical Physics* **10** no. 5, (1953) 581–582.
- [14] M. Gell-Mann, “The interpretation of the new particles as displaced charge multiplets,” *Il Nuovo Cimento* **4** no. 2, (1956) 848–866.
- [15] N. Cabibbo, “Unitary Symmetry and Leptonic Decays,” *Phys. Rev. Lett.* **10** (Jun, 1963) 531–533.
- [16] M. Kobayashi and T. Maskawa, “CP-Violation in the Renormalizable Theory of Weak Interaction,” *Progress of Theoretical Physics* **49** no. 2, (1973) 652–657.
- [17] P. Higgs, “Broken symmetries, massless particles and gauge fields,” *Physics Letters* **12** no. 2, (1964) 132 – 133.
- [18] P. W. Higgs, “Broken Symmetries and the Masses of Gauge Bosons,” *Phys. Rev. Lett.* **13** (Oct, 1964) 508–509.
- [19] P. W. Higgs, “Spontaneous Symmetry Breakdown without Massless Bosons,” *Phys. Rev.* **145** (May, 1966) 1156–1163.
- [20] F. Englert and R. Brout, “Broken Symmetry and the Mass of Gauge Vector Mesons,” *Phys. Rev. Lett.* **13** (Aug, 1964) 321–323.
- [21] T. W. B. Kibble, “Symmetry Breaking in Non-Abelian Gauge Theories,” *Phys. Rev.* **155** (Mar, 1967) 1554–1561.
- [22] J. Goldstone, “Field theories with « Superconductor » solutions,” *Il Nuovo Cimento* **19** no. 1, (1961) 154–164.
- [23] G. Landsberg, “Higgs bosons in the standard model and beyond,” [arXiv:1310.5705](https://arxiv.org/abs/1310.5705) [hep-ex].
- [24] D. Z. Freedman and P. van Nieuwenhuizen, “Properties of supergravity theory,” *Phys. Rev. D* **14** (Aug, 1976) 912–916.
- [25] D. Z. Freedman, P. van Nieuwenhuizen, and S. Ferrara, “Progress toward a theory of supergravity,” *Phys. Rev. D* **13** (Jun, 1976) 3214–3218.
- [26] S. Deser and B. Zumino, “Consistent supergravity,” *Physics Letters B* **62** no. 3, (1976) 335 – 337.
- [27] K. G. Wilson, “The renormalization group: Critical phenomena and the Kondo problem,” *Rev. Mod. Phys.* **47** (Oct, 1975) 773–840.
- [28] H. Georgi and S. L. Glashow, “Unity of All Elementary-Particle Forces,” *Phys. Rev. Lett.* **32** (Feb, 1974) 438–441.
- [29] J. C. Pati and A. Salam, “Unified Lepton-Hadron Symmetry and a Gauge Theory of the Basic Interactions,” *Phys. Rev. D* **8** (Aug, 1973) 1240–1251.

- [30] A. Buras, J. Ellis, M. Gaillard, and D. Nanopoulos, “Aspects of the grand unification of strong, weak and electromagnetic interactions,” *Nuclear Physics B* **135** no. 1, (1978) 66 – 92.
- [31] J. Ellis, J. S. Hagelin, D. Nanopoulos, and K. Tamvakis, “Weak symmetry breaking by radiative corrections in broken supergravity,” *Physics Letters B* **125** no. 4, (1983) 275 – 281.
- [32] J. F. Gunion and H. E. Haber, “Higgs bosons in supersymmetric models (I),” *Nuclear Physics B* **272** no. 1, (1986) 1 – 76.
- [33] **Planck** Collaboration, P. Ade *et al.*, “Planck 2013 results. XVI. Cosmological parameters,” [arXiv:1303.5076](https://arxiv.org/abs/1303.5076) [astro-ph.CO].
- [34] **WMAP** Collaboration, C. Bennett *et al.*, “Nine-Year Wilkinson Microwave Anisotropy Probe (WMAP) Observations: Final Maps and Results,” [arXiv:1212.5225](https://arxiv.org/abs/1212.5225) [astro-ph.CO].
- [35] P. van Nieuwenhuizen, “Supergravity,” *Physics Reports* **68** no. 4, (1981) 189 – 398.
- [36] S. Coleman and J. Mandula, “All Possible Symmetries of the S -Matrix,” *Phys. Rev.* **159** (Jul, 1967) 1251–1256.
- [37] R. Haag, J. T. Łopuszański, and M. Sohnius, “All possible generators of supersymmetries of the S -matrix,” *Nuclear Physics B* **88** no. 2, (1975) 257 – 274.
- [38] M. Drees, R. Godbole, and P. Roy, *Theory and phenomenology of sparticles : an account of four-dimensional $N = 1$ supersymmetry in high energy physics*. World Scientific, Singapore, 2005.
- [39] E. Witten, “Dynamical breaking of supersymmetry,” *Nuclear Physics B* **188** no. 3, (1981) 513 – 554.
- [40] S. Dimopoulos and H. Georgi, “Softly broken supersymmetry and $SU(5)$,” *Nuclear Physics B* **193** no. 1, (1981) 150 – 162.
- [41] H. E. Haber, “Nonminimal Higgs sectors: The Decoupling limit and its phenomenological implications,” [arXiv:hep-ph/9501320](https://arxiv.org/abs/hep-ph/9501320) [hep-ph].
- [42] P. Fayet, “Supersymmetry and weak, electromagnetic and strong interactions,” *Physics Letters B* **64** no. 2, (1976) 159 – 162.
- [43] P. Fayet, “Supergauge invariant extension of the Higgs mechanism and a model for the electron and its neutrino,” *Nuclear Physics B* **90** no. 0, (1975) 104 – 124.
- [44] H. Nilles, “Supersymmetry, supergravity and particle physics,” *Physics Reports* **110** no. 1–2, (1984) 1 – 162.
- [45] **MSSM Working Group** Collaboration, A. Djouadi *et al.*, “The Minimal supersymmetric standard model: Group summary report,” [arXiv:hep-ph/9901246](https://arxiv.org/abs/hep-ph/9901246) [hep-ph].
- [46] R. S. Chivukula, H. Georgi, and L. Randall, “A composite technicolor standard model of quarks,” *Nuclear Physics B* **292** no. 0, (1987) 93 – 108.

- [47] L. J. Hall and L. Randall, “Weak-scale effective supersymmetry,” *Phys. Rev. Lett.* **65** (Dec, 1990) 2939–2942.
- [48] A. Buras, P. Gambino, M. Gorbahn, S. Jager, and L. Silvestrini, “Universal unitarity triangle and physics beyond the standard model,” *Phys.Lett.* **B500** (2001) 161–167, [arXiv:hep-ph/0007085](#) [hep-ph].
- [49] G. D’Ambrosio, G. Giudice, G. Isidori, and A. Strumia, “Minimal flavor violation: An Effective field theory approach,” *Nucl.Phys.* **B645** (2002) 155–187, [arXiv:hep-ph/0207036](#) [hep-ph].
- [50] C. Bobeth, M. Bona, A. J. Buras, T. Ewerth, M. Pierini, *et al.*, “Upper bounds on rare K and B decays from minimal flavor violation,” *Nucl.Phys.* **B726** (2005) 252–274, [arXiv:hep-ph/0505110](#) [hep-ph].
- [51] B. Allanach, C. Balazs, G. Belanger, M. Bernhardt, F. Boudjema, *et al.*, “SUSY Les Houches Accord 2,” *Comput.Phys.Commun.* **180** (2009) 8–25, [arXiv:0801.0045](#) [hep-ph].
- [52] K.-i. Hikasa and M. Kobayashi, “Light scalar top quark at e^+e^- colliders,” *Phys. Rev. D* **36** (Aug, 1987) 724–732.
- [53] M. Mühlleitner and E. Popeno, “Light Stop Decay in the MSSM with Minimal Flavour Violation,” *JHEP* **1104** (2011) 095, [arXiv:1102.5712](#) [hep-ph].
- [54] **ATLAS** Collaboration, G. Aad *et al.*, “Search for a supersymmetric partner to the top quark in final states with jets and missing transverse momentum at $\sqrt{s} = 7$ TeV with the ATLAS detector,” *Phys.Rev.Lett.* **109** (2012) 211802, [arXiv:1208.1447](#) [hep-ex].
- [55] **ATLAS** Collaboration, G. Aad *et al.*, “Search for direct top squark pair production in final states with one isolated lepton, jets, and missing transverse momentum in $\sqrt{s} = 7$ TeV pp collisions using 4.7 fb^{-1} of ATLAS data,” *Phys.Rev.Lett.* **109** (2012) 211803, [arXiv:1208.2590](#) [hep-ex].
- [56] **ATLAS** Collaboration, G. Aad *et al.*, “Search for direct top-squark pair production in final states with two leptons in pp collisions at $\sqrt{s}=8$ TeV with the ATLAS detector,” [arXiv:1403.4853](#) [hep-ex].
- [57] **ATLAS** Collaboration, “Search for pair-produced top squarks decaying into a charm quark and the lightest neutralinos with 20.3 fb^{-1} of pp collisions at $\sqrt{s} = 8$ TeV with the ATLAS detector at the LHC,” Tech. Rep. ATLAS-CONF-2013-068, CERN, Geneva, Jul, 2013.
- [58] **CDF** Collaboration, T. Aaltonen *et al.*, “Search for Scalar Top Quark Production in $p\bar{p}$ Collisions at $\sqrt{s} = 1.96$ TeV,” *JHEP* **1210** (2012) 158, [arXiv:1203.4171](#) [hep-ex].
- [59] C. Boehm, A. Djouadi, and Y. Mambrini, “Decays of the lightest top squark,” *Phys.Rev.* **D61** (2000) 095006, [arXiv:hep-ph/9907428](#) [hep-ph].
- [60] R. Gröber, *Aspects of Higgs Physics and New Physics at the LHC*. PhD thesis, KIT, 2014.

- [61] **CMS** Collaboration, S. Chatrchyan *et al.*, “Search for top-squark pair production in the single-lepton final state in pp collisions at $\sqrt{s} = 8$ TeV,” *Eur.Phys.J.* **C73** (2013) 2677, [arXiv:1308.1586](#) [hep-ex].
- [62] **CMS** Collaboration, “Search for supersymmetry using razor variables in events with b-jets in pp collisions at 8 TeV,” Tech. Rep. CMS-PAS-SUS-13-004, CERN, Geneva, 2013.
- [63] T. Kinoshita, “Mass singularities of feynman amplitudes,” *Journal of Mathematical Physics* **3** no. 4, (1962) 650–677.
- [64] T. D. Lee and M. Nauenberg, “Degenerate systems and mass singularities,” *Phys. Rev.* **133** (Mar, 1964) B1549–B1562.
- [65] G. ’t Hooft and M. Veltman, “Regularization and renormalization of gauge fields,” *Nuclear Physics B* **44** no. 1, (1972) 189 – 213.
- [66] G. Costa and M. Tonin, “Renormalization of non-abelian local gauge theories,” *La Rivista Del Nuovo Cimento Series 2* **5** no. 1, (1975) 29–107.
- [67] J. Collins, *Renormalization*. Cambridge University Press, Cambridge, 1984.
- [68] Y. Yamada, “Gauge dependence of the on-shell renormalized mixing matrices,” *Phys.Rev.* **D64** (2001) 036008, [arXiv:hep-ph/0103046](#) [hep-ph].
- [69] A. Denner, “Techniques for calculation of electroweak radiative corrections at the one loop level and results for W physics at LEP-200,” *Fortsch.Phys.* **41** no. 4, (1993) 307–420, [arXiv:0709.1075](#) [hep-ph].
- [70] B. A. Kniehl and A. Pilaftsis, “Mixing renormalization in Majorana neutrino theories,” *Nucl.Phys.* **B474** (1996) 286–308, [arXiv:hep-ph/9601390](#) [hep-ph].
- [71] P. Gambino, P. Grassi, and F. Madricardo, “Fermion mixing renormalization and gauge invariance,” *Phys.Lett.* **B454** (1999) 98–104, [arXiv:hep-ph/9811470](#) [hep-ph].
- [72] M. Böhm, A. Denner, and H. Joos, *Gauge Theories of the Strong and Electroweak Interaction*. Teubner, Stuttgart, 2001.
- [73] S. Heinemeyer, H. Rzehak, and C. Schappacher, “Proposals for Bottom Quark/Squark Renormalization in the Complex MSSM,” *Phys.Rev.* **D82** (2010) 075010, [arXiv:1007.0689](#) [hep-ph].
- [74] A. Denner and T. Sack, “Renormalization of the quark mixing matrix,” *Nuclear Physics B* **347** no. 1–2, (1990) 203 – 216.
- [75] G. ’t Hooft and M. Veltman, “Scalar one-loop integrals,” *Nuclear Physics B* **153** no. 0, (1979) 365 – 401.
- [76] R. K. Ellis, W. J. Stirling, and B. R. Webber, *QCD and Collider Physics*. Cambridge University Press, Cambridge, 1996.
- [77] J. M. Campbell, R. K. Ellis, and F. Tramontano, “Single top production and decay at next-to-leading order,” *Phys.Rev.* **D70** (2004) 094012, [arXiv:hep-ph/0408158](#) [hep-ph].

- [78] T. Hahn, “Generating Feynman diagrams and amplitudes with FeynArts 3,” *Comput.Phys.Commun.* **140** (2001) 418–431, [arXiv:hep-ph/0012260](#) [hep-ph].
- [79] T. Hahn and M. Perez-Victoria, “Automatized one loop calculations in four-dimensions and D-dimensions,” *Comput.Phys.Commun.* **118** (1999) 153–165, [arXiv:hep-ph/9807565](#) [hep-ph].
- [80] L. Lewin, ed., *Structural properties of polylogarithms*. Mathematical surveys and monographs ; 37. American Math. Soc., Providence, RI, 1991.
- [81] W. Porod, “SPHeno, a program for calculating supersymmetric spectra, SUSY particle decays and SUSY particle production at e+ e- colliders,” *Comput.Phys.Commun.* **153** (2003) 275–315, [arXiv:hep-ph/0301101](#) [hep-ph].
- [82] W. Porod and F. Staub, “SPHeno 3.1: Extensions including flavour, CP-phases and models beyond the MSSM,” *Comput.Phys.Commun.* **183** (2012) 2458–2469, [arXiv:1104.1573](#) [hep-ph].
- [83] **ATLAS** Collaboration, “Search for direct production of charginos and neutralinos in events with three leptons and missing transverse momentum in 21 fb^{-1} of pp collisions at $\sqrt{s} = 8 \text{ TeV}$ with the ATLAS detector,” Tech. Rep. ATLAS-CONF-2013-035, CERN, Geneva, Mar, 2013.
- [84] H. E. Haber and R. Hempfling, “Can the mass of the lightest Higgs boson of the minimal supersymmetric model be larger than m_Z ?,” *Phys. Rev. Lett.* **66** (Apr, 1991) 1815–1818.
- [85] J. Ellis, G. Ridolfi, and F. Zwirner, “Radiative corrections to the masses of supersymmetric higgs bosons,” *Physics Letters B* **257** no. 1–2, (1991) 83 – 91.
- [86] **Particle Data Group** Collaboration, J. Beringer *et al.*, “2012 Review of Particle Physics,” *Phys. Rev.* **D86** (2012) 010001.
- [87] P. Bechtle, O. Brein, S. Heinemeyer, G. Weiglein, and K. E. Williams, “HiggsBounds: Confronting Arbitrary Higgs Sectors with Exclusion Bounds from LEP and the Tevatron,” *Comput.Phys.Commun.* **181** (2010) 138–167, [arXiv:0811.4169](#) [hep-ph].
- [88] P. Bechtle, O. Brein, S. Heinemeyer, G. Weiglein, and K. E. Williams, “HiggsBounds 2.0.0: Confronting Neutral and Charged Higgs Sector Predictions with Exclusion Bounds from LEP and the Tevatron,” *Comput.Phys.Commun.* **182** (2011) 2605–2631, [arXiv:1102.1898](#) [hep-ph].
- [89] P. Bechtle, O. Brein, S. Heinemeyer, O. Stal, T. Stefaniak, *et al.*, “Recent Developments in HiggsBounds and a Preview of HiggsSignals,” *PoS* (2012) 024, [arXiv:1301.2345](#) [hep-ph].
- [90] A. Djouadi, J. Kalinowski, and M. Spira, “HDECAY: a program for Higgs boson decays in the Standard Model and its supersymmetric extension,” *Computer Physics Communications* **108** (Jan., 1998) 56–74, [arXiv:hep-ph/9704448](#).
- [91] P. Z. Skands, B. Allanach, H. Baer, C. Balazs, G. Belanger, *et al.*, “SUSY Les Houches accord: Interfacing SUSY spectrum calculators, decay packages, and event generators,” *JHEP* **0407** (2004) 036, [arXiv:hep-ph/0311123](#) [hep-ph].

- [92] A. Arbey and F. Mahmoudi, “SuperIso Relic: A Program for calculating relic density and flavor physics observables in Supersymmetry,” *Comput.Phys.Commun.* **181** (2010) 1277–1292, [arXiv:0906.0369 \[hep-ph\]](#).
- [93] A. Arbey and F. Mahmoudi, “SuperIso Relic v3.0: A program for calculating relic density and flavour physics observables: Extension to NMSSM,” *Computer Physics Communications* **182** no. 7, (2011) 1582 – 1583.
- [94] F. Mahmoudi, “SuperIso: A Program for calculating the isospin asymmetry of B to $K^* \gamma$ in the MSSM,” *Comput.Phys.Commun.* **178** (2008) 745–754, [arXiv:0710.2067 \[hep-ph\]](#).
- [95] F. Mahmoudi, “SuperIso v2.3: A Program for calculating flavor physics observables in Supersymmetry,” *Comput.Phys.Commun.* **180** (2009) 1579–1613, [arXiv:0808.3144 \[hep-ph\]](#).
- [96] **CMS, LHCb** Collaboration, “Combination of results on the rare decays $B_{(s)}^0 \rightarrow \mu^+ \mu^-$ from the CMS and LHCb experiments,” Tech. Rep. CMS-PAS-BPH-13-007. CERN-LHCb-CONF-2013-012, CERN, Geneva, Jul, 2013.
- [97] **ATLAS, CDF, CMS, D0, LHCb** Collaboration, P. Eerola *et al.*, “Rare $B_{(s)}^0 \rightarrow \mu^+ \mu^-$ decays,” [arXiv:1209.3440 \[hep-ex\]](#).
- [98] **Belle** Collaboration, J. Brodzicka *et al.*, “Physics Achievements from the Belle Experiment,” *PTEP* **2012** (2012) 04D001, [arXiv:1212.5342 \[hep-ex\]](#).
- [99] **BaBar** Collaboration, J. Lees *et al.*, “Evidence of $B \rightarrow \tau \nu$ decays with hadronic B tags,” *Phys.Rev.* **D88** (2013) 031102, [arXiv:1207.0698 \[hep-ex\]](#).
- [100] **BaBar** Collaboration, J. Lees *et al.*, “Measurement of $B(B \rightarrow X_s \gamma)$, the $B \rightarrow X_s \gamma$ photon energy spectrum, and the direct CP asymmetry in $B \rightarrow X_{s+d} \gamma$ decays,” *Phys.Rev.* **D86** (2012) 112008, [arXiv:1207.5772 \[hep-ex\]](#).
- [101] B. Allanach, A. Djouadi, J. Kneur, W. Porod, and P. Slavich, “Precise determination of the neutral Higgs boson masses in the MSSM,” *JHEP* **0409** (2004) 044, [arXiv:hep-ph/0406166 \[hep-ph\]](#).
- [102] **ATLAS** Collaboration, C. Deluca *et al.*, “Searches for gluino-mediated production of third generation squarks with the ATLAS detector,” Tech. Rep. ATL-PHYS-PROC-2013-179, CERN, Geneva, Jun, 2013.
- [103] A. Djouadi, M. Mühlleitner, and M. Spira, “Decays of supersymmetric particles: The Program SUSY-HIT (SUSpect-SdecaY-Hdecay-InTerface),” *Acta Phys.Polon.* **B38** (2007) 635–644, [arXiv:hep-ph/0609292 \[hep-ph\]](#).
- [104] M. Muhlleitner, A. Djouadi, and Y. Mambrini, “SDECAY: A Fortran code for the decays of the supersymmetric particles in the MSSM,” *Comput.Phys.Commun.* **168** (2005) 46–70, [arXiv:hep-ph/0311167 \[hep-ph\]](#).
- [105] **Particle Data Group** Collaboration, C. Amsler *et al.*, “Review of Particle Physics,” *Physics Letters* **B667** (2008) 1.
- [106] C. Balazs, M. S. Carena, and C. Wagner, “Dark matter, light stops and electroweak baryogenesis,” *Phys.Rev.* **D70** (2004) 015007, [arXiv:hep-ph/0403224 \[hep-ph\]](#).

-
- [107] CMS Collaboration, S. Chatrchyan *et al.*, “Identification of b-quark jets with the CMS experiment,” *JINST* **8** (2013) P04013, [arXiv:1211.4462](#) [hep-ex].
- [108] G. Dissertori, I. Knowles, and M. Schmelling, *Quantum Chromodynamics: High energy experiments and theory International Series of Monographs on Physics No. 115*. Oxford University Press, 2003.
- [109] T. Hurth, “Present status of inclusive rare B decays,” *Rev.Mod.Phys.* **75** (2003) 1159–1199, [arXiv:hep-ph/0212304](#) [hep-ph].
- [110] R. Barbieri, D. Buttazzo, F. Sala, and D. M. Straub, “Flavour physics and flavour symmetries after the first LHC phase,” [arXiv:1402.6677](#) [hep-ph].
- [111] J. D. Bjorken and S. D. Drell, *Relativistische Quantenmechanik*. Spektrum, Akad. Verl., Heidelberg, 1998.

ACKNOWLEDGMENTS

I would particularly like to thank Prof. Dr. Margarete Mühlleitner for giving me the opportunity to write my master thesis on such an exciting and current topic. I highly appreciate her ongoing support in discussions, questions and problems and I thank her for providing help in preparation for talks and in writing this thesis. Many thanks also for enabling me to participate in a workshop in Bad Liebenzell, the Helmholtz Alliance meeting at the KIT and the annual DPG meeting in Mainz.

I would like to express my gratitude to Prof. Dr. Dieter Zeppenfeld for being the second reviewer of my master thesis.

My sincere thanks to Dr. Eva Popena who guided me through the work and answered questions anytime. In particular I thank for many fruitful discussions, comments on talks and especially for detailed proof-reading of this thesis.

Cordial thanks also to Ramona Gröber for cross-checking my calculation, discussing problems and for supplying me with the implementation of her calculations.

Thanks to all members of the ITP who made the stay at the institute a pleasant time. Especially I would like to thank the members of my working group who offered support in case of problems and in preparing talks. I also give thanks to my room mates for a nice atmosphere, for tips and comments and for reading several parts of this thesis.

My warm thanks to my friends, my family and especially to Lena for supporting me all throughout my studies.